DISSERTATION

A MODELING-EXPERIMENTAL (MODEX) APPROACH TO ADVANCE UNDERSTANDING OF GLOBAL CONTROLS AND MICROBIAL CONTRIBUTIONS TO PARTICULATE AND MINERAL-ASSOCIATED ORGANIC MATTER STORAGE

Submitted by

Paige M. Hansen

Graduate Degree Program in Ecology

In partial fulfillment of the requirements

For the Degree of Doctor of Philosophy

Colorado State University

Fort Collins, Colorado

Summer 2024

Doctoral committee:

Advisor: M. Francesca Cotrufo

Meagan Schipanski
Matt Wallenstein
Pankaj Trivedi

ABSTRACT

A MODELING-EXPERIMENTAL (MODEX) APPROACH TO ADVANCE UNDERSTANDING OF GLOBAL CONTROLS AND MICROBIAL CONTRIBUTIONS TO PARTICULATE AND MINERAL-ASSOCIATED ORGANIC MATTER STORAGE

As soils are the largest terrestrial pool of carbon (C) and provision many ecosystem services, including nutrient cycling and maintenance of plant productivity, soil C sequestration represents a promising technology to help meet urgent needs to draw down atmospheric carbon dioxide (CO_2) and prevent acceleration of climate change, as well as to help feed a rapidly growing global population. Given this, a comprehensive understanding of the mechanisms underpinning observed patterns of soil C storage is necessary to ensure a sustainable future for all. In response to this need, recent breakthroughs in our understanding of soil organic matter (SOM) dynamics have led to the development of multiple frameworks articulating how climate, soil, plant, and microbial properties interact with one another to control the formation of the two SOM constituents, particulate (POM) and mineral-associated organic matter (MAOM). Despite this, environmental controls that act on POM and MAOM storage at the global scale, as well as microbial functionality, is noticeably absent from our empirical understanding of SOM fraction formation and persistence. More advanced knowledge of these controls would enable more robust identification of where SOM is most vulnerable to loss, as well as more informed implementation of 'multi-pool' management practices aimed at enhancing C storage in both POM and MAOM. In this vein, this dissertation explores global controls on and microbial mediation of SOM dynamics at multiple scales through a combination of synthesis, modeling, and experimental (i.e., ModEx) approaches. Specifically, I first synthesized climate, soil property, and fraction C data to understand global controls on C storage in POM and MAOM. I then applied a previously developed individual-based model (Kaiser et al., 2015) to determine how emergent microbial community properties resulting from microbial social dynamics (i.e.,

interactions among microbes that produce enzymes at different rates) impact POM retention under varying degrees of MAOM saturation. Lastly, I investigated the relevance of hypothesized microbial copiotrophic and oligotrophic life history strategies to changes in POM and MAOM storage. Results from these projects indicate that global POM and MAOM storage is controlled by disparate suites of environmental variables, with POM being primarily controlled by variables that modulate microbial activity, and MAOM being controlled by a combination of C inputs and soil properties related to the potential to stabilize new MAOM. Additionally, flexible enzyme production in response to the availability of easily-assimilable, soluble substrates may contribute to POM retention under varying degrees of MAOM saturation and POM carbon:nitrogen ratio (C:N). However, variation in microbial function does not always result in changes in POM and MAOM storage – differences in growth rate, our proxy for copio- and oligotrophy, was unrelated to changes in POM and MAOM. Despite this, this dissertation indicates that microbial functions and environmental properties controlling microbial activity rates (i.e., controls on C outputs from the soil) mediate POM storage, but that MAOM is more reflective of C inputs to the soil. This indicates that microbial interventions to support soil C storage may want to focus on ecosystem-specific microbial manipulations that support community efficiency and modulate exo-enzyme production. In combination with other management strategies that increase soil C, these types of microbial interventions may help ensure that new soil C is retained in the soil for longer periods of time. Additionally, given that microbial activity is generally expected to increase with climate warming, these results indicate a premium need to preserve existing POM stocks.

ACKNOWLEDGEMENTS

There are so many individuals and organizations without whose support I would not have been able to finish this dissertation. First and foremost, I am very grateful for my doctoral mentor, Dr. Francesca Cotrufo, who has not only been critical to my success as a grad student and young scientist, but through her example, has helped me grow more confident both in my science and who I am outside of my research. I am thrilled to have the opportunity to continue working with you, both during my upcoming postdoc and into the future. Thanks so much to my committee members, Drs. Meagan Schipanski, Matt Wallenstein, and Pankaj Trivedi, whose scientific and professional advice have also helped shape me into the scientist I am today.

Thanks so much to Dr. Jocelyn Lavallee, whose advice on how to best manage and analyze the synthesized dataset used in my structural equation modeling work was critical to its success. Thanks also to Dr. Anne Hess, who shared valuable tips and resources on how to best interpret structural equation model results. Thanks to the National Ecological Observatory Network (NEON) for giving us access to archived megapit soil samples, and even more thanks to Rebecca Even for fractionating them all.

There is absolutely no way that I could have finished my incubation chapter by myself. I am especially grateful for Michelle Haddix and Rebecca Even, who assisted with my lab work in multiple ways and trained me in virtually every lab analysis I know. I got sick with COVID on the first day of my planned incubation harvest, and I have so much gratitude to Michelle, who led a huge squad of undergrads, including Louise Halaburt, Beaman Martin, Jake Brisnehan, and EARTH University intern Anthony Mbunju, in continuing the harvest for the couple days I was recovering at home. I also very much appreciate all of Rebecca's help in fractionating my harvested soils (once again) – you are truly my fraction queen! Thanks to my undergraduate research assistants Jacob Stier and Louise Halaburt, who assisted in fractionation and preparation of my soil samples for %C and ^{13}C analysis, as well as preparation of thousands of gas sampling vials for use in ^{13}C-CO_2 analysis. Thanks so much to my Research Experience for Undergraduates (REU) student Laura Moore, who helped collect, fractionate,

and recombine all the soil needed for this experiment, and who also assisted in many aspects of data collection during my trial incubation. Many thanks to Drs. Alberto Canarini and Andreas Richter at the University of Vienna, who trained me in high-throughput phospholipid fatty acid (PLFA) extraction, as well as quantification of isotopes using gas chromatography-isotope mass ratio spectroscopy (GC-IRMS). These lab analyses were crucial to my second chapter, and I am very thankful for the opportunity to learn these how to apply these techniques in my experiment (and to be able to spend a couple weeks in Vienna during Christmastime!). I am also grateful to Dan Ruess and Guy Beresford for access to the instruments in the Natural Resources Ecology Lab (NREL) EcoCore, and for training me on operation of the instruments needed for the analyses I performed for my incubation experiment. Thank you to the United States Department of Agriculture (USDA) and NEON for access to the Central Plains Experimental Range (CPER), where soils used in this experiment were collected.

Many thanks to Drs. Ksenia Guseva and Christina Kaiser at the University of Vienna, who provided access to their individual-based model for use in my modeling work, modified it model to match the needs of my project, and were a huge help in interpreting my results. Thanks also to Dr. Yao Zhang, who was a huge help in getting me started on modeling as well as interpretation of the results from this project and continues to be a huge resource to me for all things modeling.

More broadly, thank you to all the past and present members of the Cotrufo Soil Innovation Lab and MEMS modeling team. I've received so much support from you, in both small and big ways. Thanks for all the suggestions on how to improve talks, writing, statistical analyses, helping me navigate many aspects of grad school, and being all-around wonderful coworkers. I am so fortunate to be able to work with you all, and call many of you my friends.

My dissertation was financially and logistically supported through a National Science Foundation (NSF) DEB grant (#2016003) and a European Research Council (ERC)-NSF supplement. I was personally supported through a CSU Graduate Degree Program in Ecology recruitment award, as well as the Philanthropic Educational Organization (PEO) Scholar Award. It has been an absolute pleasure to receive not only this Scholar Award, but also care and support from all the amazing women in the Estes

Park PEO chapter. You are all such loving and inspiring women – I aspire to hold myself with equivalent grace one day.

Outside of research, I am incredibly grateful for the support of my friends and family. I am fortunate to have made many close friends during my time in Fort Collins – naming every single person who has positively impacted my time here would take up paragraphs of this dissertation. To all of you, including Sam, Erica, Leif, Erin, Aaron, Carli, Rafael, and especially Kristen and Jess, thanks so much for your friendship and for making my grad school experience so much more enjoyable. The same goes to my family and all my close friends from Kansas and South Dakota – to my parents, grandparents, Jack, Grace, Antoine, Theo, and Lígia, thanks for all of your continued love and friendship. And to my fiancé Ali, who is both family and my best friend, so many thanks for all you have done to support and encourage me over the past three years and beyond. You are the one person I truly could not have finished my dissertation without.

Forever and for always grateful for all of you.

DEDICATION

In honor of my dad, who taught me that being an artsy-fartsy girly-girl and a nerdy scientist are not mutually exclusive identities, and without whom I don't believe I would ever have considered a career in science.

TABLE OF CONTENTS

CHAPTER 1: Introduction

Given that soils represent the largest terrestrial carbon (C) store, enhancing and preserving soil C storage is vital to carbon dioxide (CO_2) drawdown and climate change mitigation efforts (Smith, 2016). When coupled with the need to sustain plant productivity to feed growing global populations, an intimate understanding of soil organic matter (SOM) dynamics is required to ensure our planet has a sustainable future (Smith et al., 2015). The urgent need enhance soil C storage has led to multiple breakthroughs in our understanding of SOM dynamics, especially with respect to the mechanisms controlling SOM formation and persistence (e.g., Cotrufo et al., 2013, 2015; Lehmann et al., 2020; Lehmann & Kleber, 2015; Liang et al., 2017; Schmidt et al., 2011; Sokol et al., 2019). While SOM is highly complex (Lehmann et al., 2020), current research typically conceptualizes SOM into two physically and functionally distinct fractions, particulate (POM) and mineral-associated organic matter (MAOM). POM is formed primarily from fragmentation of structural compounds in the soil, whereas MAOM is formed via sorption of low molecular weight soluble compounds to soil mineral surfaces. For both POM and MAOM, these structural and low molecular weight compounds can be of either plant or microbial origin. While the structural compounds contributing to POM formation require enzymatic depolymerization before they can be taken up by microbes, the low molecular weight, easily assimilable compounds that serve as precursors to MAOM can be readily metabolized by microbes if found in solution. However, when bound to soil minerals, these low molecular weight compounds are strongly protected from microbial degradation, giving MAOM a longer average residence time than POM (Heckman et al., 2022; Lavallee et al., 2020). Although SOM can be further subdivided into many additional constituents based on their chemical signatures, conceptualizing SOM into these two fractions is especially useful because they can be easily separated through physical fractionation in the lab, and because their disparate mechanisms of formation and persistence can aid in identification of specific processes contributing to changes in C storage. This makes POM and MAOM especially helpful in understanding how soils might

respond to climate change, as well as in identifying management practices that can be leveraged to enhance the capacity of the soil to store C (Cotrufo & Lavallee, 2022).

Soil microbes play a key role in mediating the formation and persistence of both these fractions. Structural components of microbial necromass such as cell walls can serve as precursors to POM (Cotrufo et al., 2022), while the soluble components of cells and compounds derived from POM depolymerization are capable of sorbing to mineral surfaces to form MAOM (Kallenbach et al., 2016; Liang et al., 2019). In fact, microbial necromass can account for as much as half of the total MAOM pool in some ecosystems (Angst et al., 2021; Whalen et al., 2022). As it is not protected by bonds with minerals, POM is especially susceptible to decomposition via enzyme activity, with changes in POM storage being more vulnerable to environmental changes associated with climate change than MAOM (Lugato et al., 2021; Rocci et al., 2021). As such, through their behaviors, responses to environmental conditions, and chemical composition, the structural and functional characteristics of microbes mediate C accumulation and loss in POM and MAOM.

Wide recognition that microbes play a key role in mediating SOM formation and persistence has led to the development of multiple frameworks predicting microbial structural and functional traits relevant to POM and MAOM storage. For instance, given that microbial compounds can make up nearly 50% of total MAOM C (Angst et al., 2021; Liang et al., 2019; Whalen et al., 2022), more efficient microbial processing of C substrates can lead to greater biomass production (i.e., greater carbon use efficiency; CUE), especially when litter quality is high, leading to greater MAOM storage (Cotrufo et al., 2013). Synergies among microbial trait tradeoffs may also mediate POM and MAOM formation (Malik et al., 2020; Whalen et al., 2024). For instance, high availability of soluble, easily assimilable resources may select for copiotrophic microbial communities specialized for rapid growth and biomass production (Fierer et al., 2007; Meyer, 1994), generating more necromass than can contribute to MAOM formation. Oppositely, oligotrophic microbes with low growth rates may dominate in soils with low resource availability (Fierer et al., 2007; Meyer, 1994), with their potentially more structural chemical composition and preference for structural substrates having greater impacts on POM storage. Additionally, the relative

control of soil microbes on POM and MAOM formation may depend on climate and soil properties, whereby microbial traits may more strongly mediate C cycling in mesic than in extreme environments, where POM and MAOM may be primarily controlled by climate and soil properties that place strong selection pressures on microbes (Cotrufo et al., 2021; Cotrufo & Lavallee, 2022). Given all the above, climate, soil, plant, and microbial properties likely interact with each other to determine POM and MAOM storage in different ways depending on scale, underscoring the complexity of SOM formation and the multifaceted roles playa in driving soil C storage.

Despite these recent advances in our conceptualization of the mechanisms underpinning soil C storage, we are still unable to articulate how a combination of climate, plant, and soil properties control POM and MAOM storage at the global scale. Such knowledge is critical to understanding how different forms of soil C can be gained or lost across ecosystem types, as well as identification of where soil C is most vulnerable to climate change. Also absent from our empirical understanding of controls on POM and MAOM storage are microbial functional traits (Buchkowski et al., 2017). With the exception of perhaps only CUE (e.g., Kallenbach et al., 2015, 2016; Luo et al., 2020; Wang et al., 2021), relatively few experimental and field studies have quantitatively assessed the extent to which microbial functionality mediates C gains and losses in POM and MAOM (e.g., Cotrufo et al., 2022; Craig et al., 2022; Horsch et al., 2023). Additionally, limited data on microbial functions, especially in conjunction with C fraction, data prohibits their inclusion in broader syntheses on C storage controls. It also limits robust representation of microbial communities in ecosystem models of C and nitrogen (N) cycling, with relatively few process-based models representing microbial ecology outside of a single microbial biomass pool (e.g., Georgiou et al., 2017; Sistla et al., 2014; Wang et al., 2015; Wieder et al., 2014). Given the many ways in which microbes may impact patterns of POM and MAOM storage and the many different scales at which those impacts may be most relevant, especially in conjunction with climate and soil properties known to influence C storage at the global scale, a combined modeling-experimental (ModEx) approach may be especially useful in identifying controls on SOM fraction storage relevant at a variety of spatial scales. This kind of approach could lead to a more comprehensive understanding of how a

combination of climate, soil, plant, and microbial properties control or mediate POM and MAOM formation and persistence at a variety of scales, thus greatly advance our understanding of SOM dynamics.

Given the roles that climate, plant, soil, and microbial traits play in C cycling and the importance of reducing atmospheric CO_2, a robust understanding of their contributions to SOM fraction storage is crucial. This knowledge could significantly impact both fundamental research and the development of advanced technologies for CO_2 drawdown. Incorporating controls on microbial activity and their effects on SOM fractions into process-based models would enhance the accuracy and applicability of these models across a broader range of ecosystems. Furthermore, it would enable the development of ecosystem-specific management techniques that leverage microbial activity to draw down atmospheric CO_2 or prevent further soil carbon loss. Identifying specific traits or genes to target in the development of microbial inoculants, as well as understanding how the climate, plant, and soil properties influence and interact with microbial controls on SOM storage, are essential for this approach. Additionally, management practices and inputs can be optimized to influence the ecology of particular microbial organisms beneficial for C storage. Ultimately, a thorough understanding of how microbial communities and their functions impact SOM storage in different fractions is necessary. This understanding will allow us to fully utilize decades of biogeochemical and microbial ecological research to mitigate the adverse effects of climate change effectively.

This dissertation aims to advance our understanding of global controls on POM and MAOM storage, and the contributions of microbial functionality to gains and losses in POM and MAOM through a modeling-experimental (ModEx) approach. Specifically, I use a synthesized dataset to identify controls on POM and MAOM that act at the global scale, as well as describe how these controls may interact with one another (Hansen et al., 2024). After identifying global controls on POM and MAOM storage, I then apply a previously developed individual-based model that simulates decomposition of structural SOM forms as a result of microbial social dynamics (Kaiser et al., 2015) to better understand how interactions between microbes that produce enzymes at different rates (i.e., microbial social dynamics) impacts POM

retention at varying degrees of MAOM saturation (Cotrufo, 2019; Georgiou et al., 2022; Hassink, 1997; Six et al., 2002, 2024; Stewart et al., 2007, 2008). I also speculate on the ways in which the emergent microbial properties identified through the model can be used to further development of ecosystem-level, process-based models. Lastly, I use a highly controlled incubation experiment to test the extent to which copiotrophic and oligotrophic traits are present within microbial communities, along with whether differences in the expression of those traits have impacts on changes in POM and MAOM storage. By integrating results from these synthesis, modeling, and experimental projects, I provide a comprehensive assessment of the global controls and microbial functions contributing to SOM dynamics. In addition to enhancing basic knowledge of SOM dynamics, this dissertation provides important insights on how microbial interventions can be effectively leveraged to rebuild and prevent the loss of existing C stores, thus helping mitigate the negative effects of climate change.

CHAPTER 2: Distinct, direct and climate-mediated environmental controls on global particulate and mineral-associated organic carbon storage[1]

Introduction

Maintaining and increasing soil organic carbon (SOC) stores is crucial to mitigating climate change and to enhancing the soil's capacity to provide essential ecosystem services, including nutrient recycling and maintenance of plant productivity. As such, it is imperative that we develop an advanced understanding of the environmental conditions under which SOC is most vulnerable to loss, as well as its responses to deliberate management practices aimed at increasing SOC storage. Although we can now identify how drivers of SOC storage, including climate (Jobbágy & Jackson, 2000), carbon (C) inputs, and soil properties (Hassink, 1997; Six et al., 2002) operate on a variety of spatial scales (Wiesmeier et al., 2019), we lack a quantitative framework of hierarchical controls on SOC storage that incorporates its conceptualization into separate fractions. Such knowledge could give us a more specific understanding of how different forms of SOC can be gained or can be lost across multiple ecosystem types, allowing us to better target "multi-pool management" practices (Angst et al., 2023) towards increasing or maintaining SOC storage in different fractions.

Conceptualizing SOC into particulate (POC) and mineral-associated organic carbon (MAOC) fractions can be particularly useful as a first step in building a more comprehensive understanding of global controls on SOC formation and persistence (Cotrufo & Lavallee, 2022; Lavallee et al., 2020). Particulate organic C is formed via fragmentation of structural plant inputs and is primarily protected by physical occlusion in aggregates (or in the case of pyrogenic C, through chemical recalcitrance). Limited protection from decomposition results in POC having relatively short mean residence times (von Lützow et al., 2007), except in locations where decomposition is limited by physical or physiological constraints

[1] Hansen, P. M., Even, R., King, A. E., Lavallee, J., Schipanski, M., & Cotrufo, M. F. (2023). Distinct, direct and climate-mediated environmental controls on global particulate and mineral-associated organic carbon storage. Global Change Biology, 30, e17080. https://doi.org/10.1111/gcb.17080.

on microbial activity (Cotrufo & Lavallee, 2022) where POC is found to accumulate (Herndon et al., 2017). In contrast, MAOC is formed via sorption of microbial necromass and decomposition products, as well as soluble plant inputs, to soil mineral surfaces (Haddix et al., 2016; Kallenbach et al., 2016; Liang et al., 2019). These mineral bonds make MAOC relatively inaccessible to microbial decomposition, leading to, on average, longer mean residence times than POC (von Lützow et al., 2007). Given their distinct mechanisms of formation and persistence, it is likely that global POC and MAOC storage are controlled by contrasting environmental variables.

Climate may be the primary driver of both POC and MAOC storage because of its effects on factors that influence the amount of C that enters (i.e., C inputs) and leaves the soil (i.e., C outputs; Cotrufo et al., 2021). For instance, both temperature and moisture are important controls on annual C inputs to soil (i.e., net primary production (NPP); Churkina & Running, 1998), with increased C inputs often leading to greater SOC storage (Lajtha et al., 2014; Z. Luo et al., 2017). While we lack an understanding of how C inputs separately affect POC and MAOC storage, MAOC can be expected to be more reflective of C inputs than POC, due to POC's lack of soil matrix protection from decomposition. Independent of inputs, climate may act as an additional control on SOC storage through its effects on microbial activity constraints (Cotrufo & Lavallee, 2022). For instance, POC may be particularly sensitive to climate-driven variations in decomposition (Conant et al., 2011). Temperature and moisture are key controls on microbial activity, with higher temperatures leading to accelerated decomposition (Schimel, 2018), especially for complex structural compounds that require higher activation energy to decompose (Davidson & Janssens, 2006) and when optimum soil moisture levels increase microbial access to substrates through increased diffusion (Schimel, 2018). As such, we may expect lower POC storage in warm compared to cold ecosystems, especially when microbial access to substrates is limited by low diffusion under dry conditions. Additionally, moisture may serve as a direct control on MAOC storage through its effects on dissolved organic carbon (DOC) leaching. As plant-derived DOC can make up nearly half of MAOC storage (Angst et al., 2021), leaching of DOC due to high moisture may contribute to greater MAOC stores (Haddix et al., 2020), especially in ecosystems where the majority of MAOC is

plant-derived. However, little work has focused on how temperature, moisture, and C inputs interact with one another to control POC and MAOC storage, especially at large spatial scales.

In addition to climate, soil physicochemical properties may act as a further control on POC and MAOC storage. For instance, strong associations with soil mineral surfaces may mean that the capacity of the soil to form mineral bonds with organic C molecules is an additional control on MAOC storage, with higher silt and clay contents leading to greater storage of MAOC (Hassink, 1997; Six et al., 2002). Other physicochemical properties, including exchangeable calcium (Ca) and iron (Fe) and aluminum (Al) hydroxides, may operate as additional controls on MAOC storage (King et al., 2023; Kirsten et al., 2021; Rowley et al., 2021), whose importance to C storage may be mediated by soil moisture and pH (Rasmussen et al., 2018). pH may also control POC storage through its inhibitory effects on microbial activity. Like cold temperatures, low pH can slow microbial decomposition (Rousk et al., 2009) and may contribute to greater POC storage in acidic soils. However, little work has investigated the extent to which these soil properties interact with our hypothesized overarching climatic controls in determining global patterns of POC and MAOC storage.

To identify hierarchical controls on global C storage, we synthesized POC and MAOC fraction data from 72 existing studies and databases, along with SOC fraction data we generated from the National Ecological Observatory Network (NEON) "megapit" soils (Hinckley et al., 2016). We included studies conducted in a diversity of climate and land cover types, with the goal of identifying controls on POC and MAOC that are generalizable across a variety of ecosystems. We aimed to assess the extent to which climate, NPP, and soil properties directly *versus* indirectly control C storage in POC, MAOC, and bulk SOC. Based on the observations described above, we broadly hypothesized that POC and MAOC storage would be governed by distinct, climate-mediated environmental controls (Cotrufo et al., 2021), with POC being primarily controlled by C loss processes related to microbial activity constraints, and MAOC being primarily controlled by a combination of C input limitations and soil properties related to C stabilization. Additionally, we hypothesized that linking environmental variables to POC and MAOC would exhibit

greater utility in understanding global patterns of C storage than linking the same variables to bulk SOC alone.

Materials and Methods

Global synthesis of particulate and mineral-associated organic carbon data

We constructed an observational dataset of POC and MAOC by conducting a comprehensive search on Google Scholar using various combinations of keywords including "soil carbon," "soil organic matter," "particulate and mineral-associated," "light and heavy fractions," "density fractionation," and "size fractionation," then collating all relevant data from published studies and existing databases (Figure 2.1). We chose to use Google Scholar as it may have greater geographic representation than other search engines (Harzing & Alakangas, 2016; Martín-Martín et al., 2018). For studies that fractionated soil by size or density only, we defined POC as >53-63 μm in size or <1.65-1.85 g cm^{-3} in density, and MAOC as <53-63 μm or >1.65-1.85 g cm^{-3}. For studies that fractionated soil by both size and density, we considered POC to be <1.65-1.85 g cm^{-3}, and MAOC to be >1.65-1.85 g cm^{-3} and <53-63μm. Heavy coarse fraction (>1.65-1.85 g cm^{-3} and >53-63 μm; *sensu* Leuthold et al., 2022) C and occluded SOC fraction (in the cases in which POC was separated by density before dispersion) data were retained for calculations of total SOC (see *Data processing*, below), but excluded from analyses performed on fraction data only. This was done to maintain as much consistency in SOC fraction definitions as possible, as the fractionation schemes of the studies included in our synthesis varied with both study and ecosystem type. While we focused our synthesis primarily on observational studies, we also included data from control plots (i.e., not receiving experimental treatments) of relevant field studies involving experimental N deposition, CO_2 enrichment, climate manipulations, etc. However, for experimental studies in agricultural systems where treatment represented a modified management practice, we included all reported data to account for the fact that management practices vary across the landscape, and may generate different environmental controls (e.g., NPP, pH, etc.) on POC and MAOC storage.

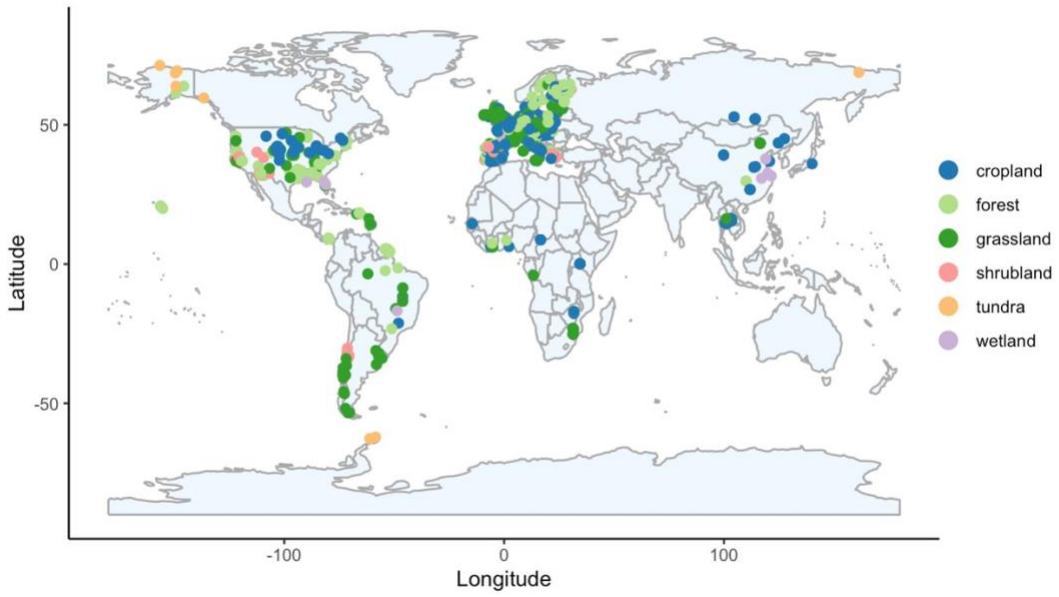

Figure 2.1. Geographic location of all data points included in our synthesis (n=901). Different colors represent the land cover type assigned to each point based on author-reported plant community composition and management information. For croplands, n=312; for forests, n=233; for grasslands, n=301; for shrublands, n=35; for tundra, n=7; and for wetlands, n=10. The distribution of our included data across Köppen-Geiger Climate Classification Zones (Beck et al., 2018) can be found in Figure A2.1. Map lines delineate study areas and do not necessarily depict accepted national boundaries.

National Ecological Observatory Network (NEON) data generation

We supplemented our synthesis with additional SOC fraction data we generated by fractionating "megapit" mineral soil samples from the National Ecological Observatory Network (NEON; Hinckley et al., 2016). Soil samples were taken from megapits, or large, temporary soil pits dug to either 2 m depth or bedrock at each of NEON's 47 terrestrial research sites, divided by horizon, then homogenized and characterized according to standard NEON protocols. A subsample of each of the 2-mm sieved, air-dried megapit soil samples was shipped to Colorado State University, where they were de-quarantined for 16 hours at 116°C according to APHIS regulation. After de-quarantining, we fractionated all soil samples by both density (1.85 g cm^{-3}) and size (53 µm) after mechanical dispersion as described in Zhang et al., 2021. Briefly, 5.5-6.0 g subsamples were first shaken in deionized (DI) water for 15 min, then centrifuged at 3400 rpm. Dissolved organic matter was decanted over a 20 µm nylon filter and stored at -20°C. Any

particulate material on the filter was set aside as part of the light particulate organic matter fraction (<1.85 g cm^{-3}). Twelve glass beads and 1.85 g cm^{-3} sodium polytungstate (SPT) were added to the soil residue and shaken for 18 h to disperse aggregates. Soils were then centrifuged for 30 min at 3400 rpm, and the remaining light particulate organic matter was aspirated onto a 20 μm nylon filter. The pellet (> 1.85 g cm^{-3}) was rinsed multiple times to remove any remaining SPT before wet-sieving to separate it into heavy coarse organic matter (>53μm), and mineral-associated organic matter (<53μm). All solid fractions were oven-dried at 60°C, then finely ground to ensure homogenization before being analyzed for %C on an elemental analyzer (Costech ECS 4010; Valencia, CA, USA). Samples that contained carbonates according to the NEON database were acid-fumigated to remove carbonates (Harris et al., 2001), then re-analyzed to obtain organic C values. For this study, we used the light POC and MAOC values from topsoil samples only (see *Data processing*, below), for a total of 47 observations for each of the fractions, as well as bulk SOC.

Auxiliary data incorporation

In addition to SOC fraction data, we incorporated auxiliary data including mean annual temperature (MAT; °C), mean annual precipitation (MAP; mm), potential evapotranspiration (PET; mm), aboveground net primary production (NPP; Mg C ha^{-1} yr^{-1}) as a proxy for annual soil C inputs, soil texture and pH, bulk density, sampling depth, plant community composition, and any applicable management practices into our synthesized dataset. In all cases, we used the site data as reported in publications or contained within the NEON database. However, if specific site data types such as MAT, MAP, PET, and NPP were not available, we used reported geographic coordinates to extract equivalent 20-year average MAT and MAP values from WorldClim 2.0 (Fick & Hijmans, 2017), and 20-year average PET and NPP values from MODIS (data products MOD16A3GF.061 and MOD17A3HGF.006, respectively; Running et al., 2021; Running & Zhao, 2019). We subtracted PET from MAP to create a metric of effective moisture (MAP-PET; mm; *sensu* Kramer & Chadwick, 2018). Additionally, we

assigned one of six broad land cover types to each soil profile (i.e., cropland, forest, grassland, shrubland, tundra, wetland; Figure 2.1) based on reported plant community composition and management information.

Data processing

After compiling both synthesis and NEON megapit data, we used reported SOC stocks, soil depth, and bulk density values to convert all SOC fraction stocks to SOC fraction concentrations (g fraction-C kg $soil^{-1}$). As mentioned above, we did not include organic C in heavy coarse organic matter or in occluded SOC fractions in our downstream analyses of fraction data. However, we retained and used any heavy coarse organic matter or occluded SOC fraction data in calculations of g SOC kg $soil^{-1}$ (i.e., sum of all fraction C values), as well as calculations of MAOC relative to bulk SOC storage (i.e., f_{MAOC}; g MAOC kg $soil^{-1}$/g SOC kg $soil^{-1}$). While our original intent was to test for variations in SOC storage drivers throughout the soil profile, there was not enough subsoil data available at the global scale to include subsoils in our downstream statistical analyses. As such, we chose to focus our analysis specifically on topsoil. We considered the first sampled depth increment or horizon reported in each study to be representative of topsoil, and applied data from that layer only in downstream analyses. Depending on study site and sampling design, topsoils included both O and A horizons, and spanned different soil depths (Figure A2.2). This was done to minimize biases associated with variation in maximum topsoil sample depth across our synthesized dataset, as methods of normalizing data to a standardized depth (e.g., Abdalla et al., 2018; Hou et al., 2020; Ogle et al., 2005) across all our data points diluted the effects of driving variables known to change along the soil profile less than, or differently from, SOC (data not shown). After filtering our data so that it contained only topsoil, we averaged all data collected at the plot level such that we had one data point per site. At the end of all data processing, our final dataset included 901 total data points (i.e., n=901 for each SOC fraction as well as bulk SOC) from 72 studies (Figures 2.1, A2.1; Table A2.1).

Statistical analyses

We first assessed broad relationships and patterns among our data using simple linear regressions. Specifically, we used linear regressions to test for relationships of MAT and MAP-PET with NPP, as well as relationships of MAT, MAP-PET, NPP, soil pH, and % sand with POC, MAOC, bulk SOC, and f_{MAOC}. We did not include multiple factors or any interactive effects in these simple regressions, such that we tested for the effects of only one explanatory variable per regression. We then used results from these analyses and literature-supported hypotheses to conduct path analyses investigating direct and indirect controls on C storage in POC, MAOC, and SOC using the R package '*lavaan*' (Rosseel, 2012). Given that many known drivers of soil C storage interact with one another, we chose to use path analyses because of their ability to test for mediation, as well as direct and indirect effects of variables on outcomes of interest (Shipley, 2016). We created two separate path analyses, one which predicted POC and MAOC storage and one which predicted storage in bulk SOC. The fit of different iterations of these path analyses was assessed using Chi square, the comparative fit index (CFI > 0.9), the root mean square error of approximation (RMSEA < 0.08), and the standardized root mean square residual (SRMR < 0.08; Hooper et al., 2008). Our final path analysis structures that exhibited the best fits allowed for direct effects of MAT, MAP-PET, NPP, pH, and % sand, as well as indirect effects of MAT and MAP-PET via NPP, on POC and MAOC storage, or bulk SOC storage. We originally included topsoil sampling depth as a covariate in our analyses to account for differences in it within and across studies but removed it due to poor fit. We assessed effects of our environmental variables (i.e., MAT, MAP-PET, NPP, pH, and % sand) by assigning coefficients to individual pathways, then multiplying coefficients to calculate indirect effects (e.g., for indirect effects of MAP-PET, we multiplied the effect of MAP-PET on NPP by the effect of NPP on MAOC). We summed direct and indirect path coefficients to estimate total effects of each variable on POC, MAOC and bulk SOC storage. In addition to determining controls on SOC storage, we compared our POC and MAOC fraction path analysis with our bulk SOC analysis to assess the utility of separating SOC into POC and MAOC in understanding global patterns of SOC formation and persistence. We also assessed differences in f_{MAOC} among land cover types using Welch's one-way Analysis of Variance

(ANOVA) to account for uneven sample size among land cover types, and further investigated our significant test result using Games-Howell *post-hoc* pairwise comparisons using the R package '*rstatix'* (Kassambara, 2023). All analyses were carried out in R version 4.1.1 (R Core Team, 2021).

Results

Broad relationships between climate, NPP, soil properties, and POC, MAOC, and bulk SOC storage

We first explored global patterns of SOC formation and persistence by conducting linear regressions between environmental variables and POC, MAOC, and SOC storage, as well as relationships between climate and NPP. We found significant, positive relationships between NPP and both MAT and MAP-PET (Figure 2.3a, b; Table A2.2), reflecting expected associations between climate and NPP. We also found significant relationships between POC and MAT, MAP-PET, NPP, and pH. MAP-PET and NPP were positively associated with POC, while MAT and pH were negatively associated with POC storage (Figure 2.3c-g; Table A2.2). Environmental controls on MAOC included MAP-PET, NPP, and % sand, with MAP-PET and NPP being positively related, and % sand being negatively related to global MAOC storage (Figure 2.3h-l; Table A2.2). All studied environmental variables were associated with bulk SOC. Specifically, MAP-PET and NPP were positively associated with SOC, while MAT, pH and % sand were negatively associated with bulk SOC storage (Figure 2.3m-q; Table A2.2). We note that the significance of the above relationships may be driven in part by high sample size, as many relationships had relatively small r^2 values (i.e., 0.0111 – 0.221).

Direct and indirect controls on global POC, MAOC, and bulk SOC storage

To assess direct and indirect effects of the above environmental variables on soil C, we constructed separate path analyses to predict C storage in POC and MAOC and bulk SOC (Figures 2.2, 2.3). Our fraction path analysis fit the data well ($X^2_{2, n=649)} = 1.239$, $p = 0.538$; CFI = 1.0; RMSEA = 0.068; SRMR = 0.007; Hooper et al., 2008), and explained 35.8% of the variation in NPP, 12.3% of the variation

in POC, and 20.5% of the variation in MAOC (Figure 2.2, Table A2.3). Consistent with our linear regression analyses, NPP was positively predicted by both MAT and MAP-PET. Global POC storage was directly predicted by MAT and pH, both of which had a negative effect on POC. Contrary to our linear regressions, however, neither MAP-PET nor NPP emerged as a significant predictor of POC, potentially because path analysis calculates partial regression coefficients that account for correlations and covariance between multiple factors, which likely reduced the already weak relevance (i.e., low r^2) of our linear regression coefficients. Global MAOC storage had direct, positive relationships with MAP-PET and NPP (and as such, indirect relationships with MAT and MAP-PET), as well as a direct, negative relationship with % sand (Figure 2.2, Table A2.3).

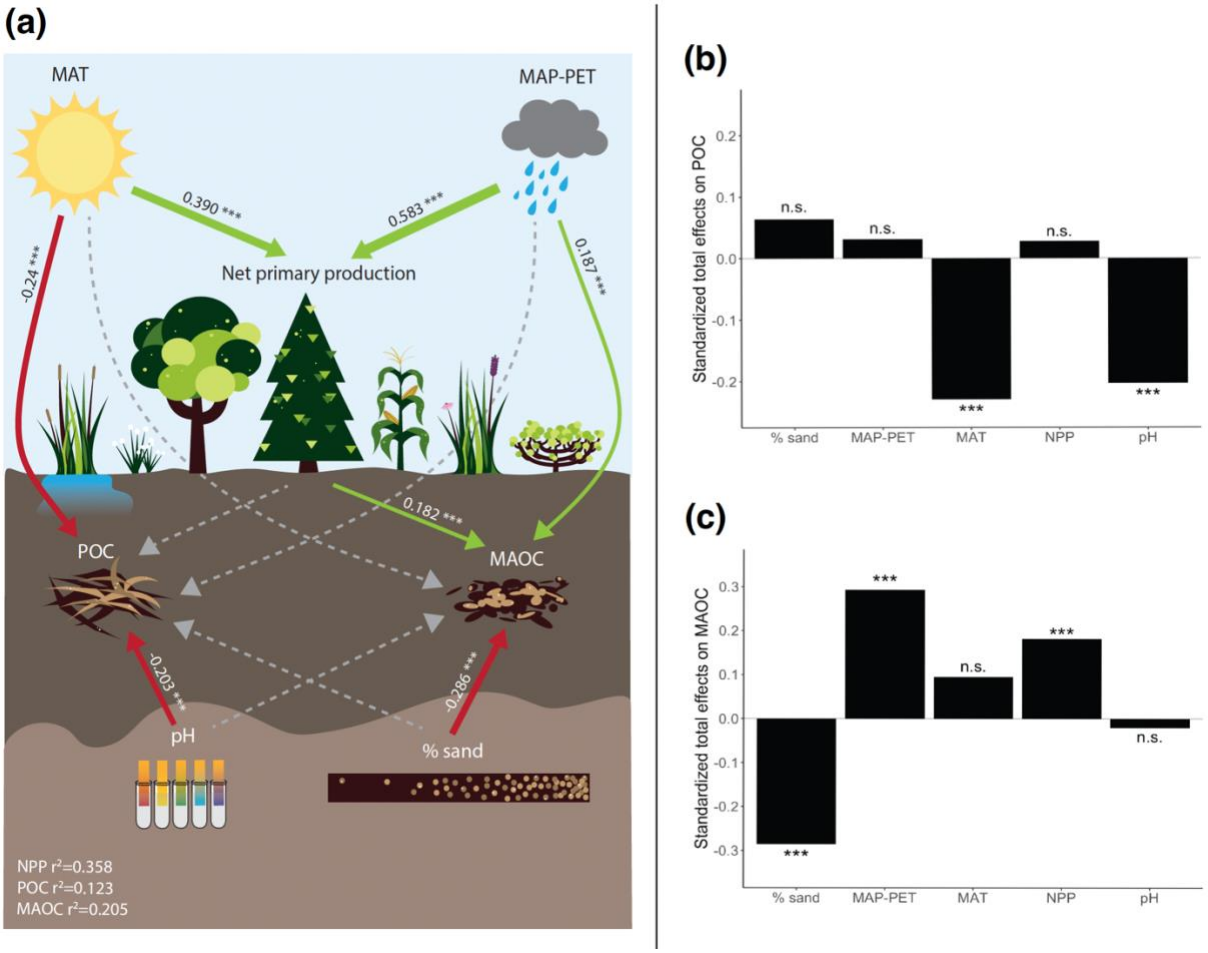

Figure 2.2. Results from path analysis showing direct and indirect effects of mean annual temperature (MAT; °C), mean annual precipitation minus potential evapotranspiration (MAP-PET; mm), net primary production (NPP; Mg C ha^{-1} yr^{-1}), soil pH, and % sand on global particulate (POC; g C kg $soil^{-1}$) and mineral-associated organic carbon (MAOC; g C kg $soil^{-1}$) storage (panel (**a**)). Green and red arrows indicate significant positive and negative effects, respectively, of the variables described above on POC and MAOC storage. Grey, dashed arrows indicate non-significant paths. The widths of the arrows correspond to standardized path coefficients, shown in numbers above each arrow. Standardized total (i.e., direct plus indirect) effects of the variables described above on POC and MAOC storage are shown in panels (**b**) and (**c**). In all cases, n.s. non-significant, * $p < 0.05$, ** $p < 0.01$, and *** $p < 0.001$. Full results and output are provided in Table A2.3.

Our SOC path analysis revealed similar trends in global C storage. Like our fraction analysis, our SOC path analysis fit our data well ($X^2_{2, n=649)} = 1.239$, $p = 0.538$; CFI = 1.0; RMSEA = 0.0; SRMR = 0.007; Hooper et al., 2008) and explained 35.8% of the variation in NPP, with both MAT and MAP-PET once again having direct, positive effects on NPP (Figure 2.3; Table A2.4). However, this path analysis explained only 12.3% of the variation in global SOC storage, which was predicted by all included

exogenous variables. MAT, pH, and % sand had direct, negative effects on SOC storage, while MAP-PET and NPP had direct, positive effects on SOC. In addition, MAT and MAP-PET had positive, indirect effects on SOC via NPP (Figure 2.3; Table A2.4).

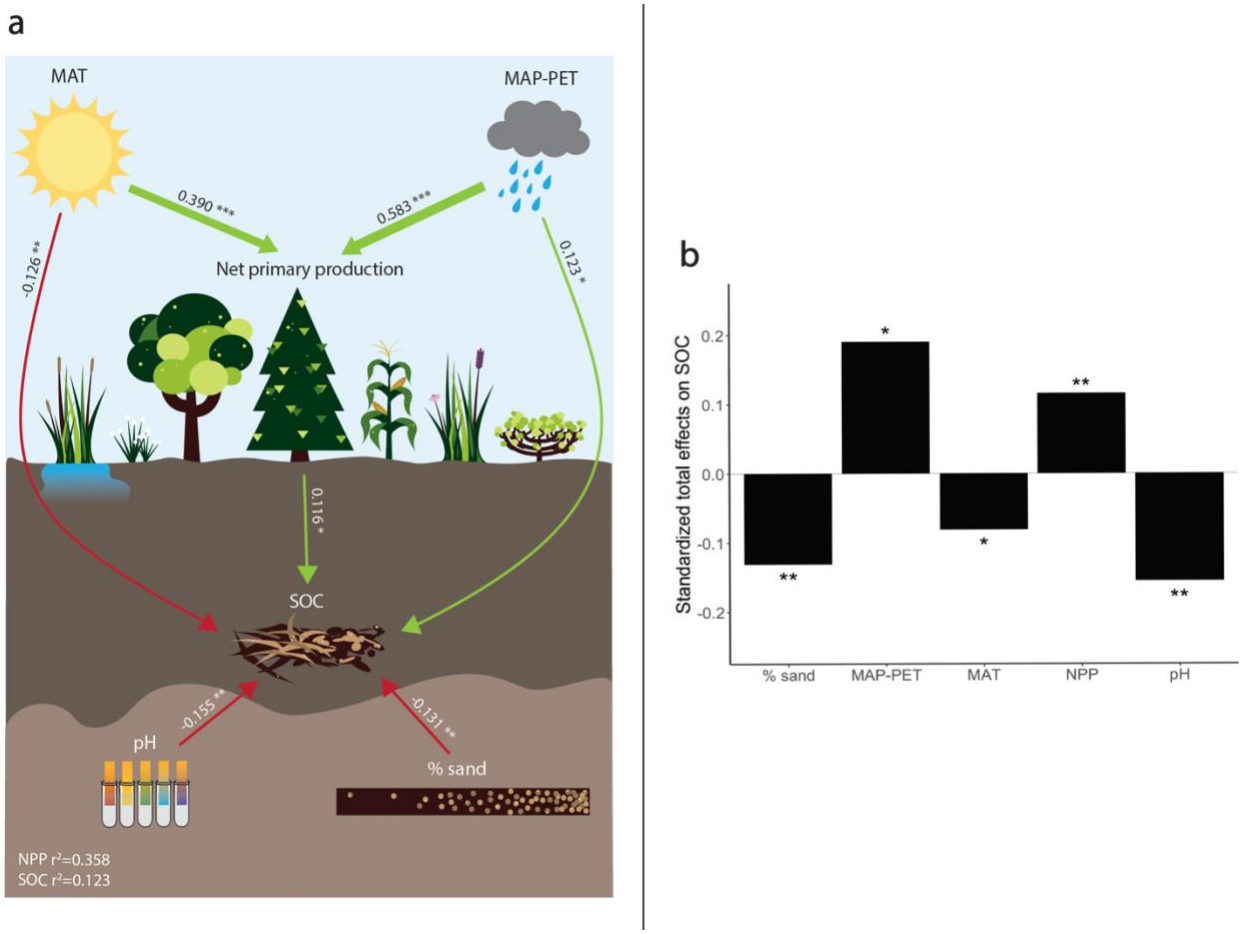

Figure 2.3. Results from our path analysis showing direct and indirect effects of mean annual temperature (MAT; °C), mean annual precipitation minus potential evapotranspiration (MAP-PET; mm), net primary production (NPP; tons C ha^{-1} yr^{-1}), soil pH, and % sand on global bulk soil organic carbon (SOC; g C kg $soil^{-1}$) storage (panel (**a**)). Green and red arrows indicate significant positive and negative effects of the variables described above on bulk SOC storage. The widths of the arrows correspond to standardized path coefficients, shown in numbers above each arrow. Standardized total (i.e., direct plus indirect) effects of the variables described above on bulk SOC storage are shown in panel (**b**). In all cases, n.s. non-significant, * $p < 0.05$, ** $p < 0.01$, and *** $p < 0.001$. Full results and output are provided in Table A2.4.

Relationships between f_{MAOC}, environmental variables, and land cover type

We next aimed to understand the extent to which the above environmental controls are reflected in the fraction of C stored in MAOC relative to total bulk SOC (i.e., f_{MAOC}), as well as across land cover types that are representative of those controls. MAT, NPP, and soil pH were positively related to f_{MAOC} while soil % sand was negatively related (Table A2.5; Figure A2.4), though these relationships were relatively weak (i.e., in all cases, $r^2 < 0.1$). We did not find any relationships between MAP-PET and f_{MAOC} (Table A2.5; Figure A2.4). Additionally, land cover was a significant predictor of f_{MAOC} ($F_{5,37.901}$=58.024; p < 2e-16; Figure 2.4), with croplands having higher f_{MAOC} than all other land cover types (Table A2.6). In addition, both shrublands and grasslands had higher f_{MAOC} than forests, wetlands, and tundra (Table A2.6). Notably, most land cover types spanned large ranges of f_{MAOC}, which declined from >75% in croplands to <50% in tundra (Figure 2.4).

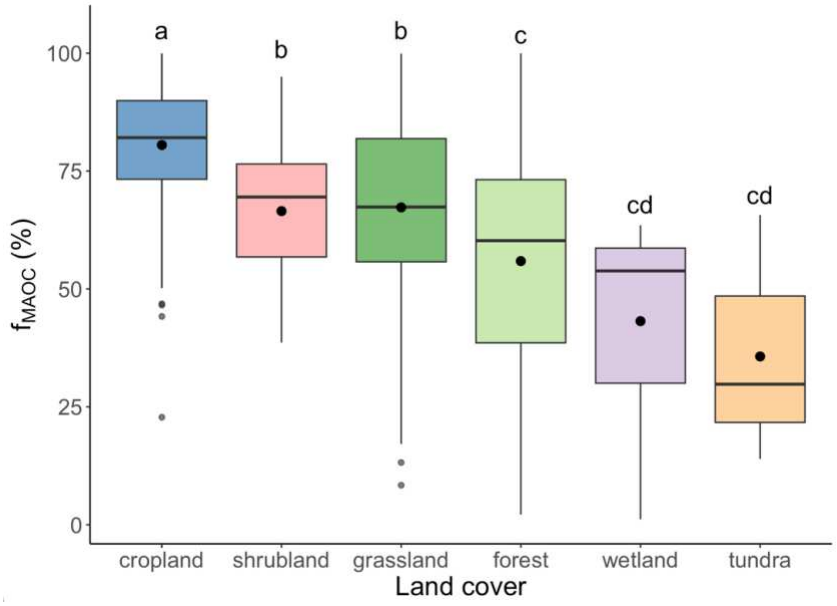

Figure 2.4. Comparison of the fraction of C stored in mineral-associated organic carbon (MAOC) relative to bulk soil organic carbon (SOC), represented as f_{MAOC} (%; (g MAOC kg $soil^{-1}$/g SOC kg $soil^{-1}$)*100), across land cover types (cropland n=312; forest n=233; grassland n=301; shrubland n=35; tundra n=7; wetland n=10). Solid black dots inside each box indicate group means, and letters above bars indicate significant differences between groups. Full *post-hoc* testing outputs are provided in Table S6. Additional information on the distribution of our mean annual temperature (MAT), mean annual precipitation minus potential evapotranspiration (MAP-PET), net primary production (NPP), soil pH, and % sand data across land cover types is provided in Figure A2.5 and Table A2.7.

Discussion

In this study, we sought to identify hierarchical controls on global POC, MAOC, and bulk SOC storage by applying path analyses to a large dataset synthesized from published papers and data we generated from NEON megapit soils. We also evaluated the utility of C fractionation in understanding global SOC storage patterns by comparing our POC and MAOC fraction path analysis to our bulk SOC analysis. Overall, climate and soil properties (i.e., pH and texture) emerged as the primary controls on SOC, with climate exerting both direct as well as indirect controls on SOC through controlling plant productivity. Separating SOC into POC and MAOC improved our ability to identify a hierarchy of controls on SOC storage, as demonstrated by identification of distinct environmental drivers of POC and MAOC storage, along with greater % variation explained in our SOC fraction path analysis compared to our bulk SOC analysis. We found that MAT and soil pH were dominant controls on POC storage, while MAP-PET, NPP, and % sand were dominant controls on MAOC storage. These results are echoed in our bulk SOC path analysis, which revealed a similar structure of controls. These results were also echoed in our analysis of f_{MAOC} across land cover types, with land cover types that tend to experience weaker constraints on SOC decomposition (i.e., croplands) having a greater fraction of SOC stored in MAOC than types that experience stronger constraints (i.e., wetlands and tundra). Altogether, these results demonstrate that POC and MAOC are controlled by separate environmental variables, with POC storage being primarily controlled by decomposition (i.e., C output) limitations, and MAOC being primarily controlled by climate-driven plant productivity (i.e., C input) limitations, as well as SOC stabilization.

Consistent with our original hypotheses, we found that global POC storage is controlled primarily by factors that impose limitations on C loss processes (Fig. 3; Table S3). The two variables most closely related to POC storage, temperature and pH, are strong controls on microbial activity, with both lower pH (Rousk et al., 2009) and lower temperatures (Schimel, 2018) contributing to slower decomposition. These findings are supported by studies conducted at smaller spatial scales, with low pH contributing to greater POC storage across the United States (Yu et al., 2022) and Europe (Lugato et al., 2021), as well as increased temperatures leading to greater POC compared to MAOC losses in lab incubations (Benbi et al.,

2014). Lower POC storage under conditions that promote microbial decomposition is consistent with this SOC fraction's turnover time (von Lützow et al., 2007) and sensitivity to disturbance (e.g., Lobe et al., 2011; Poeplau et al., 2017; Song et al., 2014; Thaysen et al., 2017; Wu et al., 2023), whereby little to no protection from microbial attack makes POC reflective of microbial physical and physiological access constraints (Cotrufo & Lavallee, 2022). This shows that POC may be most vulnerable to C losses from the soil, despite being formed primarily from structural plant inputs, and therefore represents the SOC fraction that requires protection from climate change and management disturbance, such as tillage or draining of wetlands (Ashagrie et al., 2007; Bouajila & Tahar, 2010; Lavallee et al., 2019).

We found that global MAOC storage is controlled by a different set of environmental controls from POC, including % sand, NPP, and MAP-PET (Fig. 3; Table S3). This indicates that MAOC is primarily controlled by climate-driven limitations on C inputs, moisture, and stabilization potential. Soil % sand was the largest control on MAOC. This relationship is broadly supported by the literature, with lower sand (and therefore greater silt and clay) contents contributing to greater MAOC storage (Hassink, 1997; Six et al., 2002). Our additional observed relationship between MAOC storage and MAP-PET is also consistent with previous findings, whereby MAP-PET was found to control the abundance of C retained by reactive minerals (Kramer & Chadwick, 2018). This association with effective moisture may be reflective of the direct sorption pathway of MAOC formation, with increased moisture leading to greater leaching of soluble plant inputs that are capable of sorbing directly to soil mineral surfaces (Haddix et al., 2020). Though large portions of the MAOC pool can be formed from microbial decomposition products and necromass (Huang et al., 2019; Kallenbach et al., 2016; Liang et al., 2019), this direct pathway of MAOC formation from plant compounds is increasingly recognized as a significant pathway of MAOC formation, especially in wet environments (Angst et al., 2021; Yu et al., 2022). Limitation on C inputs (i.e., NPP) represented another constraint on global MAOC storage. We interpret this relationship between MAOC and plant C inputs as the result of MAOC's protection from microbial access, making it less vulnerable to types of disturbance that accelerate decomposition and therefore more representative of C inputs to the soil than POC. Additionally, there could be interactions between the soil

matrix and plant productivity not explored in this study that contribute to greater MAOC storage. For instance, recent work indicates that increased soil mineral capacity index (MCI) leads to both greater plant productivity and MAOC storage (King et al., 2023). As Fe and Ca, key components of this MCI, are essential plant nutrients and important for mineral stabilization, factors that promote plant productivity may also promote MAOC stabilization and storage (King et al., 2023; but see Fuhrmann & Zuberer, 2021; Ramos et al., 2018). Similarly, interactions between increased silt and clay content, soil moisture, and plant productivity resulted in higher MAOC storage in dryland soils (Mao et al., *in review*).

To our knowledge, this analysis is one of the first to assess global, hierarchical controls acting on both POC and MAOC storage (though recent work has investigated the roles of climate and soil minerology in determining MAOC storage and saturation; Georgiou et al., 2022). However, the structure of controls we identified, particularly with regards to climate as an overarching driver of POC and MAOC storage, is generally consistent with studies conducted at smaller spatial scales. For instance, climate and C inputs exerted the greatest influence on total bulk SOC and POC:MAOC ratio, as well as change in bulk SOC storage, in Australian croplands (Luo et al., 2017). Increased moisture has also been associated with greater MAOC persistence at continental (Heckman et al., 2023) and global scales (Heckman et al., 2022), though in contrast to recent work on global patterns of MAOC saturation, we do not find that MAT is a significant control on global MAOC storage (Georgiou et al., 2022), potentially due to differences in data analysis or in distribution of data points among climate zones (Figure A2.1) between our studies. Our work moves beyond the above studies by expanding our understanding of SOC storage controls through explicit incorporation of both POC and MAOC, the former of which is relatively understudied in comparison to the latter, as well as by including a global distribution of climate, soil, and vegetation types.

In addition to identifying global controls on POC and MAOC storage, we compared our SOC fraction to our bulk SOC path analysis. While we were able to identify similar effects of climate, C inputs, and soil physicochemical properties on SOC storage when we considered SOC as a single pool, the effects of these variables on SOC were stronger in our fraction path analysis than in our bulk SOC

analysis. Additionally, our bulk SOC path analysis explained less variation in SOC storage than our fraction path analysis (12.3% for bulk SOC *versus* 20.5% for MAOC; Figures 2.3, 2.4; Tables A2.3, A2.4). This demonstrates the utility of separating SOC into distinct fractions to better understand controls on its formation and storage (Lavallee et al., 2020). In this study, separating SOC into POC and MAOC not only conferred greater explanatory power, but also revealed that these separate fractions are controlled by distinct environmental variables—a finding that could not be realized when considering SOC as a single pool. Building upon the findings of previous syntheses that demonstrate that SOC is not created equal, and that its component fractions respond differently to global change and management (Heckman et al., 2022; Prairie et al., 2023; Rocci et al., 2021), this study indicates that separating SOC into POC and MAOC improves our ability to understand and quantify environmental controls on SOC storage at the global scale. As such, we continue to advocate that SOC is not studied as a unique pool. In particular, as the field has gained robust knowledge of SOC dynamics from its separation into POC and MAOC, we advocate for further separation of SOC into, for example, free *versus* occluded POC and exchangeable *versus* stable MAOC, as well as further analyses on how fractionation scheme may influence predictions of SOC fraction formation and persistence (e.g., Poeplau et al., 2018; Leuthold et al., *in review*). Doing so could advance our understanding of how processes like aggregate inclusion as well as sorption and desorption of DOC to mineral surfaces impact soil C storage, thus improving our ability to predict responses of SOC to global change.

Like our bulk SOC path analysis, our comparisons of SOC storage in MAOC relative to total bulk SOC (i.e., f_{MAOC}) across our included environmental variables and across land cover types dovetail our proposed understanding of POC as controlled by C loss processes. We found that land cover types thought to experience weaker constraints on microbial decomposition, such as croplands (e.g., due to the effects of tillage (Balesdent et al., 2000; Lupwayi et al., 2004) and optimal nutrient status (Parihar et al., 2019) had a greater proportion of their total SOC pool stored in MAOC than types that tend to experience stronger decomposition constraints, such as wetlands or tundra (i.e., due to anaerobic conditions (Huang et al., 2020) or cold temperatures (Frøseth & Bleken, 2015; Figure 2.4; Table A2.5). This is mirrored in

our linear regressions between MAT, pH, and f_{MAOC}, whereby lower temperatures and lower pH confer greater proportions of SOC stored as POC (Figure A2.3; Table A2.5). These findings build upon Sokol et al., 2022 through more explicit incorporation of land cover types including wetlands and tundra, who also found that croplands and polar regions tend to have higher and lower f_{MAOC}, respectively, than both grasslands and forests. Given the large variance in f_{MAOC} within land cover types, especially in types that span a wide range of climatic conditions (e.g., grasslands and forests), this trend suggests that constraints on C inputs and losses from the soil may be a larger control on SOC fraction storage than C input quality. However, the large overlap in f_{MAOC} between forests and grasslands may also be explained by large differences in input quality within land cover types, especially for forests (Krishna & Mohan, 2017; Pérez-Harguindeguy et al., 2000). While more work is needed to confirm the effects of plant input quality on f_{MAOC}, these findings generally support the hypothesis that climate, and its effects on C inputs and decomposition-related SOC losses, represent overarching controls on SOC formation and persistence at the global scale (Cotrufo et al., 2021).

Moreover, within the context of ongoing calls to focus research efforts on building new, stable SOC to meet climate change mitigation goals (Bradford et al., 2019; Rumpel et al., 2018; Vermeulen et al., 2019), our findings highlight the importance of not just accruing new SOC, but also preventing losses of existing SOC, particularly C that is stored in POC. Our analyses support the notion that POC is highly sensitive to loss (Lobe et al., 2011; Poeplau et al., 2017; Song et al., 2014; Thaysen et al., 2017; Wu et al., 2023), and demonstrate that ecosystems that are especially vulnerable to disturbances associated with global change (e.g., wetlands, tundra) harbor SOC stores that are mostly comprised of POC (e.g., Herndon et al., 2017; Mirabito & Chambers, 2023; Sousa et al., 2015; Xu et al., 2009). Given that C loss processes exert a much greater control over POC than C inputs, and that the soils with the highest C contents (e.g., wetlands and tundra) have high POC stores, large amounts of SOC may be very difficult to rebuild if lost, particularly under a warming climate. As such, a focus on building new SOC, especially in the form of MAOC, is not enough (*sensu* Angst et al., 2023*)*— we claim that developing incentives that

maintain current SOC stores in natural lands is equally essential to preventing the negative effects of climate change.

Despite our above findings, we note that our path analyses explained only 12.3%, 20.5%, and 12.3% of the variation in POC, MAOC, and bulk SOC storage, respectively (Figure 2.3; Table A2.3), indicating that the climate, C input, and soil property variables we included in our analyses were not sufficient to describe global patterns of SOC storage. Several recent studies demonstrate that additional soil physicochemical properties not included in this study, especially exchangeable Ca and Fe- and Al-hydroxides, are better predictors of MAOC storage than % sand alone (Kirsten et al., 2021; Rowley et al., 2021; King et al., 2023). Microbial traits including mycorrhizal type (Craig et al., 2018; Horsch et al., 2023; Keller et al., 2021) and transformation efficiency may be additional modulators of both SOC fraction storage and f_{MAOC}, though the majority of studies on microbial transformations have focused primarily on their effects on microbial-derived MAOC (e.g., Craig et al., 2022; Ernakovich et al., 2021; Kallenbach et al., 2016; Liang et al., 2019). While satellite-based NPP data is often used as a proxy for C inputs to the soil (e.g., Chen et al., 2021; Eclesia et al., 2016; He et al., 2023), it may not be as applicable to agricultural systems, where depending on management strategy, plant residues are often removed from the soil. Additionally, though land cover type may be an indirect indicator of C input quality, specific litter quality traits have demonstrated effects on C storage in POC and MAOC (e.g., Córdova et al., 2018; Craig et al., 2022; Haddix et al., 2016), and may represent a secondary control on SOC fractions, after climate-driven controls. Despite their relevance to this study, there was not enough exchangeable Ca, Fe- and Al-hydroxide, microbial, or litter quality data available in conjunction with C fraction data at the global scale to include them in our synthesis, prohibiting us from testing their effects on global C storage. Furthermore, there was relatively low representation of land cover types including tundra, wetlands, and shrublands in our dataset. In addition to potentially contributing to the relatively low explanatory power of our path analyses, this limited our ability to run more comprehensive analyses of land cover-specific controls on C storage. In combination with an additional lack of standardized data reporting, particularly with regards to SOC and N fraction data, all of the above prevented us from more robustly testing several

of the hypotheses presented in the In-N-Out framework (Cotrufo et al., 2021), as was our original intent. Given the difficulties of compiling large datasets for synthesis and meta-analysis projects, we echo recent calls in advocating for more standardized collection and reporting of fraction and ancillary data in SOC studies (Todd-Brown et al., 2022). Successful harmonization of SOC fraction data is an important next step in enabling more comprehensive testing of hypotheses related to SOC storage and N recycling, including the broad, global controls we aimed to test in this work, as well as ecosystem-specific controls that aid in development of site-specific strategies to prevent C loss. Both types of knowledge are critical to realizing the potential of soils to mitigate climate change and alleviate food insecurity.

In conclusion, our analyses revealed that global POC and MAOC storage are driven by separate environmental variables. Specifically, global POC storage is controlled primarily by C loss processes, while global MAOC storage is primarily controlled by constraints on C inputs and C stabilization mechanisms. These resulted in land cover types that tend to experience more rapid decomposition having a greater portion of their total soil C pool stored in MAOC. Despite these findings and demonstrating the effectiveness of fractionation in understanding global patterns of SOC storage, we were only able to explain 12.3% and 20.5% of the variation in POC and MAOC storage. As such, our work highlights the need for increased measurement of variables, including exchangeable Ca, Fe- and Al-hydroxides, various types of microbial data, as well as fraction N, when conducting studies. Additionally, we invite the soils community to begin separating SOC into fractions beyond POC and MAOC, with the goal of improving our understanding of the likely contrasting behavior of free *versus* occluded POC and exchangeable *versus* stable MAOC. We hope that this improved measurement, combined with advancing soils data quality and reporting standards, will aid in effective data harmonization that can enable the field to build upon our findings. Doing so will allow us to develop the robust understanding of controls on soil C and N cycling needed to mitigate climate change, and ensure the soil can continue to provide essential ecosystem services well into the future.

CHAPTER 3: Microbial social dynamics and flexible enzyme production mediate patterns of particulate and mineral-associated organic matter accumulation in undersaturated soils

Introduction

Rising levels of atmospheric carbon dioxide (CO_2) significantly impact the global climate, resulting in persistent warming and necessitating the development of innovative strategies to reduce atmospheric CO_2 concentrations and prevent further emissions of carbon (C) to the atmosphere. As such, soils, which represent the largest terrestrial C store, may play a critical role in climate change mitigation efforts through sequestration of atmospheric CO_2 (Smith, 2016). In conjunction with the soil's role in provisioning many essential ecosystem services, including nutrient cycling, water filtration, and sustaining plant productivity (Smith et al., 2015), understanding the complex mechanisms that influence soil C gains and losses is crucial to climate change mitigation efforts. This includes examining processes at a variety of spatial and temporal scales, from interactions between soil microbes, who are important mediators of changes in soil C storage, at the molecular level, to large-scale ecosystem dynamics that occur over decades or centuries.

Conceptualizing SOM into physically and functionally distinct fractions, including particulate (POM) and mineral-associated organic matter (MAOM), is helpful in understanding how soils might respond to climate change, as well as the mechanisms we can leverage to enhance the capacity of the soil to store C (Cotrufo & Lavallee, 2022). POM is formed primarily from fragmentation of structural compounds in the soil, whereas MAOM is formed via sorption of low molecular weight soluble compounds (i.e., dissolved organic matter; DOM) to soil mineral surfaces. While the structural compounds contributing to POM formation require enzymatic depolymerization before they can be taken up by microbes, the low molecular weight compounds that serve as precursors to MAOM can be readily taken up and metabolized by microbes if found in solution. However, when they are bound to soil minerals in MAOM, they are strongly protected from microbial degradation, giving MAOM a longer average residence time than POM (Heckman et al., 2022; Lavallee et al., 2020). Soil microbes play a key

role in mediating the formation and persistence of both these fractions. Structural components of microbial necromass such as cell walls can serve as precursors to POM (Cotrufo et al., 2022), while the soluble components of cells and compounds derived from POM depolymerization are capable of sorbing to mineral surfaces to form MAOM (Kallenbach et al., 2016; Liang et al., 2019). In fact, microbial necromass can account for as much as half of the total MAOM pool in some ecosystems (Angst et al., 2021; Whalen et al., 2022). As it is not protected by bonds with minerals, POM is especially susceptible to decomposition via enzyme activity, whereby conditions that support microbial decomposition, including higher temperatures and optimal pH, lead to lower POM storage than in soils in colder climates or acidic soils (Hansen et al., 2024). As such, in both life and death, the structural and functional characteristics of microbes mediate C accumulation and loss in POM and MAOM.

Requiring the availability of active mineral surfaces to form, MAOM is additionally controlled by saturation dynamics, whereby the accumulation of new MAOM is limited by the proportion of mineral surfaces available for organic matter sorption (Cotrufo, 2019; Georgiou et al., 2022; Hassink, 1997; Six et al., 2002, 2024; Stewart et al., 2007, 2008). Though exact saturation limits are debated (Begill et al., 2023; Cotrufo et al., 2023; Salonen et al., 2023), many modeling and experimental studies concur that soils that are low in MAOM (i.e., are undersaturated) tend to accumulate more new C in response to inputs than those that are closer to maximum saturation (Georgiou et al., 2022; Stewart et al., 2007, 2008). Patterns of C accumulation in undersaturated soils have been fairly robustly explored, and are shown to be influenced by a combination of soil properties, C inputs, and management practices. Specifically, besides texture (Cotrufo, 2019; Hassink, 1997), mineralogy also plays a role, with soils that have more high-activity minerals having greater potential to sorb soluble C inputs than those with low-activity minerals (Georgiou et al., 2022). Carbon accrual in low-C soils is also controlled by management, whereby certain management practices are capable of building more soil C in undersaturated soils than others (West & Six, 2007).

In comparison to soil properties and management, relatively little work has investigated the extent to which microbial function influences patterns of C accumulation in undersaturated soils. Microbial

functions related to how microbes access and metabolize C substrates may be especially relevant in these soils, where high proportions of unoccupied silt and clay sorption sites mean that minerals and microbes likely compete with each other for access to DOM. Evidence that mineral surfaces are more effective at sorbing inorganic nutrients than microbes are at taking them up (Zhu et al., 2016) suggests that when the majority of mineral sorption sites are unoccupied (i.e., available for DOM sorption), DOM availability may become limiting, and microbes may be forced to produce more enzymes for the depolymerization of POM and the production of more DOM. This could mean that microbial functions, particularly those related to enzyme production and activity, in soils with low DOM availability (e.g., due to high sorption of soluble substrates) compared to soils where DOM availability is relatively high (e.g., due to high saturation of mineral surfaces and therefore low DOM sorption) could be a key mediator of whether POM is depolymerized or retained in the soil.

This proposed relationship between microbial enzyme activity and POM retention is supported by recent modeling work demonstrating that microbial social dynamics, or interactions between microbes that produce enzymes at maximal capacity (i.e., "producers") and those that produce enzymes at a lower rate or not at all (i.e., "cheaters"), promote retention of structural forms of litter and SOM (Kaiser et al., 2015). In this study, communities comprised entirely of producers had high rates of enzyme production and turnover, regardless of the soluble resources in their environment that were available for immediate uptake. This inefficient resource use created greater break down of structural SOM, and therefore low retention of that SOM pool. On the other hand, communities with cheaters had lower overall rates of enzyme production, leading to more efficient use of available resources with comparatively little waste. In this way, microbial social interactions decreased structural SOM breakdown, and led to lower loss of C from the system (Kaiser et al., 2015). Additionally, since microbes have a constrained C:N stoichiometry with low C:N ratios (Cleveland & Liptzin, 2007), they mineralize more SOM the higher is its C:N ratio (Kaiser et al., 2015). Given that the presence of cheaters within microbial communities promotes structural SOM retention, that their survival depends on the availability of DOM generated by the enzyme producers' activity, and that POM C:N modulates microbial demand for DOM, it is possible that

microbial social dynamics play a role in determining how long structural SOM forms like POM are retained in the soil, depending on the degree of MAOM saturation (i.e., DOM availability) and the C:N of POM.

Despite experimental evidence of microbial necromass contributions to C storage in POM and MAOM (Haddix et al., 2020; Kallenbach et al., 2016; Liang et al., 2019) as well as frameworks of microbial functional contributions to C storage (Malik et al., 2020), our empirical understanding of the mechanisms driving POM and MAOM formation and persistence lacks detailed insights into microbial functionality and behaviors including enzyme production and social interactions. Studies that do not incorporate microbial or enzyme traits explain low variability in POM and MAOM carbon stocks on a global scale (Hansen et al., 2024), suggesting that these traits might account for some of the unexplained variation in soil C storage. More knowledge about how specific microbial community and population interactions influence C accumulation and loss in the soil would enhance our mechanistic understanding of SOM fraction storage, thereby enabling the development of robust microbial interventions and land management strategies aimed at maximizing the retention of C inputs into the soil.

To begin filling this knowledge gap, we used the Kaiser et al. (2015) individual-based model that simulates emergent behaviors of interactions between different microbial functional groups to investigate the extent to which microbial social dynamics influence retention of POM under varying degrees of MAOM saturation. *Sensu* Kaiser et al. (2015) we hypothesized that social interactions within microbial communities would lead to greater retention of POM compared to communities consisting of producers only, where social interactions do not exist. Additionally, we hypothesized that in saturated soils (i.e., high DOM availability), high availability of immediately-assimilable C resources will require less enzyme investment, leading to long-term community maintenance and efficiency, as well as greater retention of POM, when communities contain cheaters. By contrast, in undersaturated soils with low DOM availability, we expect that higher enzyme production is needed to maintain the microbial community, leading to greater community maintenance and POM retention when communities contain microbes that produce enzymes at or very close to the maximum rate. Finally, we hypothesized that the C:N of POM

would modulate responses to MAOM saturation, with higher POM C:N requiring greater microbial enzyme investment to meet cell stoichiometric needs than when POM C:N is low.

Materials and Methods

Individual-based modeling

We applied a previously developed, individual-based, and spatially-explicit microscale model (Figure 3.1; Kaiser et al., 2015) to understand how microbial social dynamics influence emergent community behavior and POM retention under varying degrees of MAOM saturation. This model simulates a 1 x 1 mm^2 piece of decomposing organic matter as a grid of 100 x 100 microsites, each measuring 10 x 10 x 10 μm. These microsites can contain four different types of organic matter, including complex, plant-derived substrate (i.e., POM), microbial-derived C-rich and N-rich substrates, and microbial-derived soluble substrates. Unlike POM, C-, and N-rich microbial necromass, microbial-derived soluble substrates do not require enzymes to be metabolized, and contribute directly to the model's DOM pool following microbial cell death. At model initialization, 98.5% of the initial substrate pool consists of POM and 1.5% consists of microbial necromass. There is also a pool of dissolved inorganic nitrogen (DIN) that can change in size depending on microbial immobilization and mineralization rates, in the case of stoichiometric imbalances between C and N uptake (see below). There is no new input of POM throughout the simulations, though microbial necromass can accumulate depending on microbial mortality and necromass decomposition rates. Model simulations end when the amount of substrate is too low or too spatially distant to support microbial activity, and all microbes die.

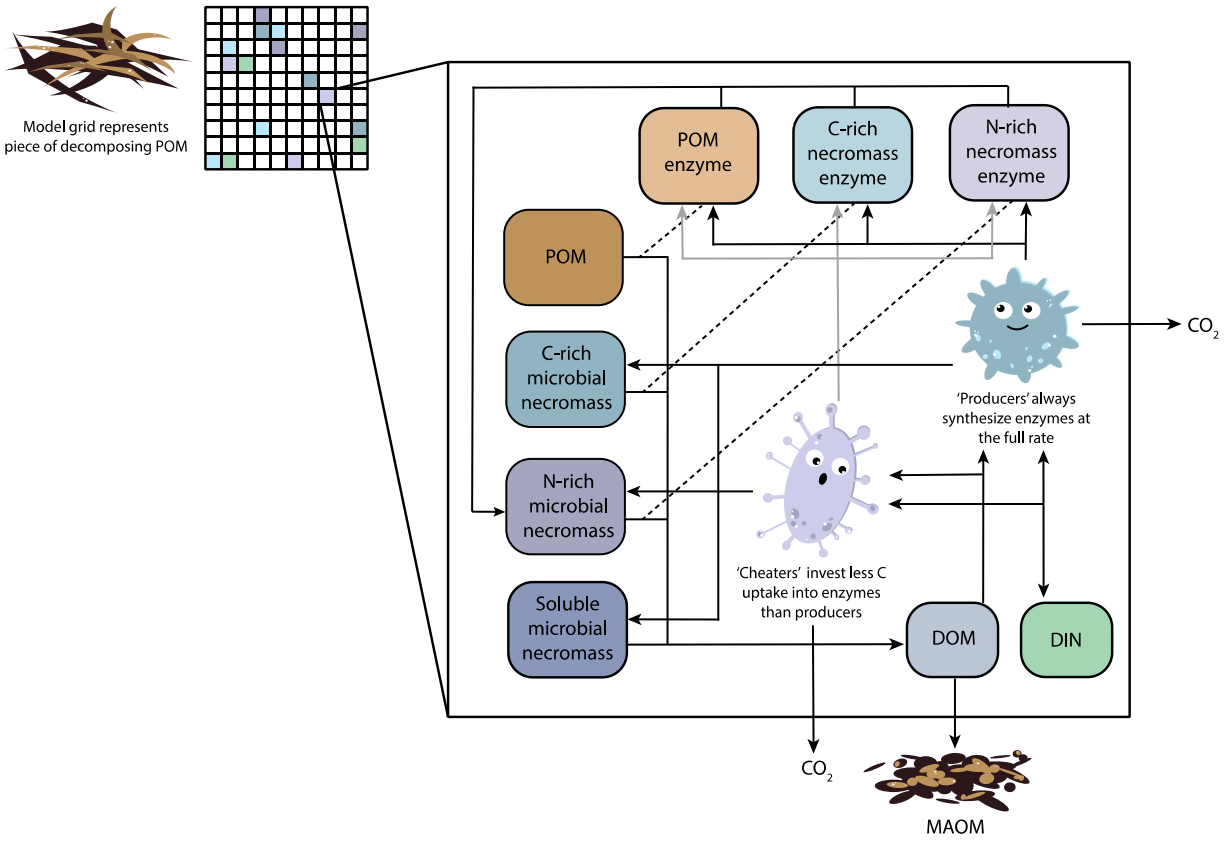

Figure 3.1. Conceptual diagram of individual-based model structure, reproduced following Kaiser et al., 2015 with modifications to match the current model. Solid arrows indicate mass flow of carbon (C) and nitrogen (N), while dotted arrows indicate the catalytic effect of an enzyme pool on the breakdown of its associated substrate (Tables 3.1, A3.1). Grey arrows associated with the enzyme production of microbial cheaters indicate that they invest less into enzyme production than microbial producers, or do not produce enzymes at all. Model results are aggregated across the entire grid at each timestep (i.e., 1 h). POM: particulate organic matter; MAOM: mineral-associated organic matter; DOM: dissolved organic matter; DIN: dissolved inorganic nitrogen.

Depending on functional group (see *Model scenarios*, below), microbes synthesize three separate enzymes that break down POM, C-rich, and N-rich necromass following Michealis-Menton kinetics:

$$d_C = k_{cat} C_{enz} \frac{C_S}{k_m + C_S} \tag{3.1}$$

Where d_C is the amount of C released by the enzyme-catalyzed reaction in the microsite within one timestep (i.e., 1 h), k_{cat} is the number of reactions catalyzed per enzyme per timestep, C_S is the amount of substrate within the microsite, C_{enz} is the amount of enzyme within the microsite, and k_m is the half saturation constant for an enzyme on its given substrate (Tables 3.1, A3.1; Figure 3.1; Kaiser et al., 2015).

Decomposition products from these reactions, along with the soluble compounds released following microbial cell death, contribute to the DOM pool and are thus available for immediate uptake (Table 3.1; Figure 3.1). All enzymes decay and contribute to the N-rich microbial necromass pool after inactivation (Table A3.1; Figure 3.1).

Table 3.1. Key parameters controlling microbial physiology and substrate availability. Additional information about model structure, assumptions, and equations can be found in Table A3.1, Kaiser et al., 2015, and the supplementary materials therewithin. Table reproduced following Kaiser et al., 2015 with modifications to match the current model.

Parameter	Description	Value
Microbial cell composition and stoichiometry		
MB_{fDOM}	Fraction of cell biomass accounting for soluble substrates available for immediate uptake by living microbes upon cell death (C:N=15)	0.06
MB_{fCR}	Fraction of cell biomass accounting for C-rich, complex substrates (e.g., cell wall compounds, lipids, starch; C:N=150)	0.37
MB_{fNR}	Fraction of cell biomass accounting for N-rich, complex substrates (e.g., proteins, DNA, RNA; C:N=5)	0.57
CN_{MB}	Resulting microbial biomass C:N	12.22
Microbial physiology and enzyme production		
MB_{fE}	Fraction of C uptake invested into enzyme production, following deduction for maintenance respiration	
	Producers	0.12
	Cheaters	0-0.1, depending on scenario
E_{fPOM}:E_{fCR}:E_{fNR}	Ratio in which enzymes are produced for degradation of POM:C-rich microbial necromass:N-rich microbial necromass	
	Producers	0.7:0.15:0.15
	Cheaters (when producing enzymes)	0.7:0.15:0.15
Microbial cell size and turnover		
MB_{Smax}	Maximum microbial cell size, at which a cell divides and colonizes a neighboring microsite	100 fmol C
MB_{Smin}	Minimum microbial cell size, at which a cell dies from starvation	10 fmol C
MB_{nC}	Maximum number of microbial cells per microsite	1
Initial pool size and C:N ratio in each microsite		
C_{POM}	Initial size of the POM pool in each microsite	8333 fmol C
CN_{POM}	Initial C:N of POM	10-100, depending on scenario
MAOM formation rates		
fr_{diff}	Parameter controlling the fraction of diffusing DOM at each timestep that is capable of sorbing to mineral surfaces; input to Eq. 2	0.0088-0.0616, depending on scenario

At model initialization, microbes begin at half of their maximum cell size and are randomly distributed across the grid. Throughout the simulation, each microbial cell takes up DOM and DIN according to their availability within local microsites. After uptake, microbes must first meet maintenance respiration needs (Table A3.1). After maintenance respiration, a functional group-specific proportion of the remaining C uptake is invested into enzyme production (Table 3.1; see *Model scenarios*, below). Any C and N remaining after both maintenance and enzyme production is invested into growth. Microbial cells that grow larger than their maximum size reproduce and can colonize empty neighboring microsites (Table 3.1) or invade an already-occupied microsite (Table A3.1). Conversely, microbes die if they are not able to access enough substrate to meet maintenance respiration needs, and their necromass is released into the C-rich, N-rich, and soluble microbial-derived substrate pools for use by surviving community members. In addition to starvation, microbes experience random catastrophic death through a stochastic mortality rate (Table A3.1). After maintenance, enzyme production, and growth needs are met, any stoichiometric imbalances between the amount of C and N acquired are accounted for by either overflow respiration (i.e., in the case of excess C), or by N mineralization or immobilization (i.e., excess N released into or taken up from the DIN pool; Figure 3.1).

At each time step, 8/9 of the total DOM and DIN in each microsite diffuses to its eight neighboring microsites such that 1/9 remains in the original microsite. A fraction of the total amount of diffusing DOM is lost from the system entirely through sorption to mineral surfaces (i.e., MAOM formation; Figure 3.1), following:

$$C_{MAOM} = n \frac{C_{DOM} \frac{fr_{diff}}{1+fr_{diff}}}{n+1} \quad (3.2)$$

Where C_{MAOM} is the amount of C leaving the system via MAOM formation, n is the number of neighboring microsites (i.e., n=8), C_{DOM} is the total amount of DOM in the microsite, and fr_{diff} is the fraction of diffusing DOM (Kaiser et al., 2014). We vary fr_{diff} to simulate the effects of altered DOM availability to microbes under different degrees of MAOM saturation, where low values of fr_{diff} approximate low sorption of DOM to mineral surfaces when soils are already saturated with MAOM, and

high values of fr_{diff} approximate high MAOM formation when soils are undersaturated (see *Model scenarios*, below).

Additional information about model structure, assumptions, and equations can be found in Table A3.1, Kaiser et al., 2015, and the supplementary materials therewithin.

Model scenarios

We compare model scenarios in which all microbes produce extracellular enzymes at the full rate (i.e., 0.12 of the C uptake at each timestep is invested into enzyme production, after deductions for maintenance respiration) with scenarios in which only half of the microbial community produces enzymes at the full rate. We define the microbes that produce enzymes at a rate less than 0.12 as "cheaters," and those that produce enzymes at the full rate as "producers." We consider 6 levels of cheating, in which cheaters produce no enzymes at all, and in which cheaters invest 0.02, 0.04, 0.06, 0.08, and 0.1 of their C uptake into enzyme production (Table 3.1). Given that all cheaters produce enzymes at a lower rate than producers (or not at all), their survival relies to at least some extent upon access to DOM that has already been produced by the enzyme activity of producers. Outside of enzyme production, all microbes invest the same amount of acquired resources into cellular maintenance and growth and possess identical cell chemical composition and stoichiometry (Table 3.1; Figure 3.1). As such, this study considers a direct comparison of communities that contain microbial cheaters *versus* those that contain producers only, without introducing any other axes of variation in microbial growth, resource acquisition, or life history traits.

In addition to enzyme production, we compare scenarios varying the C:N ratio of POM inputs as well as the rate of new MAOM formation. We consider POM C:N ratios from 10-100, in intervals of 10, corresponding to different input qualities spanning from the low C:N of leguminous plants to the high C:N of woody plants. We also consider seven different MAOM formation rates by altering the fraction of diffusing DOM that sorbs to mineral surfaces, where 0.0088, 0.0176, 0.0264, 0.0352, 0.044, 0.0528, and

0.0616 of the DOM produced at each timestep contributes to MAOM formation (Table 3.1; Figure 3.1). We interpret high MAOM formation to be representative of an undersaturated soil, where a higher proportion of diffusing DOM is inaccessible to microbes, while low MAOM formation represents a soil that is already saturated with respect to MAOM, where a higher proportion of DOM is available for immediate uptake.

We ran simulations in fully factorial combinations of scenarios varying the enzyme production capacity of microbial cheaters, initial POM C:N, and MAOM formation. As such, we were able to make comparisons on the influence and sensitivity of microbial social dynamics and POM retention across a plethora of hypothetical soil systems that vary in both substrate quality and MAOM saturation.

Model outputs and analysis

We qualitatively investigated the potential effects of microbial social dynamics on POM retention in hypothetical soils that vary in both POM C:N and MAOM saturation by first evaluating trends in several emergent microbial community properties. We chose to use qualitative methods for these assessments because it was difficult to apply quantitative methods to trends in emergent properties that varied along multiple axes, including simulation run time, the shapes of curves of variables plotted over time, as well as their maximum values over the course of the simulation. We looked specifically at the ratio of cheater to total microbial biomass (i.e., cheater:total biomass), the ratio of total enzyme production to total microbial biomass (i.e., enzyme:biomass), which indicates the proportional enzyme investment needed to support the community, and carbon use efficiency (CUE), following:

$$CUE = \frac{U_{DOC} - R - P_{enz}}{U_{DOC}} \quad (3.3)$$

Where U_{DOC} is the total amount of DOM-C taken up by all microbes on the grid, R is the total amount of C respired from the grid, and P_{enz} is the total amount of C used to synthesize extracellular enzymes by all microbes on the grid (Kaiser et al., 2015; Manzoni et al., 2012). As such, CUE is calculated from bulk C fluxes aggregated over the entire grid and represents an emergent property of the full community and soil

system. Cheater:total biomass and enzyme:biomass ratios are similarly calculated by aggregating biomass and enzyme production data from the full grid. We plotted variations in these emergent community properties over time for each scenario described above. However, for ease of interpretability, we included only those where initial POM C:N=10, 30, 50, 70, or 90 in this manuscript.

After emergent microbial community properties, we qualitatively evaluated trends in POM retention using the amount of time it took the full community to degrade their initial POM input. Given that microbial activity typically seizes soon after the available POM has been degraded, POM retention also represents the amount of time the community survived. For these comparisons, we considered scenarios with all possible combinations of microbial enzyme investment, initial POM C:N, and MAOM formation.

Results

Communities composed of enzyme producers only

To understand the influence of microbial social dynamics on POM retention across different levels of MAOM saturation, we plotted trends in enzymes:total biomass, community CUE, and POM retention across varying initial POM C:N ratios and MAOM formation rates. We first considered the dynamics of communities that contain only enzyme producers as a "control." Emergent microbial properties of these communities were insensitive to variations in MAOM formation, with all simulations consisting of only enzyme producers having approximately the same enzymes:total biomass ratio and community CUE regardless of the fraction of diffusing DOM sorbing to mineral surfaces (Figures 3.2a-f; A3.1). However, these two variables were sensitive to changes in initial POM C:N, where higher C:N values led to slightly higher enzymes:total biomass (Figures 3.2a-f; A3.1). Trends in these enzymes:total biomass and community CUE mirrored patterns of POM retention time, where the amount of time it took the community to decompose the POM pool was not affected by MAOM formation rate, but increased with initial POM C:N (Figure 3.2g).

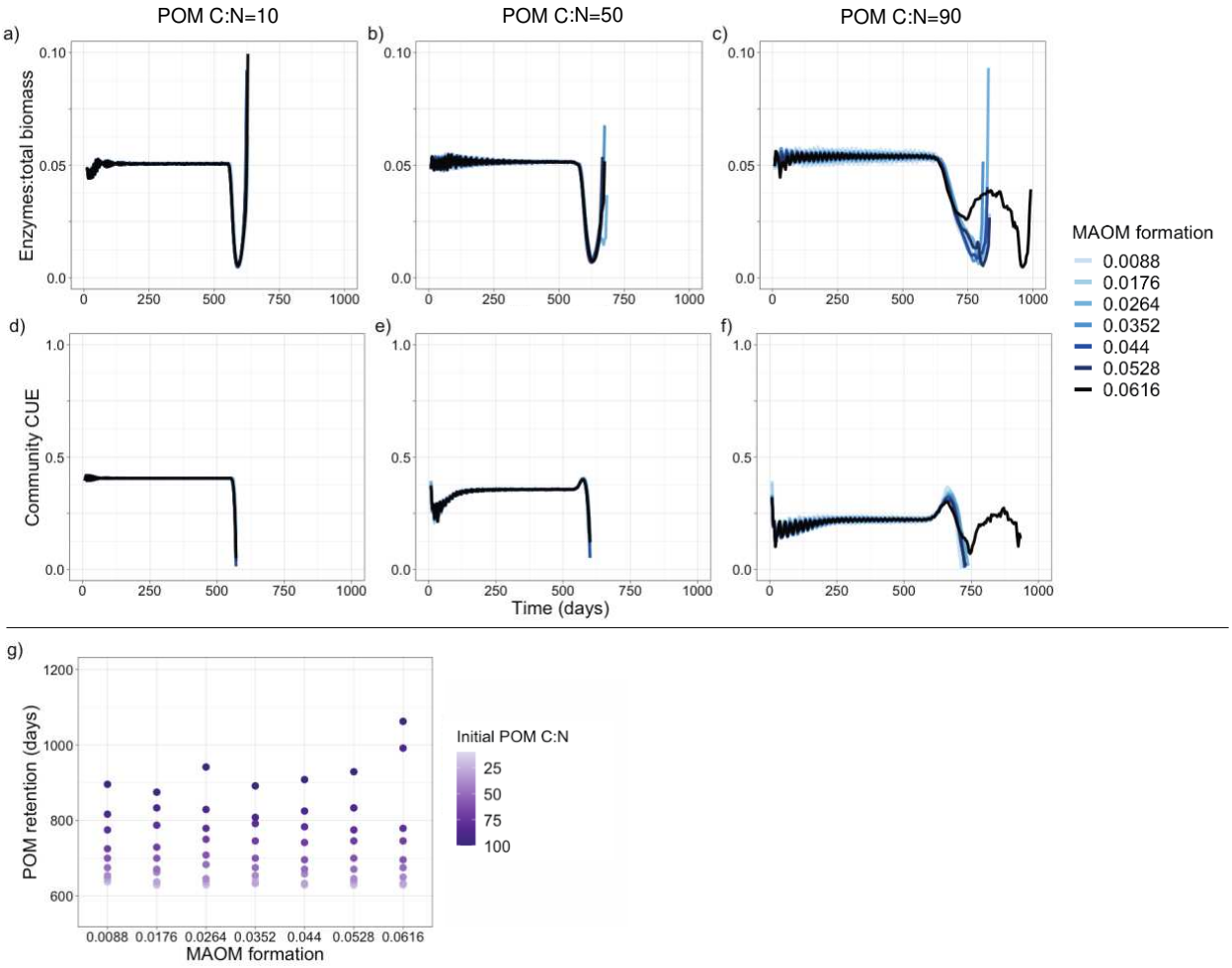

Figure 3.2. Effects of initial particulate organic matter (POM) carbon:nitrogen (C:N) ratio and mineral-associated organic matter (MAOM) formation rate on the ratio of total enzymes produced to total biomass (i.e., enzymes:total biomass; **a-c**), community carbon use efficiency (CUE; **d-f**), and POM retention time (**g**) in model simulations where microbial communities are composed entirely of producers. In **a-f**, different columns represent initial POM C:N ratios, and different shades of blue indicate MAOM formation rate. Note that these values are technically values of the parameter f_{diff} (Table 1), but are labeled "MAOM formation" for ease of interpretability, as f_{diff} controls MAOM formation rates. Results from simulations where initial POM C:N=30 and initial POM C:N=70 are found in Figure A3.1.

Emergent microbial community properties when cheaters are present

Communities that contained cheaters were sensitive to changes in both initial POM C:N and MAOM formation, especially when cheaters invested 0.06 or less of their C uptake into enzyme production. Specifically, for scenarios where cheaters invest 0.06 of C uptake or less into enzymes, as

well as four scenarios in which cheaters invest 0.08 of C uptake into enzymes (i.e., POM C:N=70 and MAOM formation=0.0616; POM C:N=90 and MAOM formation=0.044, 0.0528, and 0.0616), increases in initial POM C:N and MAOM formation both led to lower proportion of cheater to total biomass (i.e., cheater:total biomass; Figures 3.3a-o; A3.2-A3.6). MAOM formation had a larger effect on cheater:total biomass than initial POM C:N, though high POM C:N values led to greater decreases in cheater:total biomass with MAOM formation than low POM C:N. As cheater enzyme investment increased, the proportion of cheaters in the community also increased, with cheaters comprising 0.75 or more of the community at 0.06 and the four above-mentioned 0.08 enzyme investment scenarios. For the remaining 0.08 and all 0.1 investment scenarios, cheater:total biomass was largely not sensitive to changes in initial POM C:N or MAOM formation (Figures 3.3m-r; A3.6-A3.7). In these simulations, cheater biomass increased until the end of the simulation, when the community is composed almost entirely of cheaters, regardless of POM C:N and MAOM formation.

Notably, communities that contained microbial cheaters were not able to survive at all assessed combinations of cheater enzyme investment, initial POM C:N, and MAOM formation. When both POM C:N and MAOM formation were very high (i.e., POM C:N of 80 or greater and MAOM formation higher than 0.0352), communities with cheaters that invest in enzymes at a much lower rate than producers died before they were able to begin degrading their initial POM input (Figures 3.3a-i; A3.2-A3.4). Survival at these combinations of POM C:N and MAOM formation increased with enzyme investment, with communities containing cheaters that invest 0.06 of their uptake into enzymes dying rapidly only when POM C:N was 90 or greater, and the fraction of diffusing DOM sorbing to mineral surfaces was 0.0616. Only communities where cheaters invest 0.08 or 0.1 of their C uptake into enzymes (in addition to communities composed entirely of producers) were able to survive at all initial POM C:N and MAOM formation combinations.

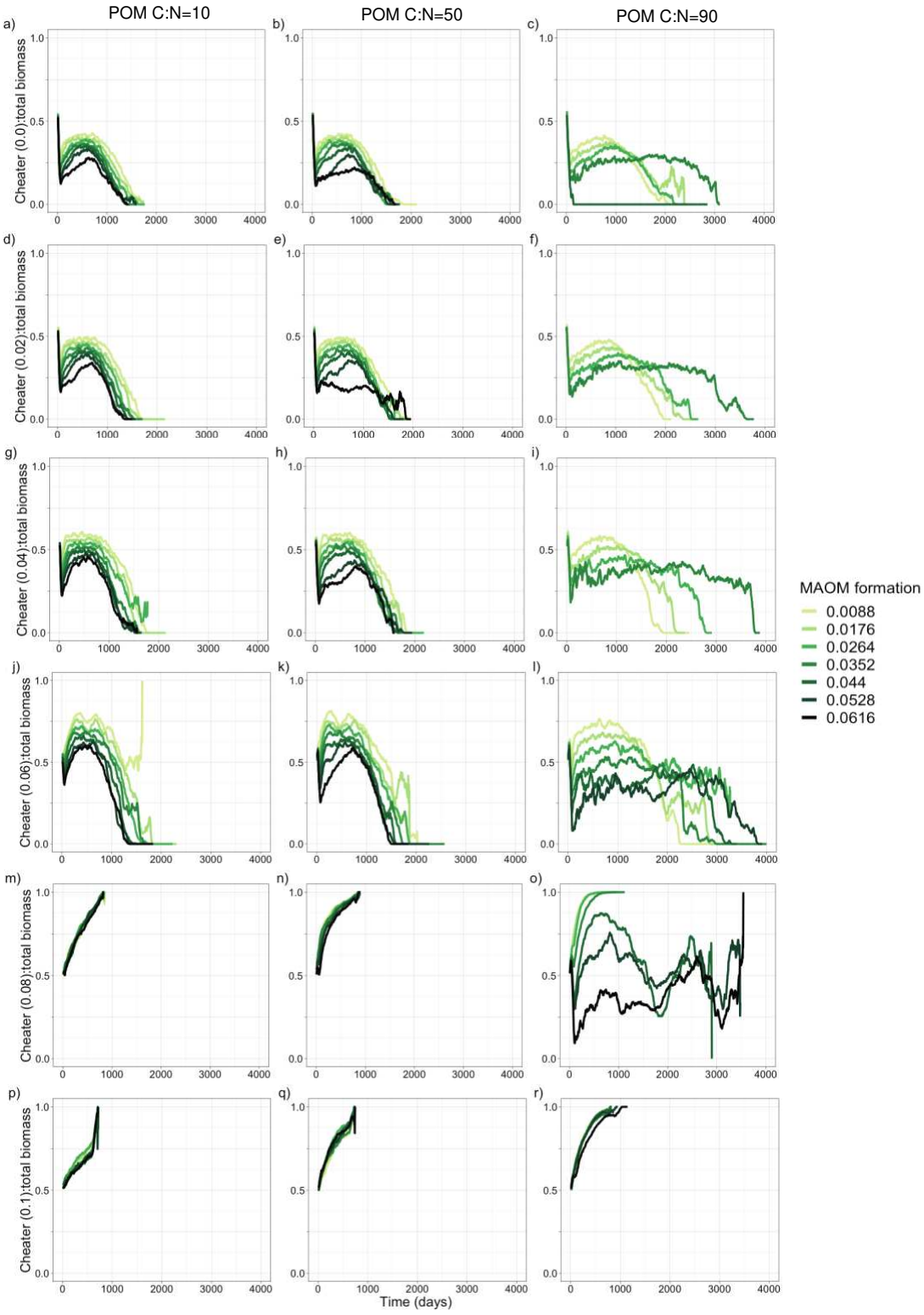

Figure 3.3. Effects of initial particulate organic matter (POM) carbon:nitrogen (C:N) ratio and mineral-associated organic matter (MAOM) formation rate on cheater:total biomass ratio in communities with cheaters that do not produce enzymes at all (**a-c**) and invest 0.02 (**d-f**), 0.04 (**g-i**), 0.06 (**j-l**), 0.08 (**m-o**), and 0.1 (**p-r**) of their C uptake into enzyme production. Different columns represent initial POM C:N

ratios and different shades of green indicate rate of MAOM formation, with darker colors representing greater amounts of diffusing dissolved organic matter (DOM) sorbing the mineral surfaces at each timestep. Note that these values are technically values of the parameter f_{diff} (Table 1), but are labeled "MAOM formation" for ease of interpretability, as f_{diff} controls MAOM formation rates. Results from simulations where initial POM C:N=30 and initial POM C:N=70 are found in Figures A3.2-A3.7.

The ratio of total enzymes produced to total biomass (i.e., a metric of how much enzyme production is needed to support the microbial community; enzymes:total biomass) generally mirrored patterns in cheater:total biomass. Enzymes:total biomass was sensitive to changes in initial POM C:N and MAOM formation when cheaters invested 0.06 or less of their C uptake into enzyme production, as well as the same four 0.08 investment scenarios described above (Figures 3.4a-l, o; A3.6-A3.7). Higher initial POM C:N and MAOM formation increased enzymes:total biomass, though increases in this ratio that were associated with higher POM C:N were smaller than those associated with MAOM formation. Additionally, enzymes:total biomass tended to decrease slightly with increases in cheater enzyme investment. For the remaining 0.08 and all 0.1 investment scenarios, enzymes:total biomass was largely not sensitive to changes in either initial POM C:N or MAOM formation (Figures 3.4m-r; A3.6-A3.7). In all simulations containing cheaters, enzymes:total biomass was higher than in simulations where communities consisted entirely of enzyme producers, regardless of cheater enzyme investment (Figures 3.1a-c; 3.4a-r).

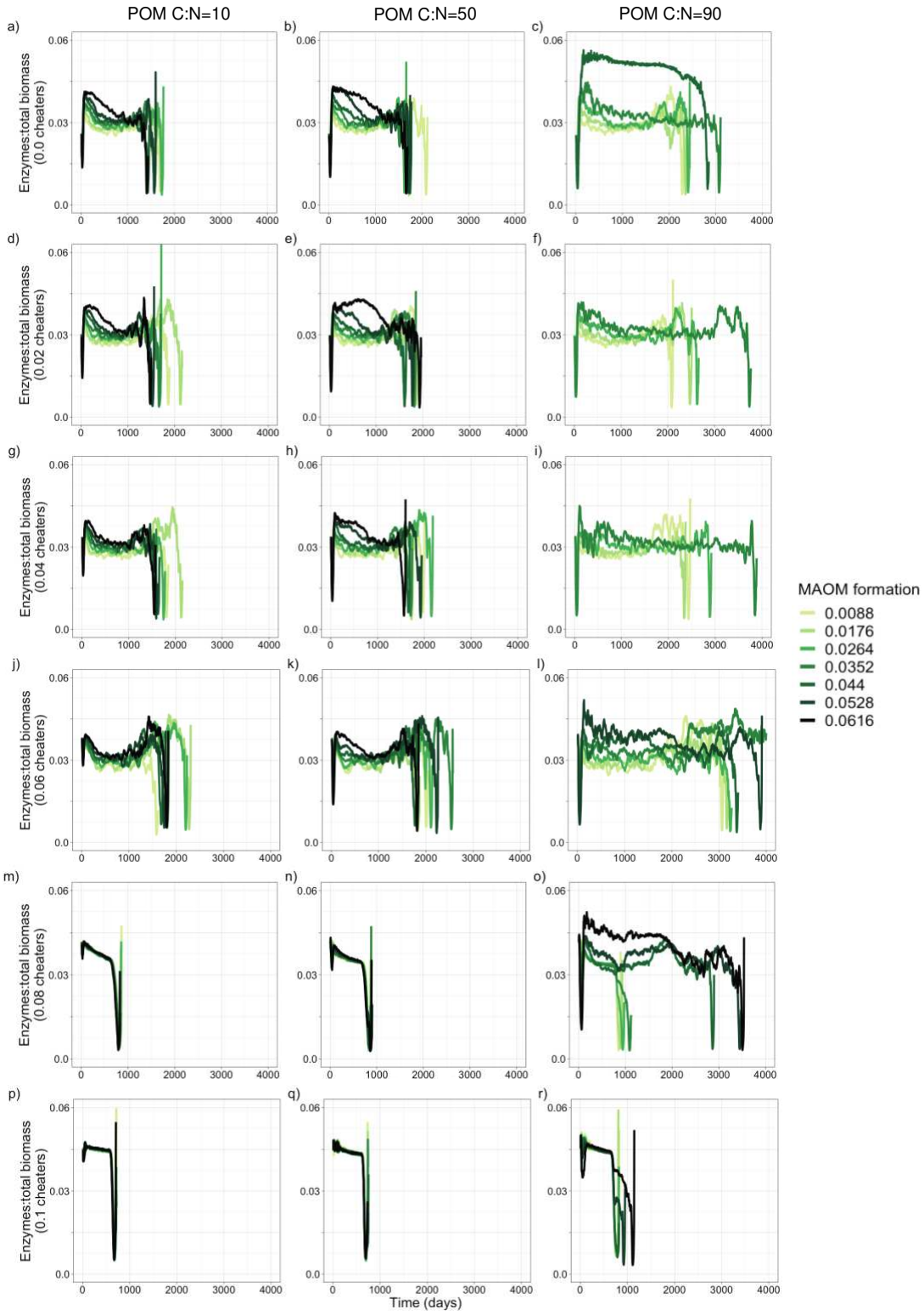

Figure 3.4. Effects of initial particulate organic matter (POM) carbon:nitrogen (C:N) ratio and mineral-associated organic matter (MAOM) formation on enzymes:total biomass ratio in communities with cheaters that do not produce enzymes at all (**a-c**) and invest 0.02 (**d-f**), 0.04 (**g-i**), 0.06 (**j-l**), 0.08 (**m-o**), and 0.1 (**p-r**) of their C uptake into enzyme production. Different columns represent initial POM C:N

ratios and different shades of green indicate rate of MAOM formation, with darker colors representing greater amounts of diffusing dissolved organic matter (DOM) sorbing the mineral surfaces at each timestep. Note that these values are technically values of the parameter f_{diff} (Table 1), but are labeled "MAOM formation" for ease of interpretability, as f_{diff} controls MAOM formation rates. Results from simulations where initial POM C:N=30 and initial POM C:N=70 are found in Figures A3.2-A3.7.

In scenarios where cheaters invested 0.06 or less of their C uptake into enzyme production, as well as the four 0.08 enzyme investment scenarios described above, responses of community CUE to MAOM formation depended on POM C:N (Figures 3.5a-l, o; A3.2-A3.7). While CUE decreased with increasing initial POM C:N, it was only sensitive to MAOM formation when POM C:N was greater than 30. Additionally, community CUE largely did not vary with increases in cheater enzyme investment. For the remaining 0.08 and all 0.1 investment scenarios, community CUE was sensitive to initial POM C:N, but not MAOM formation rate (Figures 3.5m-r; A3.2-A3.7). Like simulations where cheaters invested 0.06 or less of their C uptake into enzymes, CUE of communities with 0.08 and 0.1 enzyme investment decreased with increases in POM C:N. Additionally, similar to enzymes:total biomass, community CUE was higher than in simulations where communities contained cheaters than in those where communities consisted entirely of cheaters, regardless of cheater enzyme investment (Figures 3.1d-f; A3.5a-r).

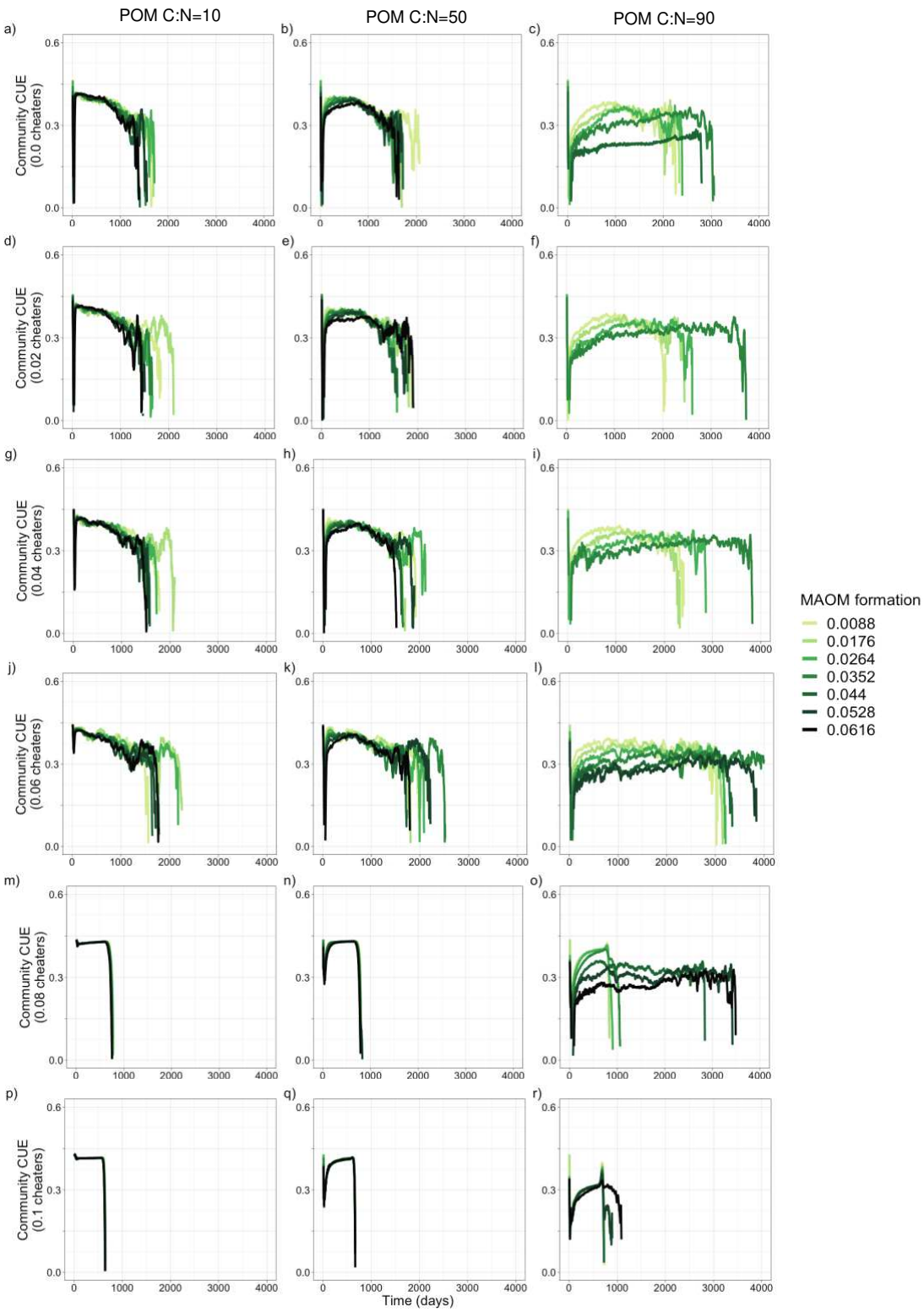

Figure 3.5. Effects of initial particulate organic matter (POM) carbon:nitrogen (C:N) ratio and mineral-associated organic matter (MAOM) formation rate on community carbon use efficiency (CUE) in communities with cheaters that do not produce enzymes at all (**a-c**), and invest 0.02 (**d-f**), 0.04 (**g-i**), 0.06 (**j-l**), 0.08 (**m-o**), and 0.1 (**p-r**) of their C uptake into enzyme production. Different columns represent

initial POM C:N ratios and different shades of green indicate rate of MAOM formation, with darker colors representing greater amounts of diffusing dissolved organic matter (DOM) sorbing the mineral surfaces at each timestep. Note that these values are technically values of the parameter f_{diff} (Table 1), but are labeled "MAOM formation" for ease of interpretability, as f_{diff} controls MAOM formation rates. Results from simulations where initial POM C:N=30 and initial POM C:N=70 are found in Figures A3.2-A3.7.

Effects of microbial social dynamics on POM retention

After assessing the extent to which trends in emergent microbial community properties varied with initial POM C:N and MAOM formation, we evaluated whether changes in POM C:N and the fraction of diffusing DOM sorbing to mineral surfaces impacted POM retention. For scenarios with 0.06 or less enzyme investment, as well as the same four scenarios with 0.08 enzyme investment described above, the presence of cheaters significantly increased POM retention time compared to communities consisting of only enzyme producers (Figures 3.1g; 3.6a-d; A3.8). When initial POM C:N was below 40, POM retention tended to stay approximately the same across all values of MAOM formation. However, when initial POM C:N was above 40, POM retention tended to increase with MAOM formation, as well as with the cheater enzyme investment. For the remaining 0.08 and all 0.1 enzyme investment scenarios, POM retention increased with increases in initial POM C:N, but did not respond to MAOM formation (Figures 1.6e-f; A1.8). Patterns of POM retention in these scenarios was more similar to simulations that contained only enzyme producers (Figures 3.1g; A3.8).

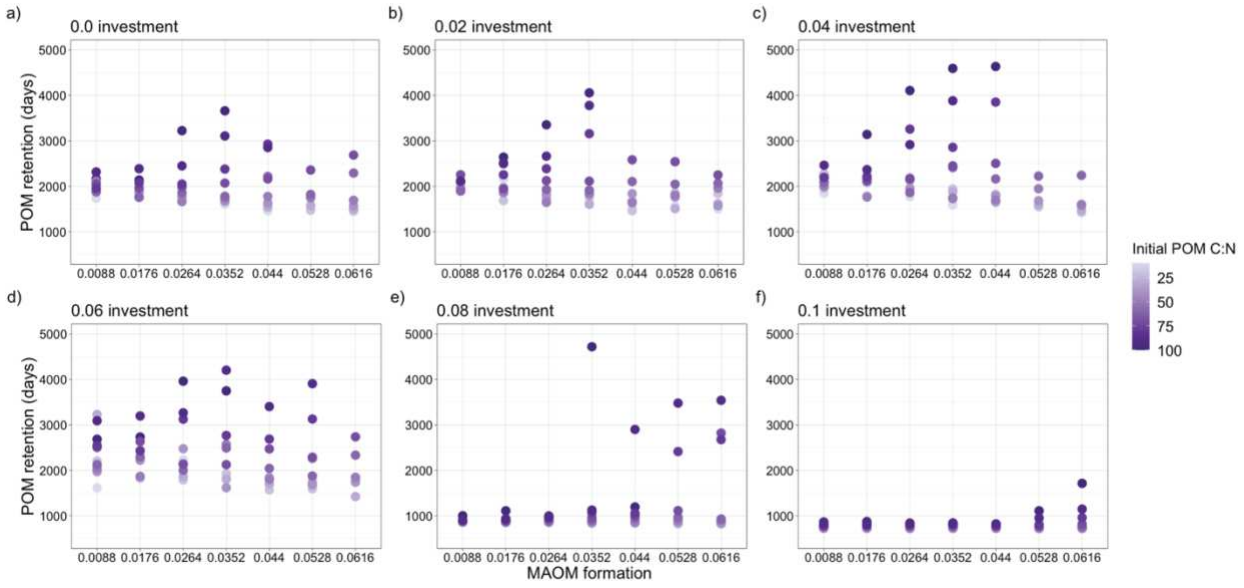

Figure 3.6. Effects of initial particulate organic matter (POM) carbon:nitrogen (C:N) ratio and mineral-associated organic matter (MAOM) formation rate on POM retention in simulations that contain microbial cheaters. Panels **a-f** represent different cheater enzyme investments. In each, the x-axis indicates MAOM formation, and the y-axis indicates the length of time POM is retained in the system. Note that values of MAOM formation values are technically values of the parameter f_{diff} (see *Materials and Methods*; Table 1) but are labeled "MAOM formation" for ease of interpretability, as f_{diff} controls MAOM formation rates. Different colors represent initial POM C:N, with darker shades of purple indicating higher C:N. Further data directly comparing POM retention in cheater simulations to its retention in producer-only simulations are found in Figure A3.8.

Discussion

In this study, we used individual-based modeling to understand the potential for microbial social dynamics to influence POM retention in hypothetical soils that vary in their degree of MAOM saturation. As hypothesized, we found that the presence of microbial social dynamics, especially when cheaters invest much less in enzymes than producers, led to greater POM retention than in producer-only communities. However, this occurred only when cheater enzyme investment was half (or less) than that of producers, or in the scenarios when both POM C:N and MAOM undersaturation were very high, when cheater enzyme investment was three-quarters that of producers. Overall, this indicates that microbial social dynamics are advantageous to community efficiency and survivability, as well as maintenance of POM stocks, but that the enzyme investment rates that produce the greatest advantages to microbial

communities depends highly on both MAOM saturation (i.e., DOM availability) and POM stoichiometry (i.e., C:N).

When considering each cheater enzyme investment scenario individually, we found that decreases in MAOM saturation (i.e., increases in MAOM formation rate) led to decreases in the proportion of cheaters present in the community, with associated increases in enzyme production relative to microbial biomass. In other words, when high sorption to mineral surfaces causes low availability of DOM, cheaters are less able to survive and greater enzyme investment is needed to break down POM to meet microbial metabolic needs. However, except for when cheater enzyme investment is very high, the presence of cheaters that can produce at least some enzymes in the community buffers CUE across MAOM saturation levels and POM qualities. This indicates that POM retention at higher structural substrate C:N and lower MAOM saturation requires additional enzyme investment to maintain the mechanisms driving efficient use of existing resources with little waste, as identified by Kaiser et al. (2015). Thus, in support of our original hypotheses, greater enzyme production is needed to minimize resource loss from the system and maintain the community when MAOM saturation is low and POM C:N is high.

In addition to more efficient use of available substrates, we found that microbial social dynamics increased POM retention in undersaturated soils in nearly all scenarios that contained microbial cheaters (apart from those in which the community did not survive long enough to begin degrading POM). This dynamic of concurrent POM retention and MAOM formation in undersaturated soils is consistent with results from many field studies and meta-analyses. For instance, long-term implementation of regenerative agricultural practices, including no- or low-till, intercropping, livestock integration, and adaptive multi-paddock grazing in traditionally-managed agricultural soils (e.g., undersaturated soils; Georgiou et al., 2022) leads to C accumulation in both POM and MAOM (Mosier et al., 2021; Prairie et al., 2023). Similar patterns occur with ecosystem restoration, where transitions from degraded croplands to native vegetation cause concurrent increases in both C fractions (Kalinina et al., 2019; Yang et al., 2022). In addition to the mechanisms of C accrual identified by the above studies, our findings support the notion that microbial social dynamics could be an additional factor driving ecosystem-scale patterns

of SOM accumulation. While our simulations do not account for the continuous C inputs that would enter field soils, high retention of the initial, one-time POM input in our model (i.e., up to ~13.5 years; Fig. 6) implies that any structural C entering the soil may also be retained. Furthermore, the initial POM input amount used in our simulations was not designed to cause any microbial limitations in itself, although its variable properties like C:N might (Kaiser et al., 2014, 2015). Though microbial social dynamics are difficult to quantify in the lab, we advocate for greater incorporation of -omics techniques, enzyme assays, stable isotope tracing, and other methods of quantifying changes in microbial function (Malik et al., 2020) within studies seeking to understand C storage dynamics in undersaturated soils to understand the extent to which social dynamics interact with and mediate the effects of known controls on C storage.

While communities that contained cheaters were more efficient and had greater POM retention than communities of producers only, we found that the cheater enzyme investment resulting in maximum community efficiency and POM retention depended highly on initial POM C:N and MAOM saturation. This indicates that static microbial enzyme investment, regardless of substrate availability or quality, does not maximize community efficiency and in some circumstances, could lead to premature community death. Subsequently, the ability for microbes to adjust enzyme production in response to the soluble substrates available in their environment would be evolutionarily advantageous to community efficiency and survival. These findings support the notion that enzyme production is not static throughout a microbe's life, but instead represents a highly responsive trait that microbes may be able to regulate depending on environmental conditions (Allison & Vitousek, 2005; Allison et al., 2007; Burns et al., 2013), sometimes within one day after a change in substrate availability (Boetius & Lochte, 1994). Downregulating enzyme production when DOM availability is high and POM C:N is medium to low could allow for greater proportion of C uptake to go to microbial growth and reproduction. Given this, maintaining high quality structural and metabolic inputs to undersaturated soils may promote both POM and MAOM formation and retention, especially in agricultural soils which typically have a high C saturation deficit (Georgiou et al., 2022; Lugato et al., 2021)

Implementing flexible enzyme investment rates as regulated by soluble resource availability in process-based models of C and N cycling may be a way to bridge gaps between experimental studies on enzyme activity, emergent microbial behaviors simulated through microscale models such as the one employed in this study, and current representation of microbial functions in process-based models. While many of these models are considered microbial-explicit in that they incorporate explicit microbial C pools or decomposition rates that are calculated based on microbial biomass (Chandel et al., 2023; Rocci et al., 2024), relatively few include specific considerations of microbial population and community ecology (e.g., Georgiou et al., 2017; Sistla et al., 2014; Wang et al., 2015; Wieder et al., 2014) that are known mediators of C change (e.g., Allison et al., 2010; Bradford et al., 2021; Buchkowski et al., 2017; Crowther et al., 2015; Hall et al., 2018; Trivedi et al., 2013), such as the social dynamics explored in this study. The ability of our microscale model to replicate the patterns of POM and MAOM formation in undersaturated soils that are observed in a variety of experimental studies demonstrates that implementing microbial social dynamics into process-based models, potentially through mediated of enzyme production based on DOM availability, could increase model precision and accuracy, particularly in ecosystems where microbial functional traits may strongly mediate C fraction storage [e.g., mesic environments; (Cotrufo et al., 2021)].

In addition to model development, relationships between microbial enzyme investment and structural SOM retention offer a valuable framework for developing microbe-centric land management strategies that increase soil C storage. For example, efforts to develop microbial inoculants for use in agricultural soils may want to focus selection of microbial strains for inoculant inclusion on promotion of efficient enzyme regulation in response to soluble substrate availability, whereby enzymes to break down structural SOM are produced only if necessitated by resource environment. In combination with other strategies to increase high-quality plant inputs, this approach could maximize microbial community efficiency in ways that retain more soil C. Alongside other regenerative practices that boost C inputs to the soil, microbial interventions aimed at retaining SOM may be able to extend the residence time of newly-formed C and prevent its loss through microbial catabolism.

In conclusion, we demonstrate that microbial social dynamics may be an additional mechanism contributing to observed patterns of C accumulation in POM and MAOM in undersaturated soils. In particular, microbial regulation of enzyme production in response to the availability of soluble substrates in the soil may support community efficiency and survival, as well as long-term retention of structural forms of SOM. While empirical work is needed to confirm the effects of flexible enzyme production on C fraction retention, our study provides a useful roadmap for more comprehensive incorporation of microbial physiology into process-based models of soil C and N cycling, as well as the development of microbial interventions to promote the formation and retention of C in agricultural soils. Ultimately, with an improved understanding of how microbial functions such as enzyme production impact SOM fractions, we may be better able to fully realize the potential of soil microbes as a tool to prevent the negative effects of global climate change.

CHAPTER 4: Copio- and oligotrophic microbial life history strategies do not mediate carbon storage in particulate and mineral-associated organic matter

Introduction

Soil microbes play a pivotal role in mediating gains and losses in soil carbon (C), with their activities in the soil and their necromass contributing both to the formation and loss of particulate organic matter (POM) and mineral-associated organic matter (MAOM). Soil microbial structural and functional traits mediate C storage in both soil organic matter (SOM) fractions, with the structural components of microbial necromass (along with structural plant litter) serving as precursors to POM (Cotrufo et al., 2022). The small, low molecular weight components of necromass sorb to mineral surfaces to form MAOM (Kallenbach et al., 2016; Liang et al., 2019). These bonds with mineral surfaces strongly protect MAOM from microbial degradation, giving it a longer average residence time than POM (Heckman et al., 2022; Lavallee et al., 2020). Because it is not protected by mineral bonds, and unless protected by fine aggregates, POM is especially susceptible to microbial decomposition, particularly under conditions that support microbial activity such as high temperatures and optimal pH (Hansen et al., 2024). Given the critical roles microbes play in mediating C storage in POM and MAOM, understanding how soil microbial functionality influences SOM gains and losses is essential to not only building more basic knowledge of soil microbial ecology, but also sheds light on how microbes may contribute to changes in soil C storage that could either accelerate C losses and climate-C feedbacks, or be leveraged in soil C sequestration strategies that could help prevent the negative effects of climate change.

The many roles microbes play in mediating C storage in POM and MAOM has led to several frameworks predicting key functional traits that strongly regulate POM and MAOM formation, particularly the efficiency with which microbes produce new biomass. More efficient biomass production may lead to more necromass that can sorb to mineral surfaces, as well as less C lost from the soil through respiration, thus leading to more efficient formation of MAOM (Cotrufo et al., 2013). These hypothesized relationships between high microbial carbon use efficiency (CUE) and increased MAOM formation (i.e.,

the Microbial Efficiency Matrix Stabilization (MEMS) hypothesis; Cotrufo et al., 2013) have been rigorously tested, though the effects of CUE on MAOM formation are generally context-dependent (Craig et al., 2022; Ernakovich et al., 2021). Relationships between CUE and MAOM formation have also spurred the development of additional frameworks describing microbial contributions to SOM formation that center around potential trade-offs between microbial traits that are desired for survival *versus* fast growth and reproductive success. For instance, under the Yield-Acquisition-Stress (YAS) framework (Malik et al., 2020), microbes specialized for quick resource acquisition (i.e., enzyme production) may lack the stress tolerance traits needed to survive under hostile environmental conditions. Alternatively, microbes specialized for stress tolerance may be outcompeted by microbes specialized for fast growth when environmental conditions are ideal. Given that microbes specialized for each of these purposes display different growth rates, have different cell stoichiometries, and produce different kinds of metabolites, the relative proportion of microbes in a community expressing a given functionality may have impacts on whether the community contributes more to POM or MAOM formation. In this way, changes in POM and MAOM storage may be modulated by multiple co-occurring life history strategies and tradeoffs among community members.

One of these tradeoff frameworks that may be of high relevance to POM and MAOM formation and storage is copiotrophic and oligotrophic life history designations. Under this framework, copiotrophic microbes represent those that can quickly access and catabolize soluble substrates, contributing to rapid growth and biomass production. On the other hand, oligotrophic microbes grow more slowly and have proportionally lower biomass production, and may catabolize primarily structural substrates (Meyer, 1994). Given their different preferences for substrate quality, it is expected that soils with high amounts of soluble organic substrates would be dominated by copiotrophs, whereas soils that are low in soluble substrates but high in structural substrates are expected to be dominated by oligotrophs (Fierer et al., 2007; Meyer, 1994). Because of their different growth and biomass production rates, these two life histories may also differentially contribute to POM and MAOM, with the fast growth rate of copiotrophs leading to high necromass production and therefore greater microbial-derived MAOM formation

(Bradford et al., 2013). Conversely, the slow growth rate, preference for structural substrates, and potential trade-offs between growth rate, resource acquisition, and stress tolerance traits (Malik et al., 2020), oligotrophs may play a greater role in dictating both gains and losses in POM storage.

While expression of copio- and oligotrophic life histories and trade-offs between microbial growth rate and enzyme activity have generally been supported (Chen et al., 2023; Fierer et al., 2007; Malik et al., 2019; Pascault et al., 2013), recent evidence indicates that soil microbial taxa can behave as either a copiotroph or an oligotroph, depending on environmental conditions (Stone et al., 2023). Additionally, expression of copio- and oligotrophy appears to more closely represent a continuum than a dichotomy, with many organisms displaying moderate to slow growth rates in response to glucose additions (Stone et al., 2023). This plasticity in copio- and oligotrophic expression limits accurate quantification of these traits, especially through classification-based tools like 16S amplicon sequencing, as well as the extent to which they influence priming of existing SOM and patterns of new SOM accumulation (Ho et al., 1017). As such, the extent to which these life histories are present within soil communities, along with their effects on C storage in POM and MAOM, has largely not been robustly explored. However, merging our current understanding of POM and MAOM with that of oligotrophs and copiotrophs, it can be hypothesized that POM supports a microbial community comprised mostly of oligotrophs, while copiotrophs would dominate in the MAOM pool.

Given the limitations of using classification-based methods of quantifying expression of copio- and oligotrophy (Ho et al., 2017; Stone et al., 2023), direct measurement of microbial growth in response to substrate changes may be a more appropriate method to test the relevance of these life history strategies to POM and MAOM formation. While this wouldn't allow sorting microbes into copio- or oligotrophic categories, it would still test the main tenet of the framework: that increased growth under high soluble substrate availability leads to greater MAOM formation. One of these methods is quantification of ^{2}H incorporation into microbial phospholipid fatty acids (PLFAs) following addition of ^{2}H-labeled water (Canarini et al., 2023; Caro et al., 2023). Given that H is required for microbial growth, high incorporation of ^{2}H would indicate high microbial growth rates, whereas low ^{2}H incorporation would

indicate little to no growth. Additionally, as this methodology relies on addition of ^{2}H-labeled water without the addition of other substrates (e.g., ^{13}C-labeled glucose), it may provide more accurate assessments of microbial growth rate in response to the substrates naturally available in their environment, avoiding potential biases from other added substrates (Canarini et al., 2023; Caro et al., 2023). As such, although direct quantification of microbial growth via ^{2}H incorporation into PLFAs does not provide direct classifications of copio- and oligotrophy, it allows for more robust testing of the expression of the traits associated with these life histories, as well as the effects they have on C storage in POM and MAOM.

In this study, we used a combination of ^{2}H and ^{13}C isotopic labeling in a highly controlled laboratory incubation experiment to understand how changes in SOM fraction storage, as well as formation of new POM and MAOM, are driven by functional traits considered to be characteristic of copio- and oligotrophy (i.e., microbial growth rate and CUE). To do so, we aimed to create variations in microbial community composition by fractionating soil by size into POM and MAOM, then recombining it in varying ratios such that approximately 25%, 50%, and 75% of the total SOC pool was stored in MAOM (f_{MAOM} treatment). We also aimed to stimulate communities dominated by copio- or oligotrophic microbes through additions of fresh, ^{13}C-labeled dissolved organic matter (DOM), whereby communities receiving greater amounts of fresh DOM would be characterized by copiotrophic behaviors such as fast growth rate, and soils receiving low additions would be characterized by oligotrophic behavior such as slow growth rate and decomposition of structural SOM forms (i.e., POM). We hypothesized that greater fresh DOM inputs would stimulate faster microbial growth, leading to greater biomass (and necromass) that would contribute to greater MAOM formation. Conversely, low availability of fresh DOM would lead to slower growth, greater losses of POM, and comparatively lower MAOM formation. Given the soil used for this work was far from C saturation in MAOM (data not shown), we did not expect our f_{MAOM} treatment to affect the formation of new MAOM derived from DOM additions. However, given the higher accessibility of POM to microbes, we expected it to be more susceptible to priming from fresh DOM additions than MAOM. Finally, we expected an interaction between f_{MAOM} and DOM addition treatments,

whereby the higher abundance of the copiotrophs in the 75% f_{MAOM} would be stimulated by the higher addition of DOM more so than the lower f_{MAOM} treatments.

Materials and Methods

Design of f_{MAOM} and soluble litter treatments

All soil used in this experiment was collected from the Central Plains Experimental Range (CPER) National Ecological Observatory Network (NEON) site in Weld County, CO (40°40′ N, 104°45′ W) in October 2022. CPER is a shortgrass steppe dominated by a combination of the C_4 grass *Bouteloua gracilis* (H.B.K.) Lag. (blue grama), and the C_3 grasses *Stipa comata* Trin and Rupr. (needle-and-thread grass) and *Pascopyrum smithii* (Rydb.) A. Love (western wheatgrass; (Pendall et al., 2004). Soil at this site is low in native SOC (i.e., 6.73 g SOC kg $soil^{-1}$), of which approximately half is stored in MAOC (i.e., 56.2%; 3.78 g MAOC kg $soil^{-1}$; Hansen et al., 2024). It also does not contain carbonates within the top 40 cm (Pendall et al., 2004), making it an ideal choice for manipulations of the fraction native SOC is stored in. Approximately 7 kg of soil was collected to a depth of ~10 cm at the CPER-NEON megapit location (Hinckley et al., 2016), and stored at 4°C until further processing and manipulation of f_{MAOM} (i.e., the fraction of C stored in MAOM relative to bulk SOM).

We created three different f_{MAOM} treatments by fractionating our collected soil by size, and then recombining it with POM and muffle-furnaced, acid-washed sand in ratios corresponding to roughly 25%, 50%, and 75% f_{MAOM}, in addition to a bulk soil control. This was done to manipulate microbial community composition, under the hypothesis that greater abundance of structural substrates in soils high in POM would select for a primarily oligotrophic community, while the greater abundance of soluble, low molecular weight substrates in high-MAOM soils would select for a primarily copiotrophic community (Fierer et al., 2007; Malik et al., 2019; Pascault et al., 2013). Following Cotrufo et al., 2019 with modifications to prevent as much disturbance to the native microbial community as possible, soils were shaken with twelve glass beads and deionized (DI) water for 18 h, then separated by wet sieving into

particulate organic matter (POM; >53 μm) and mineral-associated organic matter (MAOM; <53 μm). Fractions were dried at 40°C before they were prepared for use in the incubation. A subsample from each fraction was finely ground and measured for %C using a Velp CN 802 carbon nitrogen analyzer (Velp Scientifica, Italy). Care was taken so that SOM fractions, especially the POM fraction, retained as much of the original structural properties they had in the field before they were recombined to 25%, 50%, and 75% f_{MAOM} based on %C values from the Velp, and 60 g of each sample was weighed into 120 mL cups, and placed into 1 L mason jars. Each jar, referred to below as incubation units, contained 60 g of dry soil. Combined size and density fractionation at the end of the experiment (see *Combined size and density fractionation*, below) confirmed that our 25%, 50%, and 75% f_{MAOC} treatments maintained at 60% water-filled pore space (WFPS) with DI water only (i.e., controls not receiving any fresh DOM inputs; see below) had 2.797 ± 0.085, 3.109 ± 0.040, and 4.006 ± 0.145 mg MAOM-C g $soil^{-1}$, respectively. Additionally, our non-recombined (i.e., 2-mm sieved bulk) soil control had 3.072 ± 0.037 mg MAOM-C g $soil^{-1}$, indicating that our f_{MAOM} treatments had approximate intended effects on C storage in MAOM.

In addition to f_{MAOM}, we manipulated DOM availability through bimonthly additions of soluble litter inputs at three different rates, termed 'low,' 'medium,' and 'high,' along with a DI water control. This was done to stimulate development of copio- and oligotrophy in microbial communities separate from our f_{MAOM} treatments, with the 'high' fresh DOM treatment selecting for a copiotrophic community characterized by fast growth, and the 'low' fresh DOM and DI water control treatments selecting for an oligotrophic community characterized by slow growth (Fierer et al., 2007; Malik et al., 2019; Pascault et al., 2013). Fresh DOM addition rates were chosen to be representative of annual rhizodeposition at CPER (Pendall et al., 2004), where our "medium" treatment is equivalent to the average amount of rhizodeposition CPER soils receive over the course of a year within 16 weeks (i.e., the length of the incubation), the "low" treatment is 0.5 times "medium," and the "high" treatment is 1.5 times "medium". Soluble litter inputs were extracted from ^{13}C-, ^{15}N-labeled blue grama root litter that was grown for five months in a ^{13}C and ^{15}N continuous labeling chamber (Soong et al., 2014). We specifically chose to use

blue grama roots because blue grama is a dominant grass at CPER, and because root growth represents about 70% of the net primary production at this site (Milchunas & Lauenroth, 2001; Pendall et al., 2004). Plants were harvested after five months, and belowground material was cut at the base of the plants. Roots were washed with DI water, cut, and air dried. Dissolved organic matter from the dried roots was extracted using hot water following Soong et al., 2015. 50 g of roots were boiled in DI water at 100°C for 3 h, then filtered over a 20 µm nylon filter. Total organic C concentration of the extracted DOM was verified using a Shimadzu TOC-L/TNM-L Analyzer (Shimadzu Corporation, Kyoto, Japan) before dilution with DI to concentrations corresponding to the above input treatments. After dilution to treatment concentration, subsamples of each soluble input treatment were set aside for confirmation of DOC concentration and ^{13}C enrichment. After concentration was confirmed using the TOC analyzer, 0.05 M K_2SO_4 was added to each sample before it was freeze-dried and analyzed for %N and ^{13}C enrichment using a vario ISOTOPE cube elemental analyzer (EA; Elementar; Langenselbold, Germany) coupled to an isoprime precisION isotope ratio mass spectrometer (IRMS; Elementar; Manchester, United Kingdom). Low, medium, and high treatment concentrations corresponded to 0.5674, 1.2103, and 1.9044 mg DOM-C cumulatively added throughout the course of the 16-week incubation, as described below. Fresh DOM inputs had a C:N of 6.18, and an enrichment of 3.83 ± 0.032 atom % ^{13}C.

Both f_{MAOM} and DOM treatments were assigned to incubation units in a fully factorial design, such that every possible combination of f_{MAOM} and fresh DOM input treatment was incubated, for a total of 16 different treatments. Each treatment had five replicates, for a total of 80 incubation units or samples. Following a two-week wet-up period, all samples were incubated for 16 weeks in a constant temperature room at 25°C, during which they received fresh DOM inputs every other week.

Incubation and respiration measurements

Incubation units were set up and soils re-wet using DI water to 60% WFPS in July 2023. After being rewet, soils were allowed to sit for two weeks before receiving the bimonthly ^{13}C-labeled fresh

DOM applications described above. Every other week, samples assigned to low, medium, and high soluble litter treatments received 0.071, 0.151, or 0.238 mg of ^{13}C-labeled fresh DOM-C, respectively, in the form of 2 ml liquid addition, which was homogenously applied to the top of the soil using a pippette. All jars were flushed with CO_2-free air immediately after DOM addition. Carbon dioxide concentration in the jar headspace was then measured using a LI-COR LI 7810 infrared gas analyzer (IRGA; LI-COR Biosciences, Lincoln, NE, USA), and used as the 't_0' value in the calculations described below. After 48 h, 't_1' CO_2 concentration measurements were taken, along an additional 20 mL gas sample for ^{13}C-CO_2 analysis using a GHG IsoFLOW (Elementar, Langenselbold, Germany) coupled to the IRMS. We used the difference between CO_2 concentrations at t_1 and t_0 sampling timepoints, as well as atom % ^{13}C-CO_2 values, in calculations of both total and DOM-derived cumulative respiration, described below. After measuring respiration rate and sampling for ^{13}C-CO_2 analysis, jar lids were unscrewed but left on top of the jar such that all incubation units remained covered, but that enough moisture was allowed to evaporate from the soil so that fresh DOM could be applied again in another 12 days. In this way, soils could be maintained at 60% WFPS for the 48-h period in which the jars were tightly sealed, and soils did not become waterlogged after several DOM additions. Excluding the two-week wet-up period, this procedure was followed for 16 weeks for a total of 8 DOM applications and respiration measurements. At the end of the incubation, soils were harvested, thoroughly homogenized, and subsampled for combined size and density fraction as well as measurement of microbial community composition, mass-specific growth rate, and CUE using the methods described below.

Combined size and density fractionation

To fully understand the fate of the added DOM, as well as SOM pool transformations driven by the fresh DOM additions, at the end of the incubation we sought to separate the POM fraction by density in order to isolate it from the organic matter associated to the coarse heavy (i.e., sand) fraction of soil (CHAOM), as this pool was found to be chemically distinct from light POM (Leuthold et al., 2024). After harvest, a subsample from all soils were separated by both density (1.85 g cm^{-3}) and size (53 μm) after mechanical dispersion as described in Zhang et al., 2021. Briefly, 5.5-6.0 g of soil were shaken in DI

water for 15 min, then centrifuged at 3400 rpm. DOM was decanted over a 20 µm nylon filter and stored at -20°C. Any particulate material on the filter was set aside as part of the light POM fraction (<1.85 g cm^{-3}). Twelve glass beads and 1.85 g cm^{-3} sodium polytungstate (SPT) were added to the soil residue and shaken for 18 h to disperse aggregates. Soils were then centrifuged for 30 min at 3400 rpm, and the remaining light POM was aspirated onto a 20 µm nylon filter. The pellet (>1.85 g cm^{-3}) was rinsed multiple times to remove any remaining SPT before wet-sieving to separate it into coarse, heavy organic matter (CHAOM; >53µm), and MAOM (<53µm). All DOM extracts were analyzed for total organic C using the TOC analyzer, while all solid fractions were oven-dried at 60°C then finely ground to ensure homogenization before being analyzed for %C and ^{13}C using the EA-IRMS, as described above.

Microbial community composition, mass-specific growth rate, and CUE

We used incorporation of C and H into microbial phospholipid fatty acids (PLFAs) to quantify microbial community composition, biomass, and usage of fresh DOM inputs, as well as mass-specific microbial growth rate and community CUE. Given that microbes use H atoms from water to synthesize new cell wall components when they grow and divide, we utilized a novel ^{2}H-based method to measure directly measure growth rates of microbial functional groups via incorporation of ^{2}H-labeled water into PLFAs (Canarini et al., 2023, with modifications for liquid water).

Immediately after harvest, we set aside a 4.5 g subsample of each sample to be incubated with ^{2}H-labeled water at 60% WFPS for an additional 48 h. Subsamples were weighed into 10 mL cryovials and placed inside 50 mL centrifuge tubes. Two atom % ^{2}H-labeled water was applied homogenously to the top of each subsample using a pipette. We also incubated an additional 3 replicates per fresh DOM x f_{MAOC} treatment with the same DI water used throughout the rest of the experiment to serve as natural abundance controls in downstream isotope calculations (see *Data processing*, below). After applying either ^{2}H-labeled or natural abundance DI water, tubes containing soils to be incubated were flushed with CO_2-free air, tightly sealed with Suba Seal air-tight silicone stoppers, and measured for t_0 CO_2

concentrations. At the end of the 48-h ^{2}H incubation, respiration was measured on each sample once more (i.e., t_1) before all soils were flash-frozen in liquid N. Soils were stored at -80°C before they were freeze-dried in preparation for phospholipid fatty acid (PLFA) extraction.

Freeze-dried samples were subsampled to approximately 2 g, which were used for PLFA extraction following Gorka et al., 2023. Briefly, total lipids were extracted from the ~2 g subsamples using a chloroform:methanol:citric acid buffer mixture, then separated by solid-phase extraction on silica columns. The neutral-lipid and glycolipid fatty acid fractions were discarded before collecting the PLFA fraction by eluting columns with a 5:5:1 chloroform:methanol:water mixture. After adding an internal standard (i.e., fatty acid methyl ester 19:0), PLFAs were converted to fatty acid methyl esters (FAMEs) by transesterification. Samples were analyzed for C and H quantity, as well as ^{13}C and ^{2}H incorporation, using a Trace GC Ultra connected by a GC-IsoLink to a Delta V Advantage Mass Spectrometer (Thermo Fisher Scientific, Waltham, MA, USA). Samples were injected in splitless mode (injector temperature 300 °C) and separated on a DB5 column (60 m × 0.25 mm × 0.25 μm; Agilent, Vienna, Austria) with 1.2 ml He min^{-1} as the carrier gas (GC program: 1 min at 80 °C, 30 °C min^{-1} to 150 °C, 1 min at 150 °C, 4 °C min^{-1} to 230 °C, 30 min at 230 °C, 30 °C min^{-1} to 280 °C and 19 min at 280 °C). Sample FAMEs were identified using standard mixtures of bacterial and fungal FAMEs (i.e., Bacterial Acid Methyl Ester CP Mixture (Matreya LLC, State College, PA, USA) and 37 Comp. FAME Mix (Supelco, Bellefonte, PA, USA)), and quantified against the 19:0 internal standard. Sample atom % ^{2}H values were normalized to the Vienna Standard Mean Ocean Water (VSMOW) scale using the slope and intercept of measured values of known isotopic standards USGS70 and USGS72 (Arndt Schimmelmann, Indiana University, USA). Atom % ^{13}C values did not require this correction (Canarini et al., 2023), and were directly used in DOM-derived PLFA calculations.

We identified a total of 18 different fatty acids in both C and H data sets. We considered fatty acids 10Me17:0, 10Me18:0, i15:0, a15:0, i16:0, i17:0 and a17:0 as markers of gram-positive bacteria, with 10Me17:0 and 10Me18:0 being specific markers of actinobacteria; 16:1ω7, 19:1ω9, and cy17:0 as markers of gram-negative bacteria (Quideau et al., 2016); 18:1ω9cis and 18:2ω6,9 as markers of

saprotrophic fungi (Frostegård et al., 2011); and 16:1ω5 as a marker of arbuscular mycorrhizal fungi (AMF). We considered the remaining fatty acids 17:0Me, 18:1ω9trans, 16:0, and 17:0 to be general biomarkers that cannot be exclusively assigned to any bacterial or fungal group (Quideau et al., 2016). Additionally, while we also identified general fatty acid 18:0, large discrepancies in the quantity of this marker found in our C and H data suggested that it may have been contaminated. As such, we removed it from both data sets entirely.

We also measured microbial biomass carbon (MBC) for use in calculations of community CUE (see *Data processing*, below) using chloroform fumigation extraction (Jenkinson & Powlson, 1976; Kelly et al., 2022). Briefly, soils were divided into two 5-g subsamples. The first was immediately extracted with 25 mL of 0.05 M K_2SO_4 on a rotary shaker at 200 rpm for 2 h, then gravity-filtered through an 8 μm Whatman 40 filter. The second subsample was fumigated for 24 h with vaporized chloroform in a sealed vacuum chamber before being identically extracted. Both fumigated and unfumigated extracts were frozen at -20°C before being analyzed for total organic C using a Shimadzu TOC-L/TNM-L Analyzer. Microbial biomass C concentrations were estimated by difference between fumigated and unfumigated subsample pairs, then applying a 0.45 correction for extraction efficiency (Canarini et al., 2023).

Data processing and calculations

Respiration and C fraction data processing

We first converted all our respiration rate data to μg C respired g soil^{-1} day^{-1} (C_{resp}) following:

$$C_{resp} = \frac{C_{t1} - C_{t0}}{t} \quad (4.1)$$

Where C_{t1} is the C-CO_2 concentration at t_1 sampling timepoints, C_{t0} is the C-CO_2 concentration at t_0 sampling timepoints, and t is the amount of time that passed being samplings. We also converted all C fraction data to mg fraction-C g soil^{-1} before calculating the proportion of C derived from the added DOM using an isotope mixing model, following:

$$F_{label} = \frac{at\%^{13}C_{sample} - at\%^{13}C_{control}}{at\%^{13}C_{label} - at\%^{13}C_{control}} \quad (4.2)$$

Where F_{label} is the proportion of CO_2 respired or fraction C derived from the ^{13}C-labeled litter, $at\%^{13}C_{sample}$ is the ^{13}C enrichment of CO_2 or specific C pool of a given sample, $at\%^{13}C_{control}$ is the average enrichment of that sample's corresponding natural abundance control (i.e., DI water) treatment, and $at\%^{13}C_{label}$ is the enrichment of our applied soluble litter inputs (i.e., 3.83 atom %). After calculating $F_{label,}$ we multiplied it by respiration rate and the C concentration of each fraction to determine DOM-derived respiration rate (μg litter-derived C g soil^{-1} day^{-1}) and DOM-derived C fraction concentration (μg fraction-C g soil^{-1}).

Because incubation jars were left covered but unsealed to prevent the soil from becoming waterlogged after several soluble litter applications, we were unable to directly measure cumulative total and DOM-derived respiration over the course of the incubation. As such, DOM-derived respiration was assumed to be the difference between the C applied as DOM and the DOM-C recovered in SOM at the end of the incubation. We estimated cumulative total respiration using the trapezoidal method, assuming that rates of native soil C respiration were fairly constant from one sampling time point to another unlike fresh DOM, which might be expected to be respired very quickly after application (i.e., DOM-derived respiration peaked very quickly after application). Lines were drawn from one sampling point to another, creating trapezoids. The area of these trapezoids was calculated and summed to approximate the cumulative total amount of C respired throughout the incubation.

We calculated the efficiency of litter-derived C incorporation into each C pool relative to the amount of soluble litter added. We also calculated change in total C pools relative to DI water control treatments, by subtracting the average DI water control from its corresponding fraction treatment to get change in C. We used this method as opposed to subtracting from initial fraction values because different fractionation schemes were employed at the beginning and end of the incubation, and fractions from different separation schemes are not equivalent in chemical composition (Leuthold et al., 2024). These values, along with the total amount of native and litter-derived C in each C pool, were applied in downstream statistical analyses.

Microbial community composition and fresh DOM incorporation

Carbon and H PLFA data sets were processed separately. As described above, we used the C data set for assessments of microbial community composition, biomass, and incorporation of soluble litter inputs. To assess community composition and biomass, we calculated the concentration of each fatty acid in ng C g soil^{-1} relative to the 19:0 internal standard, then summed these values according to the functional group designations described above (Canarini et al., 2023).

To quantify microbial incorporation of fresh DOM inputs, we determined the amount of DOM-derived C in each fatty acid (i.e., $C_{DOM\_derived}$) by calculating atom % excess, following:

$$C_{DOM\_derived} = \frac{at\%^{13}C_{FA} - at\%^{13}C_{controlFA}}{at\%^{13}C_{label}} \times C_{FA\_C} \quad (4.3)$$

Where $at\%^{13}C_{FA}$ is the ^{13}C enrichment of a specific fatty acid in a given sample, $at\%^{13}C_{controlFA}$ is the average enrichment of that fatty acid in the sample's corresponding natural abundance control (i.e., DI water) treatment, $at\%^{13}C_{label}$ is the enrichment of the applied soluble litter (i.e., 3.83 atom % ^{13}C), and C_{FA_C} is the C concentration of that fatty acid relative to the 19:0 internal standard (i.e., the values used for community composition and biomass assessments). We then summed values of $C_{DOM\_derived}$ in groups corresponding to the functional group designations described above to calculate the amount of soluble litter incorporated by gram positive and negative bacteria, actinomycetes, general fungi, AMF, and general microbes.

Mass-specific microbial growth rate and community CUE

We used our H PLFA data for assessing mass-specific microbial growth rate and community CUE following Canarini et al., 2023. We first determined the newly produced C in each fatty acid (C_{prodFA}) in ng C g soil^{-1} over the course of the 48 h ^{2}H incubation by calculating atom % excess, following:

$$C_{prodFA} = \frac{at\%^{2}H_{FA} - at\%^{2}H_{controlFA}}{a \times at\%^{2}H_{label}} \times C_{FA\_H} \quad (4.4)$$

Where $at\%^{2}H_{FA}$ is the ^{2}H enrichment of a specific fatty acid in a given sample, $at\%^{2}H_{control}$ is the average enrichment of that fatty acid in the sample's corresponding natural abundance control (i.e., DI water) treatment, $at\%^{2}H_{label}$ is the enrichment of the water applied in the 48-h ^{2}H incubation (i.e., 2 atom

%), a is the assimilation efficiency of ^2H into fatty acids (i.e., 0.71; Caro et al., 2023; Kopf et al., 2015), and C_{FA_H} is the C concentration of the fatty acid calculated relative to the 19:0 internal standard, using our H data set. We then calculated mass-specific growth rate for each fatty acid in mg C g MBC^{-1} h^{-1} (C_{prodFA_rate}) following:

$$C_{prodFA\_rate} = \frac{C_{prodFA}}{C_{FA\_H} \times t} \quad (4.5)$$

Where t represents the amount of time in h soils were incubated with ^2H-labeled water. We summed these calculated values according to the same functional group designations used for our C PLFA data set to determine mass-specific growth of gram positive and negative bacteria, actinomycetes, general fungi, AMF, and general microbes. We also summed values for all fatty acids together to calculate mass-specific growth for the whole community.

To calculate community CUE, we first calculated the amount of C that microbes allocated to growth (C_{growth}) following:

$$C_{growth} = \frac{C_{prod\_total} \times MBC}{C_H \times t} \quad (4.6)$$

Where C_{prod_total} is the total amount of fatty acids produced over the 48 h ^2H incubation (i.e., sum of C_{prod} for all fatty acids), MBC is microbial biomass C measured using chloroform fumigation extraction in µg C g $soil^{-1}$, after applying a 0.45 extraction efficiency correction (Canarini et al., 2023; Vance et al., 1987), and C_H is total microbial biomass measured using our H PLFA data (i.e., sum of C_{H_FA} for all fatty acids). We then used values of C_{growth} to calculate CUE following:

$$CUE = \frac{C_{growth}}{C_{growth} + C_{resp}} \quad (4.7)$$

Where C_{resp} is the total amount of C respired over the 48 h ^2H incubation (Manzoni et al., 2012). Along with the mass-specific growth rate values for the whole community and individual microbial functional groups, we applied these community CUE values in downstream statistical analyses.

Statistical analyses

We first assessed the extent to which f_{MAOM} impacted differences in microbial communities respiring on fresh DOM inputs, as well as the full community. To do so, we applied permutational Analysis of Variance (PERMANOVA) and permutational dispersion (PERMDISP) tests through the R package *vegan* (Oksanen et al., 2012) to Euclidean distance matrices of our PLFA data. PERMANOVAs were performed using the *adonis2*() function, and allowed for direct and interactive effects of fresh DOM inputs and f_{MAOC} treatments. Separate PERMDISP tests were performed using the *betadisper*() function for the effects of fresh DOM and f_{MAOM}, and any significant differences in dispersion were further investigated using Tukey *post hoc* pairwise comparisons. Differences in community composition and dispersion were visualized using Principal Coordinates Analysis (PCoA).

Unfortunately, the f_{MAOM} treatments did not generate the expected differences in community composition as they were designed to (see *Results*, below). As such, we excluded f_{MAOM} from our remaining statistical analyses, and focused our efforts specifically on the effects of fresh DOM additions on microbial physiology, DOM-derived fraction formation efficiency, and changes in total C, independent of f_{MAOM}. We applied one-way ANOVAs with DOM inputs as the predictor variable to all microbial physiological traits, DOM-derived and total fractions and cumulative respiration, DOM-derived fraction formation efficiency, and change in total fraction C pools. Like tests of community dispersion, any significant differences were further investigated using Tukey *post hoc* pairwise comparisons.

After quantifying how fresh DOM additions affected microbial community physiology and SOM fractions, we assessed relationships among physiological traits that are expected to influence each other, including CUE, growth rate, and total biomass, as well as CUE, growth rate, and DOM incorporation efficiency, using simple linear regressions. We then used these same analyses to understand how these physiological traits impacted the formation efficiency of each fraction, as well as changes in total pool size of each fraction caused by DOM additions (e.g., priming), regardless of the effects of fresh DOM treatment on any of the above variables. Specifically, we regressed each of the above four microbial traits with both formation efficiency and C change in each fraction. All data were transformed as necessary to

meet assumptions of the above statistical tests, and we considered p values less than 0.05 to be statistically significant. All analyses were carried out in R version 4.1.1 (R Core Team, 2021).

Results

Effects of f_{MAOM} and fresh DOM additions on microbial communities

We first assessed whether our variations in f_{MAOM}, designed to manipulation microbial community composition, had intended effects on community composition and dispersion. Contrary to our expectations, we found no significant differences in the composition of the full community ($F_{3,78}$=4.721, p=1) or of the community metabolizing DOM inputs with f_{MAOM} ($F_{3,45}$=5.9538, p=1; Fig. 4.1). The same pattern occurred with community dispersion, with only marginally significant differences in dispersion among f_{MAOM} treatments for full communities ($F_{3,75}$=2.494, p=0.066) and no differences in dispersion among communities respiring on fresh DOM ($F_{3,53}$=1.56, p=0.21). Similarly, DOM inputs did not significantly impact the composition of full communities ($F_{3,78}$=1.872, p=1), or those respiring on applied DOM ($F_{3,63}$=34.39, p=1). While full community dispersion did not differ with DOM inputs ($F_{3,75}$=1.49, p=0.224), those metabolizing fresh DOM in the high input treatment more dispersed than communities in both medium (p=0.037) and low (p=4.26e-5) treatments ($F_{2,54}$=11.41, p=7.37e-5; Fig. 4.1). Based on this, we focused the rest of this study on the effects of fresh DOM addition only, across all three f_{MAOM} treatments and the non-recombined soil control.

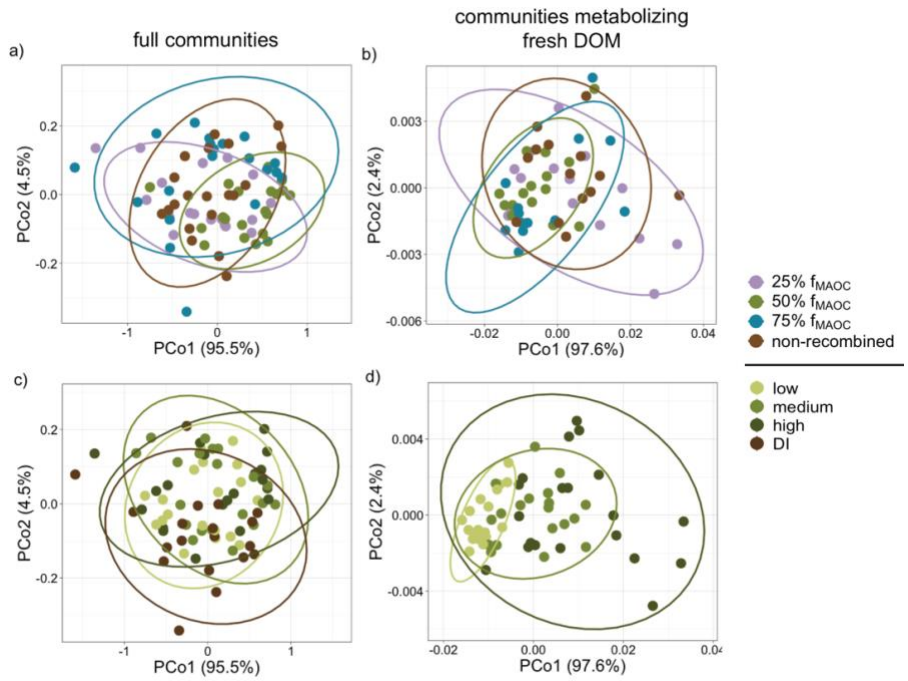

Figure 4.1. Differences in composition and dispersion in full microbial communities (**a**, **c**) and microbial communities metabolizing fresh dissolved organic matter (DOM) additions (**b, d**). Different colors in **a)** and **b)** indicate f_{MAOC} treatments, and colors in **c)** and **d)** indicate DOM treatments. In all panels, ellipses indicate 95% confidence intervals.

Fresh DOM additions did not impact microbial growth rate ($F_{3,75}$=0.73, p=0.538), community CUE ($F_{3,75}$=0.727, p=0.539), or total microbial biomass ($F_{3,75}$=0.82, p=0.487; Fig. 4.2). Except for the total biomass of general PLFA markers, which had higher biomass in the DI water control compared to fresh DOM input treatments (Tables A4.3; Figures. A4.3), similar patterns occurred in the growth rate and total biomass of individual microbial groups (Tables A4.1, A4.3; Figures A2.1, A2.3). Fresh DOM additions, however, did affect the efficiency of fresh DOM incorporation by microbes ($F_{2,57}$=5.498, p=0.0066), with the low addition treatment having greater incorporation efficiency than the high (p=0.0052). While the DOM incorporation efficiencies of actinomycetes and saprotrophic fungi were unaffected by DOM addition treatments, incorporation efficiencies of gram positive and negative bacteria, AMF, and general PLFA biomass followed the same trends as that of the total community (Table A4.2, Figure A4.2). Although growth rate, CUE, and biomass were not related to DOM additions, all three were significantly related to each other (Figure 4.3). Specifically, greater CUE led to increases in mass-specific

growth ($F_{1,76}$=27.34, p=1.454e-6; r^2=0.265), which led to greater total microbial biomass ($F_{1,76}$=4.442, p=0.038; r^2=0.055). These relationships were corroborated by a positive association between CUE and total biomass ($F_{1,76}$=8.289, p=0.0052; r^2=0.098). Additionally, while CUE had a positive relationship with DOM incorporation efficiency into microbial biomass ($F_{1,57}$=8.964, p=0.0041; r^2=0.136), growth rate was not related to the incorporation efficiency of fresh DOM into microbial biomass ($F_{1,57}$=1.178, p=0.282; Figure 4.3).

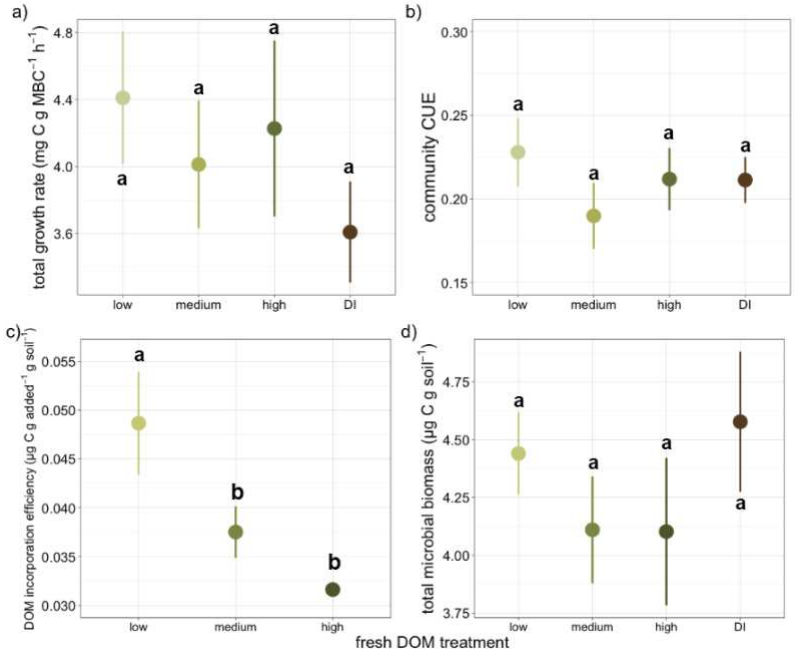

Figure 4.2. Effects of fresh dissolved organic matter (DOM) additions on **a**) total microbial growth rate, **b**) community CUE, **c**) DOM incorporation efficiency into microbial biomass, and **d**) total microbial biomass. Points and error bars represent group means and standard error, and statistical significance is indicated by letters above each data point.

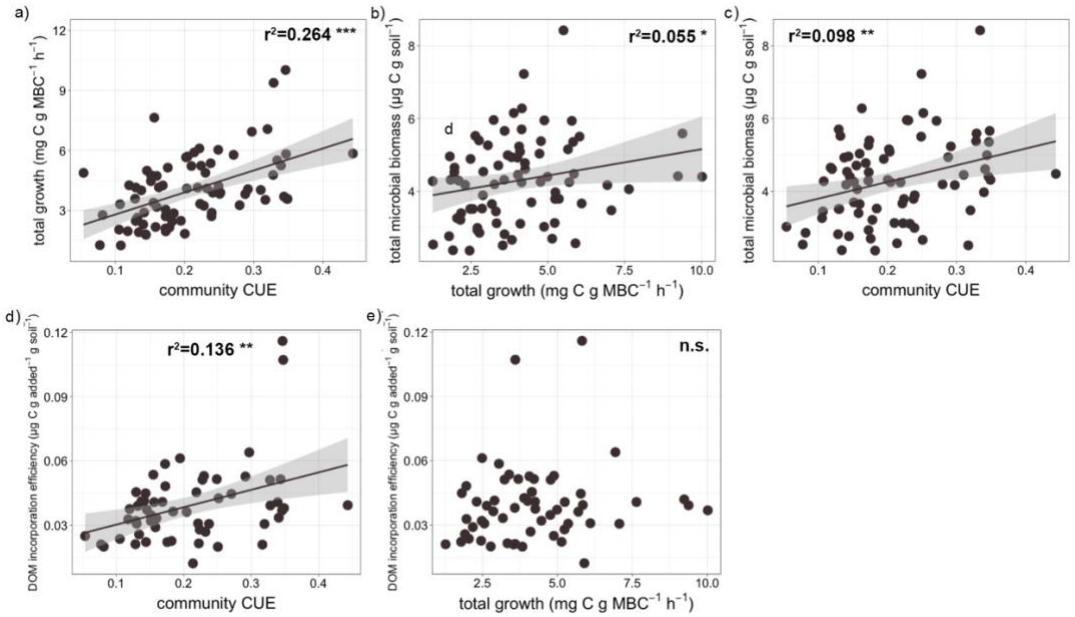

Figure 4.3. Relationships between **a**) carbon use efficiency (CUE) and total growth rate, **b**) growth rate and total microbial biomass, **c**) CUE and total microbial biomass, **d**) CUE and DOM incorporation efficiency into microbial biomass, and **e**) total growth and DOM incorporation efficiency into microbial biomass. Regression lines are only shown in statistically significant relationships, indicated by asterisks (p<0.05*, p<0.01**, p<0.001***, *n.s.* non-signficant).

Fate and incorporation efficiency of fresh DOM inputs

Across all C fractions, there was more DOM-derived C under high DOM inputs than medium or low (Table A4.4, Figure A4.4). Cumulative litter-derived respiration responded similarly, with more DOM-derived C being respired under high inputs than medium or low (Table A4.4, Figure A4.4). Despite this, there was more cumulative DOM-derived C respired relative to the total amount of fresh DOM added when inputs were medium or high than when they were low ($F_{2,47}$=3.442, p=0.0401; Figure 4.4). Additionally, DOM-derived MAOM ($F_{2,47}$=3.442, p=0.0401) and soil DOM ($F_{2,47}$=3.442, p=0.0401) formation efficiencies were greatest under high inputs. There were no effects of fresh DOM additions on DOM-derived light POM ($F_{2,47}$=3.442, p=0.0401) or CHAOM ($F_{2,47}$=3.442, p=0.0401) formation efficiencies (Figure 4.4)

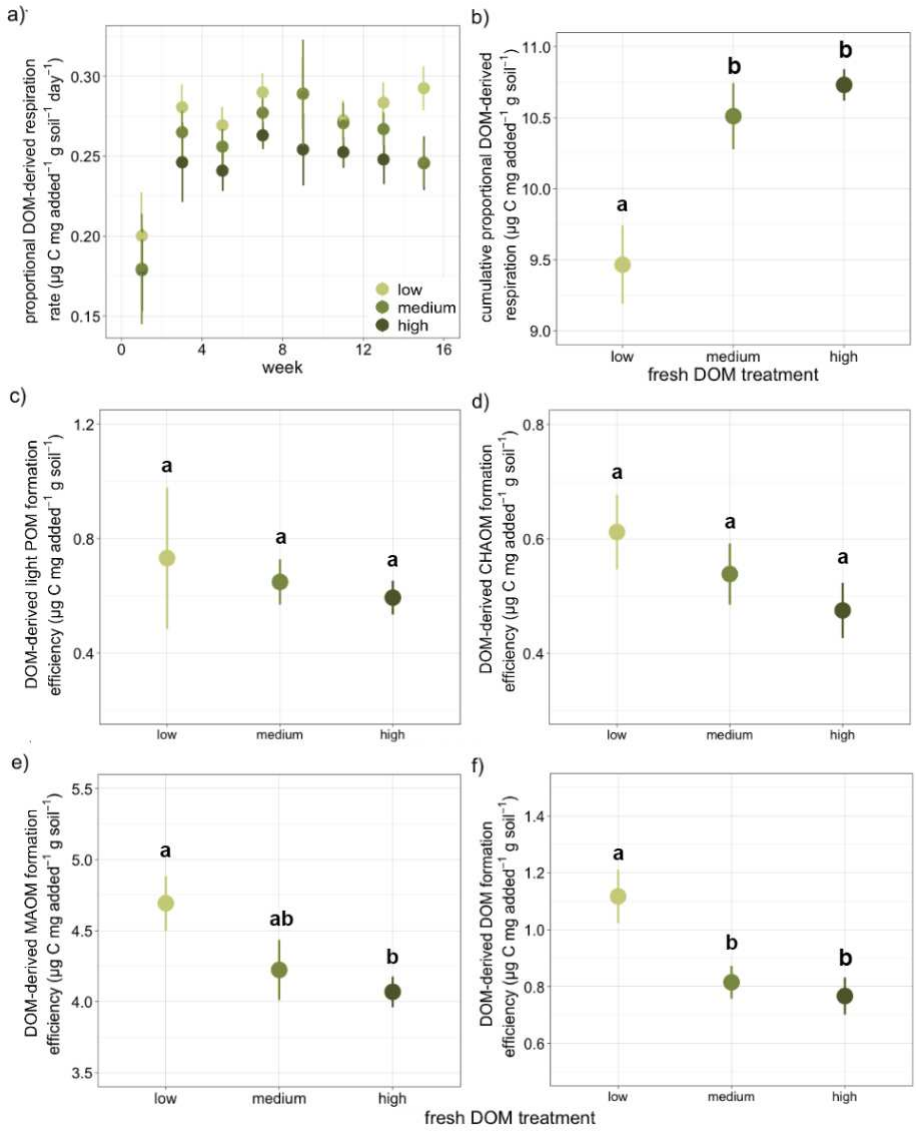

Figure 4.4. Proportion of fresh dissolved organic matter (DOM) additions found in each pool. Panel **a**) indicates proportional DOM-derived respiration rate and **b**) indicates cumulative proportional DOM-derived respiration. Panels **c-f** indicate formation efficiency of DOM-derived C in **c**) light particulate organic matter (POM), d) organic matter associated with coarse, heavy minerals (e.g., sand; CHAOM), **e**) mineral-associated organic matter (MAOM), and **f**) DOM. Data points and error bars represent group means and standard error. Any statistically significant differences are noted in letters above data points.

Effects of fresh DOM addition on changes in total C pools

Total C storage in all fractions and cumulative respiration varied with DOM addition treatment (Table A4.5, Figure A4.5). By the end of the incubation, addition of fresh DOM resulted in higher cumulative respiration and increased C storage in CHAOM, MAOM, and DOM as compared to control

soils receiving only DI water, while it primed the decomposition of light POM (Figure 4.5). In fact, POM had significantly lower C in the DOM-amended soils than in the DI water control soils (Table A2.5, Figure A4.5). However, there were no differences in C storage changes over the incubation time among DOM addition treatments, and light POM ($F_{2,57}$=0.475, p=0.624), CHAOM ($F_{2,57}$=0.021, p=0.979), MAOM ($F_{2,57}$=0.522, p=0.596), and DOM ($F_{2,55}$=0.611, p=0.547) had similar amounts of C at the end of the incubation across fresh DOM addition treatments (Figure 4.5).

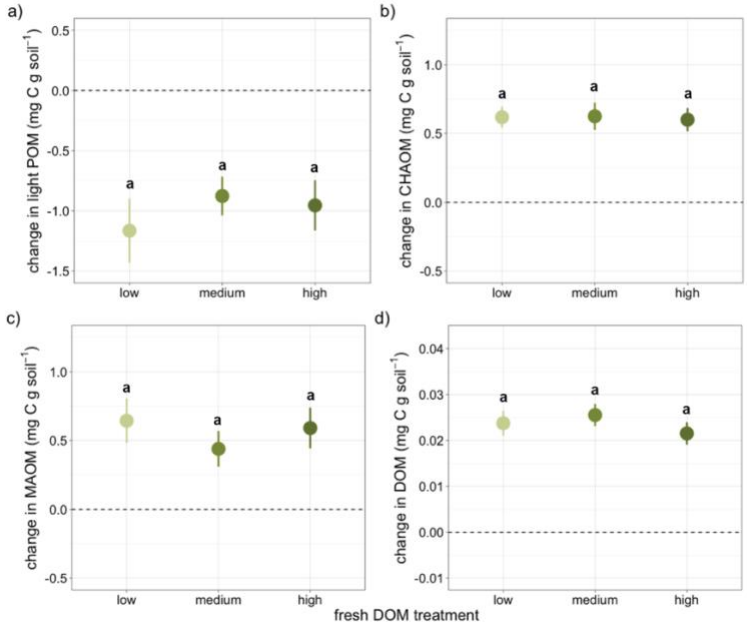

Figure 4.5. Effects of fresh dissolved organic matter (DOM) addition on change in total carbon (C) storage in **a**) light particulate organic matter (POM), **b**) organic matter associated with coarse, heavy minerals (CHAOM), **c**) mineral-associated organic matter (MAOM), and **d**) dissolved organic matter (DOM). Data points and error bars represent group means and standard error. We did not find any significant differences the change in any fraction among fresh DOM addition treatments.

Microbial functional contributions to fraction formation efficiency and change

After assessing how fresh DOM additions impacted microbial physiology, DOM-derived fraction formation efficiency, and changes in fraction C storage, we quantified the extent to which fraction formation efficiency and total fraction change were influenced by microbial physiology. None of the microbial traits assessed in this study, including growth rate, community CUE, DOM incorporation

efficiency, and total microbial biomass, were related to either DOM-derived fraction formation efficiency or total fraction change (Figure 4.6; Table A4.6).

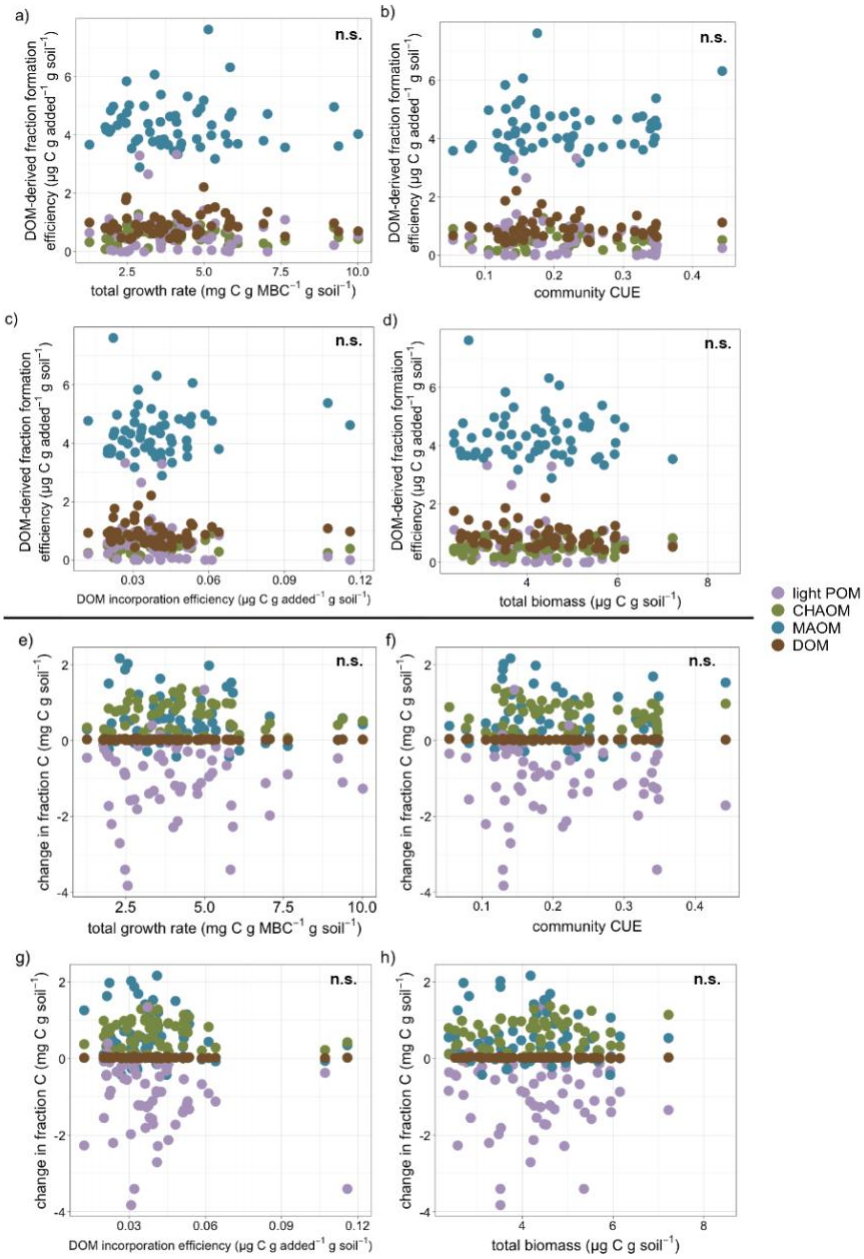

Figure 4.6. Effects of microbial traits, including mass-specific growth rate (**a, e**), community carbon use efficiency (CUE; **b, f**), dissolved organic matter (DOM) incorporation efficiency into microbial biomass (**c, g**), and total biomass (**d, h**) on fresh DOM-derived fraction formation efficiency (**a-d**) and change in fraction C storage relative to DI water controls (**e-h**). Different colors indicate each fraction, including light particulate organic matter (POM), organic matter associated with coarse, heavy minerals (CHAOM), mineral-associated organic matter (MAOM), and DOM. We did not find any significant relationships

between the assessed microbial traits and either DOM-derived fraction formation efficiency or change in fraction C.

Discussion

In this study, we used isotopic labeling in a controlled laboratory incubation to assess the extent to which copiotrophic and oligotrophic microbial life history strategies, proxied through direct measurement of microbial growth rate, impact the formation efficiency of fresh DOM-derived C, as well as changes in existing C pools receiving fresh DOM inputs compared to their associated DI water control treatments. We found little evidence that supports application of copio- and oligotrophy to assessments of microbial community ecology or SOM fraction storage, whereby none of the microbial traits measured were related to DOM inputs, C fraction formation efficiency, or change in C fraction storage. However, fresh DOM inputs did lead to differences in MAOM formation efficiency, with low inputs leading to the most efficient MAOM formation. Additionally, we found that positive priming affected only the light POM fraction, providing preliminary evidence that CHAOM and MAOM may share some mechanisms of formation and persistence (Samson et al., 2020; Zhang et al., 2021).

While we observed expected trends in relationships among the microbial traits measured, whereby greater CUE led to greater growth and greater biomass production, we did not find any relationships or interactions between f_{MAOM}, fresh DOM additions, and microbial traits. Although our DOM additions may have been too low or too similar to one another to illicit statistically difference microbial physiological responses, and the taxonomic resolution of our PLFA analyses may not have been fine enough to identify differential expression of copio- and oligotrophic behaviors (Stone et al., 2023), this finding indicates that microbial growth rate is not responsive to differences in small substrate availability, or to variations in which fraction C is stored in. This is contrary to assessments of growth rate responses to climatic changes, whereby microbes can rapidly adjust growth rates in responses to changes in both temperature and moisture (i.e., drought; Canarini et al., 2023). In combination with DNA-based evidence that microbes do not reliably express copio- or oligotrophy (Stone et al., 2023), this study

demonstrates that copiotrophic and oligotrophic life history strategies do not apply to microbial communities associated with SOM fractions, thus making them unapplicable to changes in POM and MAOM storage. It is possible that growth rate may be more strongly controlled by a separate suite of environmental variables, such as climate (Canarini et al., 2023), rather than by the availability of soluble substrates in the soil. As such, we recommend that the soils community move on from copiotrophic and oligotrophic designations as a conceptualization of microbial responses to resource availability. Furthermore, the microbiome of specific SOM physical fractions should be characterized across multiple soils. Our expectations that size-separated POM and MAOM would be characterized by contrasting microbial communities was not supported (Figure 4.1). Recent evidence also corroborated by this study that POM is better separated by density due to its distinct chemical composition from CHAOM (Leuthold et al., 2024), and that it may behave more like MAOM (Samson et al., 2020), indicates that microbiome characterization of SOM fractions should be done on POM, CHAOM, and MAOM that have been separated using a combined density and size fractionation scheme.

In addition to the lack of effects of fresh DOM additions on microbial growth and CUE, microbial traits did not have any impacts on DOM-derived fraction formation efficiency or the changes in fractions relative to their associated DI water controls. This lack of relationship between microbial physiological traits is supported by recent work on microbial mediation of litter quality effects on MAOM formation, where microbial physiology did not influence MAOM storage (Craig et al., 2022). As stated above, it may be that climatic, ecosystem, and soil properties such as temperature (Schimel, 2018), litter quality (Cleveland et al., 2014; Cruz-Paredes & Rousk, 2024), and pH (Rousk et al., 2009) are stronger controls on microbial growth and activity than soluble resource availability (Das et al., 2024; Rui et al., 2022). Variation in these properties may illicit changes in microbial behavior large enough to impact fraction C storage, especially in POM (Hansen et al., 2024). In addition to providing further support to the notion that copio- and oligotrophic life histories are not applicable to microbes or changes in soil C storage, these speculations are in line with recent frameworks of controls on C storage in POM and

MAOM, whereby microbial effects on SOM fractions are strongly controlled by a combination of climate, litter quality, and soil properties, especially under climatic extremes (Cotrufo et al., 2021).

Despite the lack of relationships between microbial traits and SOM fraction storage, we found that fresh DOM additions led to differences in the fraction of C respired relative to the amount applied, as well as the formation efficiency of DOM and MAOM. While greater DOM additions lead to greater DOM-derived C formation, lower additions were associated with proportionally lower DOM-derived respiration and higher DOM-derived MAOC formation efficiency. This indicates that lower additions of soluble substrates stimulate more efficient processing of that input, despite leading to less new C formation. While rhizodeposition and inputs of low molecular weight C substrates have overall higher new C formation efficiencies than structural root and leaf litter (Villarino et al., 2021), this finding challenges the representation of first order decomposition kinetics found in many of the most commonly used process-based models, including DAYCENT (Parton et al., 1998) and RothC (Coleman & Jenkinson, 1996). Though preliminary, our results suggest that the amount of C input affects its fate, as well as the relative distribution of the pathways it can follow as it is transformed into SOM. While further work is needed to confirm whether low DOM inputs also result in the greatest MAOM formation efficiency in the field, these findings provide early evidence of additional influences on MAOM formation that could be used to improve development of models predicting C cycling in a variety of ecosystems.

In addition to greater MAOM formation efficiency under low DOM inputs, we found that all DOM addition rates, regardless of amount, stimulated changes in each fraction, relative to its associated DI water control. Specifically, we found that positive priming of native SOM occurred only in light POM, with decreases in light POM being accompanied by proportional increases in CHAOM, MAOM, and soil DOM. The exact mechanism behind these findings are unclear, as changes in fraction C storage were not related to fresh DOM addition rate or any of the microbial traits measured in this study. However, given that increases in CHAOM, MAOM, and soil DOM (i.e., averages of 0.614 ± 0.04, 0.558 ± 0.084, and 0.024 ± 0.001 mg C g $soil^{-1}$, respectively) were all greater than fresh DOM-derived increases in C storage, and that their sum corresponded approximately to the amount of C lost from light POM (i.e., -0.998 ±

0.124 mg C g soil^{-1}) it is reasonable to assume that they represent C transfer from light POM decomposition (Soong & Cotrufo, 2015), which may have followed either a direct *ex-vivo* pathway, or first undergone microbial uptake and incorporation before being sorbed to coarse (i.e., CHAOM) and fine minerals (i.e., MAOM) as microbial products and necromass. It could also be that light POM decomposition products were first transferred to CHAOM, which may represent an intermediate pool where POM decomposition products are transiently stored before stabilization in MAOM (Leuthold et al., 2024; Samson et al., 2020), although the singular harvest in this experiment prohibits testing of this idea. Regardless, these findings provide evidence that priming occurs mainly in the light POM fraction. They are also in line with previous work indicating that addition of soluble substrates induce priming of relatively unprotected SOM fractions, while resulting in increases in C storage of coarse- and fine mineral-associated SOM fractions (Olayemi et al., 2022). Furthermore, consistent increases in both CHAOM and MAOM in soils receiving fresh DOM inputs compared to their associated DI water controls indicate that the processes driving CHAOM formation are more similar to MAOM than those of light POM. Though characterization of the chemical signatures of these fractions through Fourier Transform-Infrared (FTIR) spectroscopy or similar technologies are needed to confirm the source of these increases (i.e., plant or microbial; structural or soluble; e.g., Grandy et al., 2007; Kallenbach et al., 2016; Neurath et al., 2021; Simpson et al., 2007), it appears that CHAOM may be formed from the decomposition products of POM, and possibly serve as precursor to MAOM formation (Leuthold, 2024). Though speculatory, these findings provide preliminary information on CHAOM formation mechanisms that could be used to develop further hypotheses on the roles it plays in C storage dynamics and more generally, the specific ecosystem services its accumulation provides.

More broadly, the lack of evidence in this study, as well as others (Craig et al., 2022; Stone et al., 2023) for expression of copio- and oligotrophy in microbial communities and for direct relationships (i.e., not controlled by other ecosystem or climatic properties) between microbial growth and MAOM formation indicates that growth rate and activity, when considered without environmental or taxonomic context, may not be a significant controls on C storage in POM or MAOM. As such, microbial

interventions in agricultural soils aimed at enhancing soil C storage may want to focus efforts on identification of environment-specific traits that can promote POM retention or MAOM formation within a specific soil or climate type. Given that environment appears to much a stronger control on microbial mediation of C cycling than microbial functionality itself, identifying environment-specific traits, as opposed to selecting physiologies that could enhance C storage without consideration of the specific climate or soil type in which that intervention would be applied, could lead to more effective implementation of microbe-centric climate change mitigation strategies.

In conclusion, this study demonstrates that copiotrophic and oligotrophic life history strategies as approximated by direct measurements of microbial growth rate and CUE, are likely not applicable to either microbial physiology or changes in C storage of POM or MAOM. Despite a complete lack of relationships with microbial physiology, DOM-derived fraction formation efficiency, and change in C storage in each fraction, we show that lower additions of soluble inputs are incorporated into MAOM more efficiently and with proportionally less C lost through respiration than higher additions. Additionally, we show that fresh DOM additions stimulated positive priming in the light POM fraction, with concurrent increases in both CHAOM and MAOM. While more work is needed to identify the specific mechanisms behind this, as well as greater formation efficiency of stable C fractions under lower soluble inputs, these results indicate that CHAOM may be formed through mechanisms that are more similar to MAOM than light POM. With further research on microbial structural and functional influences on SOM formation, we may be able to more comprehensively apply microbial community ecology to climate change mitigation efforts that involve soil C sequestration.

CHAPTER 5: Conclusion

Given the lack of studies investigating global controls in C storage in POM and MAOM, as well as the extent to which microbial traits related to microbial functionality mediate POM and MAOM, this dissertation sought to fill knowledge gaps about global controls on and microbial contributions to SOM cycling through a combination of data syntheses, individual-based modeling, and experimental work. First, my synthesis and path analysis work indicates that at the global scale, POM storage is controlled primarily by variables that regulate microbial activity, while MAOM storage is primarily controlled by variables related to C inputs to the soil, as well as the availability of soil minerals for stabilization of low molecular weight compounds. Second, my individual-based modeling work indicates that microbial social interactions (i.e., interactions between microbes that produce enzymes at different rates) can generated emergent behaviors that support community survival, efficiency, as well as retention of POM under wide variety of substrate quality (C:N) and MAOM saturation levels. This work is highly relevant to continued development of process-based models, where implementation of flexible enzyme production based on soluble substrate availability may be a way to simulate these emergent behaviors at the ecosystem scale. Lastly, although my incubation experiment on copio- and oligotrophic life history strategies demonstrates that these traits are likely not relevant to microbial communities or to changes in POM and MAOM storage, it indicates that priming in response to DOM additions occurs primarily within the light POM fraction, and that MAOM and CHAOM may have similar mechanisms of formation. Broadly, all of the above indicates that microbial functionality may be a control on the retention of POM but not on MAOM formation, which appears to be more strongly controlled by a combination of C inputs to the soil and soil properties.

The idea that microbial functionality is a stronger control on POM than MAOM is supported by other work relating abundance of C degradation gene pathways to POM storage, but not any other fractions (Gao et al., 2024). However, given that microbial traits themselves do not always control POM and MAOM storage, they may represent a secondary regulator on C storage. Because climate and certain

soil conditions like anoxia are strong controls on microbial activity, it may be that extremes in climate and other broad-scale influences on microbial activity represent a first control on microbial mediation of POM storage. The specific traits of microbial decomposers may be more relevant to patterns of SOM storage at smaller spatial scales, where microbes can be expected to be within the same climate or ecosystem type, or in more mesic environments, where extreme conditions may not create a strong selection pressure for specific microbial ecologies (Cotrufo et al., 2021; Cotrufo & Lavallee, 2022). However, greater measurement of microbial community traits, in conjunction with SOM fractions, litter quality, and a variety of soil properties, at scale is needed to robustly test this hypothesis.

In combination with other work investigating contributions of microbial necromass to SOM formation, this work also points to the hypothesis that an entirely different suite of microbial traits may be related to MAOM formation, including the chemical composition of microbial necromass (Buckeridge et al., 2022; Camenzind et al., 2023). While unexplored in this dissertation, variations in the proportion of necromass composed of structural *versus* low molecular weight compounds could dictate whether necromass contributes to MAOM (if it is more soluble in composition), to POM (if it is more structural), or whether it is catabolized by living microbes (Buckeridge et al., 2022; Camenzind et al., 2023; Kindler et al., 2006; Schweigert et al., 2015). Further, given that MAOM storage is reflective of C inputs to the soil (Hansen et al., 2024), mutualisms between plants and soil microbes, especially mycorrhizae, may be an indirect mechanism by which microbes contribute to MAOM formation. In promoting plant productivity (Klironomos et al., 2000; Van Der Heijden et al., 2006, 2008), these mutualisms may stimulate C inputs to the soil, which could then lead to new MAOM formation through either *ex vivo* or *in vivo* formation pathways (Keller et al., 2021). Additionally, though also unexplored in this dissertation, interactions between arbuscular mycorrhizae, ectomycorrhizae, and saprotrophic fungi (i.e., Gadgil effects; Gadgil & Gadgil, 1971) could also impact microbial contributions to MAOM (Frey, 2019; Hicks Pries et al., 2023; Horsch et al., 2023). While further work is needed to explore these hypotheses, they underscore the complexity of SOM formation and the multifaceted roles that microbial processes play in driving soil C storage.

Ultimately, this dissertation highlights a need to focus research efforts not just on how microbes can be leveraged to enhance soil C storage, but also on the specific traits contributing to maintenance *versus* loss of soil C stored in POM. This is particularly important for retention of C in ecosystems that are extremely sensitive to climate change, such as tundras and wetlands, where the highest C densities in the world are stored in POM. If we are not able to protect these POM stores, increases in global temperatures could promote microbial activity and POM decomposition, leading to further climate-C feedbacks, degradation of these ecosystems, and exacerbation the negative effects of global climate change. Additionally, given that specific microbial functionalities (e.g., flexible enzyme production) promote POM retention, combining microbial interventions that promote these functionalities with other regenerative management strategies that increase C inputs to the soil could be an effective way to prevent loss of those new inputs. As such, while soil microbes may not be the 'silver bullet' in the fight against climate change they are often purported to be in popular science, their functionalities are a useful tool to prevent additional losses of soil C that could accelerate global climate change.

REFERENCES

Abdalla, M., Hastings, A., Chadwick, D. R., Jones, D. L., Evans, C. D., Jones, M. B., Rees, R. M., & Smith, P. (2018). Critical review of the impacts of grazing intensity on soil organic carbon storage and other soil quality indicators in extensively managed grasslands. *Agriculture, Ecosystems & Environment*, *253*, 62–81. https://doi.org/10.1016/j.agee.2017.10.023

Allison, S. D., & Vitousek, P. M. (2005). Responses of extracellular enzymes to simple and complex nutrient inputs. *Soil Biology and Biochemistry*, *37*(5), 937–944. https://doi.org/10.1016/j.soilbio.2004.09.014

Allison, S. D., Wallenstein, M. D., & Bradford, M. A. (2010). Soil-carbon response to warming dependent on microbial physiology. *Nature Geoscience*, *3*(5), 336–340. https://doi.org/10.1038/ngeo846

Allison, V. J., Condron, L. M., Peltzer, D. A., Richardson, S. J., & Turner, B. L. (2007). Changes in enzyme activities and soil microbial community composition along carbon and nutrient gradients at the Franz Josef chronosequence, New Zealand. *Soil Biology and Biochemistry*, *39*(7), 1770–1781. https://doi.org/10.1016/j.soilbio.2007.02.006

Angst, G., Mueller, K. E., Castellano, M. J., Vogel, C., Wiesmeier, M., & Mueller, C. W. (2023). Unlocking complex soil systems as carbon sinks: Multi-pool management as the key. *Nature Communications*, *14*(1), Article 1. https://doi.org/10.1038/s41467-023-38700-5

Angst, G., Mueller, K. E., Nierop, K. G. J., & Simpson, M. J. (2021). Plant- or microbial-derived? A review on the molecular composition of stabilized soil organic matter. *Soil Biology and Biochemistry*, *156*, 108189. https://doi.org/10.1016/j.soilbio.2021.108189

Ashagrie, Y., Zech, W., Guggenberger, G., & Mamo, T. (2007). Soil aggregation, and total and particulate organic matter following conversion of native forests to continuous cultivation in Ethiopia. *Soil and Tillage Research*, *94*(1), 101–108. https://doi.org/10.1016/j.still.2006.07.005

Balesdent, J., Chenu, C., & Balabane, M. (2000). Relationship of soil organic matter dynamics to physical protection and tillage. *Soil and Tillage Research*, *53*(3), 215–230. https://doi.org/10.1016/S0167-1987(99)00107-5

Beck, H. E., Zimmermann, N. E., McVicar, T. R., Vergopolan, N., Berg, A., & Wood, E. F. (2018). Present and future Köppen-Geiger climate classification maps at 1-km resolution. *Scientific Data*, *5*(1), 180214. https://doi.org/10.1038/sdata.2018.214

Begill, N., Don, A., & Poeplau, C. (2023). No detectable upper limit of mineral-associated organic carbon in temperate agricultural soils. *Global Change Biology*, gcb.16804. https://doi.org/10.1111/gcb.16804

Benbi, D. K., Boparai, A. K., & Brar, K. (2014). Decomposition of particulate organic matter is more sensitive to temperature than the mineral associated organic matter. *Soil Biology and Biochemistry*, *70*, 183–192. https://doi.org/10.1016/j.soilbio.2013.12.032

Boetius, A., & Lochte, K. (1994). Regulation of microbial enzymatic degradation of organic matter in deep-sea sediments. *Marine Ecology Progress Series*, *104*, 299–307. https://doi.org/10.3354/meps104299

Bouajila, A., & Tahar, G. (2010). Land use effect on soil and particulate organic carbon, and aggregate stability in some soils in Tunisia. *African Journal of Agricultural Research*, *5*.

Bradford, M. A., Carey, C. J., Atwood, L., Bossio, D., Fenichel, E. P., Gennet, S., Fargione, J., Fisher, J. R. B., Fuller, E., Kane, D. A., Lehmann, J., Oldfield, E. E., Ordway, E. M., Rudek, J., Sanderman, J., & Wood, S. A. (2019). Soil carbon science for policy and practice. *Nature Sustainability*, *2*(12), Article 12. https://doi.org/10.1038/s41893-019-0431-y

Bradford, M. A., Keiser, A. D., Davies, C. A., Mersmann, C. A., & Strickland, M. S. (2013). Empirical evidence that soil carbon formation from plant inputs is positively related to microbial growth. *Biogeochemistry*, *113*(1), 271–281. https://doi.org/10.1007/s10533-012-9822-0

Bradford, M. A., Wood, S. A., Addicott, E. T., Fenichel, E. P., Fields, N., González-Rivero, J., Jevon, F. V., Maynard, D. S., Oldfield, E. E., Polussa, A., Ward, E. B., & Wieder, W. R. (2021). Quantifying microbial control of soil organic matter dynamics at macrosystem scales. *Biogeochemistry*, *156*(1), 19–40. https://doi.org/10.1007/s10533-021-00789-5

Buchkowski, R. W., Bradford, M. A., Grandy, A. S., Schmitz, O. J., & Wieder, W. R. (2017). Applying population and community ecology theory to advance understanding of belowground biogeochemistry. *Ecology Letters*, *20*(2), 231–245. https://doi.org/10.1111/ele.12712

Buckeridge, K. M., Creamer, C., & Whitaker, J. (2022). Deconstructing the microbial necromass continuum to inform soil carbon sequestration. *Functional Ecology*, *36*(6), 1396–1410. https://doi.org/10.1111/1365-2435.14014

Burns, R. G., DeForest, J. L., Marxsen, J., Sinsabaugh, R. L., Stromberger, M. E., Wallenstein, M. D., Weintraub, M. N., & Zoppini, A. (2013). Soil enzymes in a changing environment: Current knowledge and future directions. *Soil Biology and Biochemistry*, *58*, 216–234. https://doi.org/10.1016/j.soilbio.2012.11.009

Camenzind, T., Mason-Jones, K., Mansour, I., Rillig, M. C., & Lehmann, J. (2023). Formation of necromass-derived soil organic carbon determined by microbial death pathways. *Nature Geoscience*. https://doi.org/10.1038/s41561-022-01100-3

Canarini, A., Fuchslueger, L., Schnecker, J., Metze, D., Nelson, D. B., Kahmen, A., Watzka, M., Pötsch, E. M., Schaumberger, A., Bahn, M., & Richter, A. (2023). *Soil fungi remain active and invest in storage compounds during drought independent of future climate conditions*. https://doi.org/10.1101/2023.10.23.563577

Caro, T. A., McFarlin, J., Jech, S., Fierer, N., & Kopf, S. (2023). Hydrogen stable isotope probing of lipids demonstrates slow rates of microbial growth in soil. *Proceedings of the National Academy of Sciences*, *120*(16), e2211625120. https://doi.org/10.1073/pnas.2211625120

Chandel, A. K., Jiang, L., & Luo, Y. (2023). Microbial Models for Simulating Soil Carbon Dynamics: A Review. *Journal of Geophysical Research: Biogeosciences*, *128*(8), e2023JG007436. https://doi.org/10.1029/2023JG007436

Chen, Q., Hu, Y., Hu, A., Niu, B., Yang, X., Jiao, H., Xu-Ri, Song, L., & Zhang, G. (2021). Shifts in the dynamic mechanisms of soil organic matter transformation with nitrogen addition: From a soil carbon/nitrogen-driven mechanism to a microbe-driven mechanism. *Soil Biology and Biochemistry*, *160*, 108355. https://doi.org/10.1016/j.soilbio.2021.108355

Chen, R., Yin, L., Wang, X., Chen, T., Jia, L., Jiang, Q., Lyu, M., Yao, X., & Chen, G. (2023). Mineral-associated organic carbon predicts the variations in microbial biomass and specific enzyme activities in a subtropical forest. *Geoderma*, *439*, 116671. https://doi.org/10.1016/j.geoderma.2023.116671

Churkina, G., & Running, S. W. (1998). Contrasting Climatic Controls on the Estimated Productivity of Global Terrestrial Biomes. *Ecosystems*, *1*(2), 206–215. https://doi.org/10.1007/s100219900016

Cleveland, C. C., & Liptzin, D. (2007). C:N:P stoichiometry in soil: Is there a "Redfield ratio" for the microbial biomass? *Biogeochemistry*, *85*(3), 235–252. https://doi.org/10.1007/s10533-007-9132-0

Cleveland, C. C., Reed, S. C., Keller, A. B., Nemergut, D. R., O'Neill, S. P., Ostertag, R., & Vitousek, P. M. (2014). Litter quality versus soil microbial community controls over decomposition: A quantitative analysis. *Oecologia*, *174*(1), 283–294. https://doi.org/10.1007/s00442-013-2758-9

Coleman, K., & Jenkinson, D. S. (1996). RothC-26.3—A Model for the turnover of carbon in soil. In D. S. Powlson, P. Smith, & J. U. Smith (Eds.), *Evaluation of Soil Organic Matter Models* (pp. 237–246). Springer. https://doi.org/10.1007/978-3-642-61094-3_17

Conant, R. T., Ryan, M. G., Ågren, G. I., Birge, H. E., Davidson, E. A., Eliasson, P. E., Evans, S. E., Frey, S. D., Giardina, C. P., Hopkins, F. M., Hyvönen, R., Kirschbaum, M. U. F., Lavallee, J. M., Leifeld, J., Parton, W. J., Megan Steinweg, J., Wallenstein, M. D., Martin Wetterstedt, J. Å., & Bradford, M. A. (2011). Temperature and soil organic matter decomposition rates – synthesis of

current knowledge and a way forward. *Global Change Biology*, *17*(11), 3392–3404. https://doi.org/10.1111/j.1365-2486.2011.02496.x

Córdova, S. C., Olk, D. C., Dietzel, R. N., Mueller, K. E., Archontouilis, S. V., & Castellano, M. J. (2018). Plant litter quality affects the accumulation rate, composition, and stability of mineral-associated soil organic matter. *Soil Biology and Biochemistry*, *125*, 115–124. https://doi.org/10.1016/j.soilbio.2018.07.010

Cotrufo, M. F. (2019). Soil carbon storage informed by particulate and mineral-associated organic matter. *Nature Geoscience*, *12*, 8.

Cotrufo, M. F., Haddix, M. L., Kroeger, M. E., & Stewart, C. E. (2022). The role of plant input physical-chemical properties, and microbial and soil chemical diversity on the formation of particulate and mineral-associated organic matter. *Soil Biology and Biochemistry*, *168*, 108648. https://doi.org/10.1016/j.soilbio.2022.108648

Cotrufo, M. F., & Lavallee, J. M. (2022). Soil organic matter formation, persistence, and functioning: A synthesis of current understanding to inform its conservation and regeneration. In *Advances in Agronomy* (Vol. 172, pp. 1–66). Elsevier. https://doi.org/10.1016/bs.agron.2021.11.002

Cotrufo, M. F., Lavallee, J. M., Six, J., & Lugato, E. (2023). The robust concept of mineral-associated organic matter saturation: A letter to Begill et al., 2023. *Global Change Biology*, *29*(21), 5986–5987. https://doi.org/10.1111/gcb.16921

Cotrufo, M. F., Lavallee, J. M., Zhang, Y., Hansen, P. M., Paustian, K. H., Schipanski, M., & Wallenstein, M. D. (2021). I n -N-O ut: A hierarchical framework to understand and predict soil carbon storage and nitrogen recycling. *Global Change Biology*, *27*(19), 4465–4468. https://doi.org/10.1111/gcb.15782

Cotrufo, M. F., Soong, J. L., Horton, A. J., Campbell, E. E., Haddix, M. L., Wall, D. H., & Parton, W. J. (2015). Formation of soil organic matter via biochemical and physical pathways of litter mass loss. *Nature Geoscience*, *8*(10), 776–779. https://doi.org/10.1038/ngeo2520

Cotrufo, M. F., Wallenstein, M. D., Boot, C. M., Denef, K., & Paul, E. (2013). The Microbial Efficiency-Matrix Stabilization (MEMS) framework integrates plant litter decomposition with soil organic matter stabilization: Do labile plant inputs form stable soil organic matter? *Global Change Biology*, *19*(4), 988–995. https://doi.org/10.1111/gcb.12113

Craig, M. E., Geyer, K. M., Beidler, K. V., Brzostek, E. R., Frey, S. D., Stuart Grandy, A., Liang, C., & Phillips, R. P. (2022). Fast-decaying plant litter enhances soil carbon in temperate forests but not through microbial physiological traits. *Nature Communications*, *13*(1), 1229. https://doi.org/10.1038/s41467-022-28715-9

Craig, M. E., Turner, B. L., Liang, C., Clay, K., Johnson, D. J., & Phillips, R. P. (2018). Tree mycorrhizal type predicts within-site variability in the storage and distribution of soil organic matter. *Global Change Biology*, *24*(8), 3317–3330. https://doi.org/10.1111/gcb.14132

Crowther, T. W., Sokol, N. W., Oldfield, E. E., Maynard, D. S., Thomas, S. M., Bradford, M. A., Crowther, T. W., Sokol, N. W., Oldfield, E. E., Maynard, D. S., Thomas, S. M., & Bradford, M. A. (2015). Environmental stress response limits microbial necromass contributions to soil organic carbon. *Soil Biology and Biochemistry*, *Complete*(85), 153–161. https://doi.org/10.1016/j.soilbio.2015.03.002

Cruz-Paredes, C., & Rousk, J. (2024). Controls of microbial carbon use efficiency along a latitudinal gradient across Europe. *Soil Biology and Biochemistry*, *193*, 109394. https://doi.org/10.1016/j.soilbio.2024.109394

Das, S., Pendall, E., Malik, A. A., Nannipieri, P., & Kim, P. J. (2024). Microbial control of soil organic matter dynamics: Effects of land use and climate change. *Biology and Fertility of Soils*, *60*(1), 1–3. https://doi.org/10.1007/s00374-023-01788-4

Davidson, E. A., & Janssens, I. A. (2006). Temperature sensitivity of soil carbon decomposition and feedbacks to climate change. *Nature*, *440*(7081), Article 7081. https://doi.org/10.1038/nature04514

Eclesia, R. P., Jobbagy, E. G., Jackson, R. B., Rizzotto, M., & Piñeiro, G. (2016). Stabilization of new carbon inputs rather than old carbon decomposition determines soil organic carbon shifts following woody or herbaceous vegetation transitions. *Plant and Soil*, *409*(1–2), 99–116. https://doi.org/10.1007/s11104-016-2951-9

Ernakovich, J. G., Baldock, J., Creamer, C., Sanderman, J., Kalbitz, K., & Farrell, M. (2021). A combined microbial and ecosystem metric of carbon retention efficiency explains land cover-dependent soil microbial biodiversity–ecosystem function relationships. *Biogeochemistry*, *153*(1), 1–15. https://doi.org/10.1007/s10533-020-00736-w

Fick, S. E., & Hijmans, R. J. (2017). WorldClim 2: New 1-km spatial resolution climate surfaces for global land areas. *International Journal of Climatology*, *37*(12), 4302–4315. https://doi.org/10.1002/joc.5086

Fierer, N., Bradford, M. A., & Jackson, R. B. (2007). TOWARD AN ECOLOGICAL CLASSIFICATION OF SOIL BACTERIA. *Ecology*, *88*(6), 1354–1364. https://doi.org/10.1890/05-1839

Frey, S. D. (2019). Mycorrhizal Fungi as Mediators of Soil Organic Matter Dynamics. *Annual Review of Ecology, Evolution, and Systematics*, *50*(1), 237–259. https://doi.org/10.1146/annurev-ecolsys-110617-062331

Frøseth, R. B., & Bleken, M. A. (2015). Effect of low temperature and soil type on the decomposition rate of soil organic carbon and clover leaves, and related priming effect. *Soil Biology and Biochemistry*, *80*, 156–166. https://doi.org/10.1016/j.soilbio.2014.10.004

Frostegård, Å., Tunlid, A., & Bååth, E. (2011). Use and misuse of PLFA measurements in soils. *Soil Biology and Biochemistry*, *43*(8), 1621–1625. https://doi.org/10.1016/j.soilbio.2010.11.021

Fuhrmann, J. J., & Zuberer, D. A. (2021). Carbon transformations and soil organic matter formation. In *Principles and Applications of Soil Microbiology* (pp. 327–361). Elsevier. https://doi.org/10.1016/B978-0-12-820202-9.00013-7

Gadgil, R. L., & Gadgil, P. D. (1971). Mycorrhiza and Litter Decomposition. *Nature*, *233*(5315), 133–133. https://doi.org/10.1038/233133a0

Gao, Y., Huang, D., Zhang, Y., McLaughlin, N., Zhang, Y., Wang, Y., Chen, X., Zhang, S., Lu, Y., & Liang, A. (2024). Precipitation increment reinforced warming-induced increases in soil mineral-associated and particulate organic matter under agricultural ecosystem. *Applied Soil Ecology*, *196*, 105301. https://doi.org/10.1016/j.apsoil.2024.105301

Georgiou, K., Abramoff, R. Z., Harte, J., Riley, W. J., & Torn, M. S. (2017). Microbial community-level regulation explains soil carbon responses to long-term litter manipulations. *Nature Communications*, *8*(1), 1223. https://doi.org/10.1038/s41467-017-01116-z

Georgiou, K., Jackson, R. B., Vindušková, O., Abramoff, R. Z., Ahlström, A., Feng, W., Harden, J. W., Pellegrini, A. F. A., Polley, H. W., Soong, J. L., Riley, W. J., & Torn, M. S. (2022). Global stocks and capacity of mineral-associated soil organic carbon. *Nature Communications*, *13*(1), 3797. https://doi.org/10.1038/s41467-022-31540-9

Gorka, S., Darcy, S., Horak, J., Imai, B., Mohrlok, M., Salas, E., Richter, A., Schmidt, H., Wanek, W., Kaiser, C., & Canarini, A. (2023). Beyond PLFA: Concurrent extraction of neutral and glycolipid fatty acids provides new insights into soil microbial communities. *Soil Biology and Biochemistry*, *187*, 109205. https://doi.org/10.1016/j.soilbio.2023.109205

Grandy, A. S., Neff, J. C., & Weintraub, M. N. (2007). Carbon structure and enzyme activities in alpine and forest ecosystems. *Soil Biology and Biochemistry*, *39*(11), 2701–2711. https://doi.org/10.1016/j.soilbio.2007.05.009

Haddix, M. L., Gregorich, E. G., Helgason, B. L., Janzen, H., Ellert, B. H., & Francesca Cotrufo, M. (2020). Climate, carbon content, and soil texture control the independent formation and persistence of particulate and mineral-associated organic matter in soil. *Geoderma*, *363*, 114160. https://doi.org/10.1016/j.geoderma.2019.114160

Haddix, M. L., Paul, E. A., & Cotrufo, M. F. (2016). Dual, differential isotope labeling shows the preferential movement of labile plant constituents into mineral-bonded soil organic matter. *Global Change Biology*, *22*(6), 2301–2312. https://doi.org/10.1111/gcb.13237

Hall, E. K., Bernhardt, E. S., Bier, R. L., Bradford, M. A., Boot, C. M., Cotner, J. B., del Giorgio, P. A., Evans, S. E., Graham, E. B., Jones, S. E., Lennon, J. T., Locey, K. J., Nemergut, D., Osborne, B. B., Rocca, J. D., Schimel, J. P., Waldrop, M. P., & Wallenstein, M. D. (2018). Understanding how microbiomes influence the systems they inhabit. *Nature Microbiology*, *3*(9), 977–982. https://doi.org/10.1038/s41564-018-0201-z

Hansen, P. M., Even, R., King, A. E., Lavallee, J., Schipanski, M., & Cotrufo, M. F. (2024). Distinct, direct and climate-mediated environmental controls on global particulate and mineral-associated organic carbon storage. *Global Change Biology*, *30*(1), e17080. https://doi.org/10.1111/gcb.17080

Harris, D., Horwáth, W. R., & van Kessel, C. (2001). Acid fumigation of soils to remove carbonates prior to total organic carbon or CARBON-13 isotopic analysis. *Soil Science Society of America Journal*, *65*(6), 1853–1856. https://doi.org/10.2136/sssaj2001.1853

Harzing, A.-W., & Alakangas, S. (2016). Google Scholar, Scopus and the Web of Science: A longitudinal and cross-disciplinary comparison. *Scientometrics*, *106*(2), 787–804. https://doi.org/10.1007/s11192-015-1798-9

Hassink, J. (1997). The capacity of soils to preserve organic C and N by their association with clay and silt particles. *Plant and Soil*, *191*(1), 77–87. https://doi.org/10.1023/A:1004213929699

He, X., Abramoff, R., Abs, E., Georgiou, K., Zhang, H., & Goll, D. S. (2023). *Contribution of carbon inputs to soil carbon accumulation cannot be neglected* [Preprint]. Ecology. https://doi.org/10.1101/2023.07.17.549330

Heckman, K. A., Possinger, A. R., Badgley, B. D., Bowman, M. M., Gallo, A. C., Hatten, J. A., Nave, L. E., SanClements, M. D., Swanston, C. W., Weiglein, T. L., Wieder, W. R., & Strahm, B. D. (2023). Moisture-driven divergence in mineral-associated soil carbon persistence. *Proceedings of the National Academy of Sciences*, *120*(7), e2210044120. https://doi.org/10.1073/pnas.2210044120

Heckman, K., Hicks Pries, C. E., Lawrence, C. R., Rasmussen, C., Crow, S. E., Hoyt, A. M., Fromm, S. F., Shi, Z., Stoner, S., McGrath, C., Beem-Miller, J., Berhe, A. A., Blankinship, J. C., Keiluweit, M., Marín-Spiotta, E., Monroe, J. G., Plante, A. F., Schimel, J., Sierra, C. A., … Wagai, R. (2022). Beyond bulk: Density fractions explain heterogeneity in global soil carbon abundance and persistence. *Global Change Biology*, *28*(3), 1178–1196. https://doi.org/10.1111/gcb.16023

Herndon, E., AlBashaireh, A., Singer, D., Roy Chowdhury, T., Gu, B., & Graham, D. (2017). Influence of iron redox cycling on organo-mineral associations in Arctic tundra soil. Geochimica et Cosmochimica Acta, 207, 210–231. https://doi.org/10.1016/j.gca.2017.02.034

Hicks Pries, C. E., Lankau, R., Ingham, G. A., Legge, E., Krol, O., Forrester, J., Fitch, A., & Wurzburger, N. (2023). Differences in soil organic matter between EcM- and AM-dominated forests depend on tree and fungal identity. *Ecology*, *104*(3), e3929. https://doi.org/10.1002/ecy.3929

Hinckley, E.-L. S., Bonan, G. B., Bowen, G. J., Colman, B. P., Duffy, P. A., Goodale, C. L., Houlton, B. Z., Marín-Spiotta, E., Ogle, K., Ollinger, S. V., Paul, E. A., Vitousek, P. M., Weathers, K. C., & Williams, D. G. (2016). The soil and plant biogeochemistry sampling design for The National Ecological Observatory Network. *Ecosphere*, *7*(3), e01234. https://doi.org/10.1002/ecs2.1234

Ho, A., Di Lonardo, D. P., & Bodelier, P. L. E. (2017). Revisiting life strategy concepts in environmental microbial ecology. *FEMS Microbiology Ecology*, *93*(3). https://doi.org/10.1093/femsec/fix006

Hooper, D., Coughlan, J., & Mullen, M. R. (2008). *Structural Equation Modelling: Guidelines for Determining Model Fit*. *6*(1).

Horsch, C. C. A., Antunes, P. M., Fahey, C., Grandy, A. S., & Kallenbach, C. M. (2023). Trait-based assembly of arbuscular mycorrhizal fungal communities determines soil carbon formation and retention. *New Phytologist*, nph.18914. https://doi.org/10.1111/nph.18914

Hou, G., Delang, C. O., Lu, X., & Gao, L. (2020). A meta-analysis of changes in soil organic carbon stocks after afforestation with deciduous broadleaved, sempervirent broadleaved, and conifer tree species. *Annals of Forest Science*, *77*(4), Article 4. https://doi.org/10.1007/s13595-020-00997-3

Huang, W., Ye, C., Hockaday, W. C., & Hall, S. J. (2020). Trade-offs in soil carbon protection mechanisms under aerobic and anaerobic conditions. *Global Change Biology*, *26*(6), 3726–3737. https://doi.org/10.1111/gcb.15100

Huang, Y., Liang, C., Duan, X., Chen, H., & Li, D. (2019). Variation of microbial residue contribution to soil organic carbon sequestration following land use change in a subtropical karst region. *Geoderma*, *353*, 340–346. https://doi.org/10.1016/j.geoderma.2019.07.028

Jenkinson, D. S., & Powlson, D. S. (1976). The effects of biocidal treatments on metabolism in soil—I. Fumigation with chloroform. *Soil Biology and Biochemistry*, *8*(3), 167–177. https://doi.org/10.1016/0038-0717(76)90001-8

Jobbágy, E. G., & Jackson, R. B. (2000). The Vertical Distribution of Soil Organic Carbon and Its Relation to Climate and Vegetation. *Ecological Applications*, *10*(2), 423–436. https://doi.org/10.1890/1051-0761(2000)010[0423:TVDOSO]2.0.CO;2

Kaiser, C., Franklin, O., Dieckmann, U., & Richter, A. (2014). Microbial community dynamics alleviate stoichiometric constraints during litter decay. *Ecology Letters*, *17*(6), 680–690. https://doi.org/10.1111/ele.12269

Kaiser, C., Franklin, O., Richter, A., & Dieckmann, U. (2015). Social dynamics within decomposer communities lead to nitrogen retention and organic matter build-up in soils. *Nature Communications*, *6*(1), 8960. https://doi.org/10.1038/ncomms9960

Kalinina, O., Cherkinsky, A., Chertov, O., Goryachkin, S., Kurganova, I., Lopes De Gerenyu, V., Lyuri, D., Kuzyakov, Y., & Giani, L. (2019). Post-agricultural restoration: Implications for dynamics of soil organic matter pools. *CATENA*, *181*, 104096. https://doi.org/10.1016/j.catena.2019.104096

Kallenbach, C. M., Frey, S. D., & Grandy, A. S. (2016). Direct evidence for microbial-derived soil organic matter formation and its ecophysiological controls. *Nature Communications*, *7*(1), 13630. https://doi.org/10.1038/ncomms13630

Kallenbach, C. M., Grandy, A. S., Frey, S. D., & Diefendorf, A. F. (2015). Microbial physiology and necromass regulate agricultural soil carbon accumulation. *Soil Biology and Biochemistry*, *91*, 279–290. https://doi.org/10.1016/j.soilbio.2015.09.005

Keller, A. B., Brzostek, E. R., Craig, M. E., Fisher, J. B., & Phillips, R. P. (2021). Root-derived inputs are major contributors to soil carbon in temperate forests, but vary by mycorrhizal type. *Ecology Letters*, *24*(4), 626–635. https://doi.org/10.1111/ele.13651

Kelly, C., Haddix, M. L., Byrne, P. F., Cotrufo, M. F., Schipanski, M. E., Kallenbach, C. M., Wallenstein, M. D., & Fonte, S. J. (2022). Long-term compost amendment modulates wheat genotype differences in belowground carbon allocation, microbial rhizosphere recruitment and nitrogen acquisition. *Soil Biology and Biochemistry*, *172*, 108768. https://doi.org/10.1016/j.soilbio.2022.108768

Kindler, R., Miltner, A., Richnow, H.-H., & Kästner, M. (2006). Fate of gram-negative bacterial biomass in soil—Mineralization and contribution to SOM. *Soil Biology and Biochemistry*, *38*(9), 2860–2870. https://doi.org/10.1016/j.soilbio.2006.04.047

King, A. E., Amsili, J. P., Córdova, S. C., Culman, S., Fonte, S. J., Kotcon, J., Liebig, M., Masters, M. D., McVay, K., Olk, D. C., Schipanski, M., Schneider, S. K., Stewart, C. E., & Cotrufo, M. F. (2023). A soil matrix capacity index to predict mineral-associated but not particulate organic carbon across a range of climate and soil pH. *Biogeochemistry*, *165*(1), 1–14. https://doi.org/10.1007/s10533-023-01066-3

Kirsten, M., Mikutta, R., Vogel, C., Thompson, A., Mueller, C. W., Kimaro, D. N., Bergsma, H. L. T., Feger, K.-H., & Kalbitz, K. (2021). Iron oxides and aluminous clays selectively control soil carbon storage and stability in the humid tropics. *Scientific Reports*, *11*, 5076. https://doi.org/10.1038/s41598-021-84777-7

Klironomos, J. N., McCune, J., Hart, M., & Neville, J. (2000). The influence of arbuscular mycorrhizae on the relationship between plant diversity and productivity. *Ecology Letters*, *3*(2), 137–141. https://doi.org/10.1046/j.1461-0248.2000.00131.x

Kopf, S. H., McGlynn, S. E., Green-Saxena, A., Guan, Y., Newman, D. K., & Orphan, V. J. (2015). Heavy water and ^{15} N labelling with N ano SIMS analysis reveals growth rate-dependent metabolic heterogeneity in chemostats. *Environmental Microbiology*, *17*(7), 2542–2556. https://doi.org/10.1111/1462-2920.12752

Kramer, M. G., & Chadwick, O. A. (2018). Climate-driven thresholds in reactive mineral retention of soil carbon at the global scale. *Nature Climate Change*, *8*(12), Article 12. https://doi.org/10.1038/s41558-018-0341-4

Krishna, M. P., & Mohan, M. (2017). Litter decomposition in forest ecosystems: A review. *Energy, Ecology and Environment*, *2*(4), 236–249. https://doi.org/10.1007/s40974-017-0064-9

Lajtha, K., Townsend, K. L., Kramer, M. G., Swanston, C., Bowden, R. D., & Nadelhoffer, K. (2014). Changes to particulate versus mineral-associated soil carbon after 50 years of litter manipulation in forest and prairie experimental ecosystems. *Biogeochemistry*, *119*(1), 341–360. https://doi.org/10.1007/s10533-014-9970-5

Lavallee, J. M., Conant, R. T., Haddix, M. L., Follett, R. F., Bird, M. I., & Paul, E. A. (2019). Selective preservation of pyrogenic carbon across soil organic matter fractions and its influence on calculations of carbon mean residence times. *Geoderma*, *354*, 113866. https://doi.org/10.1016/j.geoderma.2019.07.024

Lavallee, J. M., Soong, J. L., & Cotrufo, M. F. (2020). Conceptualizing soil organic matter into particulate and mineral-associated forms to address global change in the 21st century. *Global Change Biology*, *26*(1), 261–273. https://doi.org/10.1111/gcb.14859

Lehmann, J., Hansel, C. M., Kaiser, C., Kleber, M., Maher, K., Manzoni, S., Nunan, N., Reichstein, M., Schimel, J. P., Torn, M. S., Wieder, W. R., & Kögel-Knabner, I. (2020). Persistence of soil organic carbon caused by functional complexity. *Nature Geoscience*, *13*(8), 529–534. https://doi.org/10.1038/s41561-020-0612-3

Lehmann, J., & Kleber, M. (2015). The contentious nature of soil organic matter. *Nature*, *528*(7580), 60–68. https://doi.org/10.1038/nature16069

Leuthold, S. J., Haddix, M. L., Lavallee, J., & Cotrufo, M. F. (2022). Physical fractionation techniques. In *Reference Module in Earth Systems and Environmental Sciences* (p. B9780128229743000677). Elsevier. https://doi.org/10.1016/B978-0-12-822974-3.00067-7

Leuthold, S., Lavallee, J. M., Haddix, M. L., & Cotrufo, M. F. (2024). Contrasting properties of soil organic matter fractions isolated by different physical separation methodologies. *Geoderma*, *445*, 116870. https://doi.org/10.1016/j.geoderma.2024.116870

Liang, C., Amelung, W., Lehmann, J., & Kästner, M. (2019). Quantitative assessment of microbial necromass contribution to soil organic matter. *Global Change Biology*, *25*(11), 3578–3590. https://doi.org/10.1111/gcb.14781

Liang, C., Schimel, J. P., & Jastrow, J. D. (2017). The importance of anabolism in microbial control over soil carbon storage. *Nature Microbiology*, *2*(8), Article 8. https://doi.org/10.1038/nmicrobiol.2017.105

Lobe, I., Sandhage-Hofmann, A., Brodowski, S., du Preez, C. C., & Amelung, W. (2011). Aggregate dynamics and associated soil organic matter contents as influenced by prolonged arable cropping in the South African Highveld. *Geoderma*, *162*(3), 251–259. https://doi.org/10.1016/j.geoderma.2011.02.001

Lugato, E., Lavallee, J. M., Haddix, M. L., Panagos, P., & Cotrufo, M. F. (2021). Different climate sensitivity of particulate and mineral-associated soil organic matter. *Nature Geoscience*, *14*(5), 295–300. https://doi.org/10.1038/s41561-021-00744-x

Luo, R., Kuzyakov, Y., Liu, D., Fan, J., Luo, J., Lindsey, S., He, J.-S., & Ding, W. (2020). Nutrient addition reduces carbon sequestration in a Tibetan grassland soil: Disentangling microbial and

physical controls. *Soil Biology and Biochemistry*, *144*, 107764. https://doi.org/10.1016/j.soilbio.2020.107764

Luo, Z., Feng, W., Luo, Y., Baldock, J., & Wang, E. (2017). Soil organic carbon dynamics jointly controlled by climate, carbon inputs, soil properties and soil carbon fractions. *Global Change Biology*, *23*(10), 4430–4439. https://doi.org/10.1111/gcb.13767

Lupwayi, N. Z., Clayton, G. W., O'Donovan, J. T., Harker, K. N., Turkington, T. K., & Rice, W. A. (2004). Decomposition of crop residues under conventional and zero tillage. *Canadian Journal of Soil Science*, *84*(4), 403–410. https://doi.org/10.4141/S03-082

Malik, A. A., Martiny, J. B. H., Brodie, E. L., Martiny, A. C., Treseder, K. K., & Allison, S. D. (2020). Defining trait-based microbial strategies with consequences for soil carbon cycling under climate change. *The ISME Journal*, *14*(1), Article 1. https://doi.org/10.1038/s41396-019-0510-0

Malik, A. A., Puissant, J., Goodall, T., Allison, S. D., & Griffiths, R. I. (2019). Soil microbial communities with greater investment in resource acquisition have lower growth yield. *Soil Biology and Biochemistry*, *132*, 36–39. https://doi.org/10.1016/j.soilbio.2019.01.025

Manzoni, S., Taylor, P., Richter, A., Porporato, A., & Ågren, G. I. (2012). Environmental and stoichiometric controls on microbial carbon-use efficiency in soils. *New Phytologist*, *196*(1), 79–91. https://doi.org/10.1111/j.1469-8137.2012.04225.x

Martín-Martín, A., Orduna-Malea, E., Thelwall, M., & Delgado López-Cózar, E. (2018). Google Scholar, Web of Science, and Scopus: A systematic comparison of citations in 252 subject categories. *Journal of Informetrics*, *12*(4), 1160–1177. https://doi.org/10.1016/j.joi.2018.09.002

Meyer, O. (1994). Functional Groups of Microorganisms. In E.-D. Schulze & H. A. Mooney (Eds.), *Biodiversity and Ecosystem Function* (pp. 67–96). Springer. https://doi.org/10.1007/978-3-642-58001-7_4

Milchunas, D. G., & Lauenroth, W. K. (2001). Belowground Primary Production by Carbon Isotope Decay and Long-term Root Biomass Dynamics. *Ecosystems*, *4*(2), 139–150. https://doi.org/10.1007/s100210000064

Mirabito, A. J., & Chambers, L. G. (2023). Quantifying mineral-associated organic matter in wetlands as an indicator of the degree of soil carbon protection. Geoderma, 430, 116327. https://doi.org/10.1016/j.geoderma.2023.11632

Mosier, S., Apfelbaum, S., Byck, P., Calderon, F., Teague, R., Thompson, R., & Cotrufo, M. F. (2021). Adaptive multi-paddock grazing enhances soil carbon and nitrogen stocks and stabilization through mineral association in southeastern U.S. grazing lands. *Journal of Environmental Management*, *288*, 112409. https://doi.org/10.1016/j.jenvman.2021.112409

Neurath, R. A., Pett-Ridge, J., Chu-Jacoby, I., Herman, D., Whitman, T., Nico, P. S., Lipton, A. S., Kyle, J., Tfaily, M. M., Thompson, A., & Firestone, M. K. (2021). Root Carbon Interaction with Soil Minerals Is Dynamic, Leaving a Legacy of Microbially Derived Residues. *Environmental Science & Technology*, *55*(19), 13345–13355. https://doi.org/10.1021/acs.est.1c00300

Ogle, S. M., Breidt, F. J., & Paustian, K. (2005). Agricultural management impacts on soil organic carbon storage under moist and dry climatic conditions of temperate and tropical regions. *Biogeochemistry*, *72*(1), 87–121. https://doi.org/10.1007/s10533-004-0360-2

Oksanen, J., Blanchet, F. G., Kindt, R., Legendre, P., Minchin, P. R., O'Hara, R. B., Simpson, G. L., Sólymos, P., Stevens, M. H. H., & Wagner, H. (Directors). (2012). *vegan: Community Ecology Package*.

Olayemi, O. P., Kallenbach, C. M., & Wallenstein, M. D. (2022). Distribution of soil organic matter fractions are altered with soil priming. *Soil Biology and Biochemistry*, *164*, 108494. https://doi.org/10.1016/j.soilbio.2021.108494

Parihar, C. M., Singh, A. K., Jat, S. L., Ghosh, A., Dey, A., Nayak, H. S., Parihar, M. D., Mahala, D. M., Yadav, R. K., Rai, V., Satayanaryana, T., & Jat, M. L. (2019). Dependence of temperature sensitivity of soil organic carbon decomposition on nutrient management options under conservation agriculture in a sub-tropical Inceptisol. *Soil and Tillage Research*, *190*, 50–60. https://doi.org/10.1016/j.still.2019.02.016

Parton, W. J., Hartman, M., Ojima, D., & Schimel, D. (1998). DAYCENT and its land surface submodel: Description and testing. *Global and Planetary Change*, *19*(1), 35–48. https://doi.org/10.1016/S0921-8181(98)00040-X

Pascault, N., Ranjard, L., Kaisermann, A., Bachar, D., Christen, R., Terrat, S., Mathieu, O., Lévêque, J., Mougel, C., Henault, C., Lemanceau, P., Péan, M., Boiry, S., Fontaine, S., & Maron, P.-A. (2013). Stimulation of Different Functional Groups of Bacteria by Various Plant Residues as a Driver of Soil Priming Effect. *Ecosystems*, *16*(5), 810–822. https://doi.org/10.1007/s10021-013-9650-7

Pendall, E., Mosier, A. R., & Morgan, J. A. (2004). Rhizodeposition stimulated by elevated CO_2 in a semiarid grassland. *New Phytologist*, *162*(2), 447–458. https://doi.org/10.1111/j.1469-8137.2004.01054.x

Pérez-Harguindeguy, N., Díaz, S., Cornelissen, J. H. C., Vendramini, F., Cabido, M., & Castellanos, A. (2000). Chemistry and toughness predict leaf litter decomposition rates over a wide spectrum of functional types and taxa in central Argentina. *Plant and Soil*, *218*(1/2), 21–30.

Poeplau, C., Kätterer, T., Leblans, N. I. W., & Sigurdsson, B. D. (2017). Sensitivity of soil carbon fractions and their specific stabilization mechanisms to extreme soil warming in a subarctic grassland. *Global Change Biology*, *23*(3), 1316–1327. https://doi.org/10.1111/gcb.13491

Prairie, A. M., King, A. E., & Cotrufo, M. F. (2023). Restoring particulate and mineral-associated organic carbon through regenerative agriculture. *Proceedings of the National Academy of Sciences*, *120*(21), e2217481120. https://doi.org/10.1073/pnas.2217481120

Quideau, S. A., McIntosh, A. C. S., Norris, C. E., Lloret, E., Swallow, M. J. B., & Hannam, K. (2016). Extraction and Analysis of Microbial Phospholipid Fatty Acids in Soils. *Journal of Visualized Experiments*, *114*, 54360. https://doi.org/10.3791/54360

R Core Team. (2021). *R: A language and environment for statistical computing* (4.1.1) [Computer software]. R Foundation for Statistical Computing. https://www.R-project.org/

Ramos, F. T., Dores, E. F. D. C., Weber, O. L. D. S., Beber, D. C., Campelo, J. H., & Maia, J. C. D. S. (2018). Soil organic matter doubles the cation exchange capacity of tropical soil under no-till farming in Brazil. *Journal of the Science of Food and Agriculture*, *98*(9), 3595–3602. https://doi.org/10.1002/jsfa.8881

Rasmussen, C., Heckman, K., Wieder, W. R., Keiluweit, M., Lawrence, C. R., Berhe, A. A., Blankinship, J. C., Crow, S. E., Druhan, J. L., Hicks Pries, C. E., Marin-Spiotta, E., Plante, A. F., Schädel, C., Schimel, J. P., Sierra, C. A., Thompson, A., & Wagai, R. (2018). Beyond clay: Towards an improved set of variables for predicting soil organic matter content. *Biogeochemistry*, *137*(3), 297–306. https://doi.org/10.1007/s10533-018-0424-3

Rocci, K. S., Cotrufo, M. F., Ernakovich, J., Foster, E., Frey, S., Georgiou, K., Grandy, A. S., Malhotra, A., Reich, P. B., Schlerman, E. P., & Wieder, W. R. (2024). Bridging 20 Years of Soil Organic Matter Frameworks: Empirical Support, Model Representation, and Next Steps. *Journal of Geophysical Research: Biogeosciences*, *129*(6), e2023JG007964. https://doi.org/10.1029/2023JG007964

Rocci, K. S., Lavallee, J. M., Stewart, C. E., & Cotrufo, M. F. (2021). Soil organic carbon response to global environmental change depends on its distribution between mineral-associated and particulate organic matter: A meta-analysis. *Science of The Total Environment*, *793*, 148569. https://doi.org/10.1016/j.scitotenv.2021.148569

Rosseel, Y. (2012). **lavaan**: An *R* Package for Structural Equation Modeling. *Journal of Statistical Software*, *48*(2). https://doi.org/10.18637/jss.v048.i02

Rowley, M. C., Grand, S., Spangenberg, J. E., & Verrecchia, E. P. (2021). Evidence linking calcium to increased organo-mineral association in soils. *Biogeochemistry*, *153*(3), 223–241. https://doi.org/10.1007/s10533-021-00779-7

Rui, Y., Jackson, R., Cotrufo, M. F., Sanford, G., Spiesman, B., Deiss, L., Culman, S., Liang, C., & Ruark, M. (2022). Persistent soil carbon enhanced in Mollisols by well-managed grasslands but

not annual grain or dairy forage cropping systems. *Proceedings of the National Academy of Sciences*, *119*, e2118931119. https://doi.org/10.1073/pnas.2118931119

Rumpel, C., Amiraslani, F., Koutika, L.-S., Smith, P., Whitehead, D., & Wollenberg, E. (2018). Put more carbon in soils to meet Paris climate pledges. *Nature*, *564*(7734), 32–34. https://doi.org/10.1038/d41586-018-07587-4

Running, S., Mu, Q., Zhao, M., & Moreno, A. (2021). *MODIS/Terra Net Evapotranspiration Gap-Filled Yearly L4 Global 500m SIN Grid V061* [dataset]. NASA EOSDIS Land Processes DAAC. https://doi.org/10.5067/MODIS/MOD16A3GF.061

Running, S., & Zhao, M. (2019). *MOD17A3HGF MODIS/Terra Net Primary Production Gap-Filled Yearly L4 Global 500 m SIN Grid V006* [dataset]. NASA EOSDIS Land Processes DAAC. https://doi.org/10.5067/MODIS/MOD17A3HGF.006

Salonen, A.-R., Soinne, H., Creamer, R., Lemola, R., Ruoho, N., Uhlgren, O., De Goede, R., & Heinonsalo, J. (2023). Assessing the effect of arable management practices on carbon storage and fractions after 24 years in boreal conditions of Finland. *Geoderma Regional*, *34*, e00678. https://doi.org/10.1016/j.geodrs.2023.e00678

Samson, M.-É., Chantigny, M. H., Vanasse, A., Menasseri-Aubry, S., & Angers, D. A. (2020). Coarse mineral-associated organic matter is a pivotal fraction for SOM formation and is sensitive to the quality of organic inputs. *Soil Biology and Biochemistry*, *149*, 107935. https://doi.org/10.1016/j.soilbio.2020.107935

Schmidt, M. W. I., Torn, M. S., Abiven, S., Dittmar, T., Guggenberger, G., Janssens, I. A., Kleber, M., Kögel-Knabner, I., Lehmann, J., Manning, D. A. C., Nannipieri, P., Rasse, D. P., Weiner, S., & Trumbore, S. E. (2011). Persistence of soil organic matter as an ecosystem property. *Nature*, *478*(7367), 49–56. https://doi.org/10.1038/nature10386

Schweigert, M., Herrmann, S., Miltner, A., Fester, T., & Kästner, M. (2015). Fate of ectomycorrhizal fungal biomass in a soil bioreactor system and its contribution to soil organic matter formation. *Soil Biology and Biochemistry*, *88*, 120–127. https://doi.org/10.1016/j.soilbio.2015.05.012

Shipley, B. (2016). *Cause and Correlation in Biology: A User's Guide to Path Analysis, Structural Equations and Causal Inference with R* (2nd ed.). Cambridge University Press. https://doi.org/10.1017/CBO9781139979573

Simpson, A. J., Simpson, M. J., Smith, E., & Kelleher, B. P. (2007). Microbially Derived Inputs to Soil Organic Matter: Are Current Estimates Too Low? *Environmental Science & Technology*, *41*(23), 8070–8076. https://doi.org/10.1021/es071217x

Sistla, S. A., Rastetter, E. B., & Schimel, J. P. (2014). Responses of a tundra system to warming using SCAMPS: A stoichiometrically coupled, acclimating microbe–plant–soil model. *Ecological Monographs*, *84*(1), 151–170. https://doi.org/10.1890/12-2119.1

Six, J., Conant, R. T., Paul, E. A., & Paustian, K. (2002). Stabilization mechanisms of soil organic matter: Implications for C-saturation of soils. *Plant and Soil*, *241*, 155–176.

Six, J., Doetterl, S., Laub, M., Müller, C. R., & Van De Broek, M. (2024). The six rights of how and when to test for soil C saturation. *SOIL*, *10*(1), 275–279. https://doi.org/10.5194/soil-10-275-2024

Smith, P. (2016). Soil carbon sequestration and biochar as negative emission technologies. *Global Change Biology*, *22*(3), 1315–1324. https://doi.org/10.1111/gcb.13178

Smith, P., Cotrufo, M. F., Rumpel, C., Paustian, K., Kuikman, P. J., Elliott, J. A., McDowell, R., Griffiths, R. I., Asakawa, S., Bustamante, M., House, J. I., Sobocká, J., Harper, R., Pan, G., West, P. C., Gerber, J. S., Clark, J. M., Adhya, T., Scholes, R. J., & Scholes, M. C. (2015). Biogeochemical cycles and biodiversity as key drivers of ecosystem services provided by soils. *SOIL*, *1*(2), 665–685. https://doi.org/10.5194/soil-1-665-2015

Sokol, N. W., Sanderman, J., & Bradford, M. A. (2019). Pathways of mineral-associated soil organic matter formation: Integrating the role of plant carbon source, chemistry, and point of entry. *Global Change Biology*, *25*(1), 12–24. https://doi.org/10.1111/gcb.14482

Song, B., Niu, S., Li, L., Zhang, L., & Yu, G. (2014). Soil carbon fractions in grasslands respond differently to various levels of nitrogen enrichments. *Plant and Soil*, *384*(1), 401–412. https://doi.org/10.1007/s11104-014-2219-1

Soong, J. L., & Cotrufo, M. F. (2015). Annual burning of a tallgrass prairie inhibits C and N cycling in soil, increasing recalcitrant pyrogenic organic matter storage while reducing N availability. *Global Change Biology*, *21*(6), 2321–2333. https://doi.org/10.1111/gcb.12832

Soong, J. L., Parton, W. J., Calderon, F., Campbell, E. E., & Cotrufo, M. F. (2015). A new conceptual model on the fate and controls of fresh and pyrolized plant litter decomposition. *Biogeochemistry*, *124*(1–3), 27–44. https://doi.org/10.1007/s10533-015-0079-2

Soong, J. L., Reuss, D., Pinney, C., Boyack, T., Haddix, M. L., Stewart, C. E., & Cotrufo, M. F. (2014). Design and Operation of a Continuous ^{13}C and ^{15}N Labeling Chamber for Uniform or Differential, Metabolic and Structural, Plant Isotope Labeling. *Journal of Visualized Experiments*, *83*, 51117. https://doi.org/10.3791/51117

Sousa, R. F. D., Brasil, E. P. F., Figueiredo, C. C. D., & Leandro, W. M. (2015). Soil organic matter fractions in preserved and disturbed wetlands of the Cerrado biome. Revista Brasileira de Ciência Do Solo, 39(1), 222–231. https://doi.org/10.1590/01000683rbcs20150048

Stewart, C. E., Paustian, K., Conant, R. T., Plante, A. F., & Six, J. (2007). Soil carbon saturation: Concept, evidence and evaluation. *Biogeochemistry*, *86*(1), 19–31. https://doi.org/10.1007/s10533-007-9140-0

Stewart, C. E., Paustian, K., Conant, R. T., Plante, A. F., & Six, J. (2008). Soil carbon saturation: Evaluation and corroboration by long-term incubations. *Soil Biology and Biochemistry*, *40*(7), 1741–1750. https://doi.org/10.1016/j.soilbio.2008.02.014

Stone, B. W. G., Dijkstra, P., Finley, B. K., Fitzpatrick, R., Foley, M. M., Hayer, M., Hofmockel, K. S., Koch, B. J., Li, J., Liu, X. J. A., Martinez, A., Mau, R. L., Marks, J., Monsaint-Queeney, V., Morrissey, E. M., Propster, J., Pett-Ridge, J., Purcell, A. M., Schwartz, E., & Hungate, B. A. (2023). Life history strategies among soil bacteria—Dichotomy for few, continuum for many. *The ISME Journal*. https://doi.org/10.1038/s41396-022-01354-0

Thaysen, E. M., Reinsch, S., Larsen, K. S., & Ambus, P. (2017). Decrease in heathland soil labile organic carbon under future atmospheric and climatic conditions. *Biogeochemistry*, *133*(1), 17–36. https://doi.org/10.1007/s10533-017-0303-3

Todd-Brown, K. E. O., Abramoff, R. Z., Beem-Miller, J., Blair, H. K., Earl, S., Frederick, K. J., Fuka, D. R., Guevara Santamaria, M., Harden, J. W., Heckman, K., Heran, L. J., Holmquist, J. R., Hoyt, A. M., Klinges, D. H., LeBauer, D. S., Malhotra, A., McClelland, S. C., Nave, L. E., Rocci, K. S., … Younger, M. L. (2022). Reviews and syntheses: The promise of big diverse soil data, moving current practices towards future potential. *Biogeosciences*, *19*(14), 3505–3522. https://doi.org/10.5194/bg-19-3505-2022

Trivedi, P., Anderson, I. C., & Singh, B. K. (2013). Microbial modulators of soil carbon storage: Integrating genomic and metabolic knowledge for global prediction. *Trends in Microbiology*, *21*(12), 641–651. https://doi.org/10.1016/j.tim.2013.09.005

Van Der Heijden, M. G. A., Bardgett, R. D., & Van Straalen, N. M. (2008). The unseen majority: Soil microbes as drivers of plant diversity and productivity in terrestrial ecosystems. *Ecology Letters*, *11*(3), 296–310. https://doi.org/10.1111/j.1461-0248.2007.01139.x

Van Der Heijden, M. G. A., Streitwolf-Engel, R., Riedl, R., Siegrist, S., Neudecker, A., Ineichen, K., Boller, T., Wiemken, A., & Sanders, I. R. (2006). The mycorrhizal contribution to plant productivity, plant nutrition and soil structure in experimental grassland. *New Phytologist*, *172*(4), 739–752. https://doi.org/10.1111/j.1469-8137.2006.01862.x

Vance, E. D., Brookes, P. C., & Jenkinson, D. S. (1987). An extraction method for measuring soil microbial biomass C. *Soil Biology and Biochemistry*, *19*(6), 703–707. https://doi.org/10.1016/0038-0717(87)90052-6

Vermeulen, S., Bossio, D., Lehmann, J., Luu, P., Paustian, K., Webb, C., Augé, F., Bacudo, I., Baedeker, T., Havemann, T., Jones, C., King, R., Reddy, M., Sunga, I., Von Unger, M., & Warnken, M.

(2019). A global agenda for collective action on soil carbon. *Nature Sustainability*, *2*(1), Article 1. https://doi.org/10.1038/s41893-018-0212-z

Villarino, S. H., Pinto, P., Jackson, R. B., & Piñeiro, G. (2021). Plant rhizodeposition: A key factor for soil organic matter formation in stable fractions. *Science Advances*, *7*(16), eabd3176. https://doi.org/10.1126/sciadv.abd3176

von Lützow, M., Kögel-Knabner, I., Ekschmitt, K., Flessa, H., Guggenberger, G., Matzner, E., & Marschner, B. (2007). SOM fractionation methods: Relevance to functional pools and to stabilization mechanisms. *Soil Biology and Biochemistry*, *39*(9), 2183–2207. https://doi.org/10.1016/j.soilbio.2007.03.007

Wang, B., An, S., Liang, C., Liu, Y., & Kuzyakov, Y. (2021). Microbial necromass as the source of soil organic carbon in global ecosystems. *Soil Biology and Biochemistry*, *162*, 108422. https://doi.org/10.1016/j.soilbio.2021.108422

Wang, G., Jagadamma, S., Mayes, M. A., Schadt, C. W., Megan Steinweg, J., Gu, L., & Post, W. M. (2015). Microbial dormancy improves development and experimental validation of ecosystem model. *The ISME Journal*, *9*(1), 226–237. https://doi.org/10.1038/ismej.2014.120

West, T. O., & Six, J. (2007). Considering the influence of sequestration duration and carbon saturation on estimates of soil carbon capacity. *Climatic Change*, *80*(1), 25–41. https://doi.org/10.1007/s10584-006-9173-8

Whalen, E. D., Grandy, A. S., Geyer, K. M., Morrison, E. W., & Frey, S. D. (2024). *Microbial trait multifunctionality drives soil organic matter formation potential* (p. 2024.05.24.595733). bioRxiv. https://doi.org/10.1101/2024.05.24.595733

Whalen, E. D., Grandy, A. S., Sokol, N. W., Keiluweit, M., Ernakovich, J., Smith, R. G., & Frey, S. D. (2022). Clarifying the evidence for microbial- and plant-derived soil organic matter, and the path toward a more quantitative understanding. *Global Change Biology*, *28*(24), 7167–7185. https://doi.org/10.1111/gcb.16413

Wieder, W. R., Grandy, A. S., Kallenbach, C. M., & Bonan, G. B. (2014). Integrating microbial physiology and physio-chemical principles in soils with the MIcrobial-MIneral Carbon Stabilization (MIMICS) model. *Biogeosciences*, *11*(14), 3899–3917. https://doi.org/10.5194/bg-11-3899-2014

Wiesmeier, M., Urbanski, L., Hobley, E., Lang, B., von Lützow, M., Marin-Spiotta, E., van Wesemael, B., Rabot, E., Ließ, M., Garcia-Franco, N., Wollschläger, U., Vogel, H.-J., & Kögel-Knabner, I. (2019). Soil organic carbon storage as a key function of soils—A review of drivers and indicators at various scales. *Geoderma*, *333*, 149–162. https://doi.org/10.1016/j.geoderma.2018.07.026

Wu, J., Zhang, H., Pan, Y., Cheng, X., Zhang, K., & Liu, G. (2023). Particulate organic carbon is more sensitive to nitrogen addition than mineral-associated organic carbon: A meta-analysis. *Soil and Tillage Research*, *232*, 105770. https://doi.org/10.1016/j.still.2023.105770

Xu, C., Guo, L., Ping, C.-L., & White, D. M. (2009). Chemical and isotopic characterization of size-fractionated organic matter from cryoturbated tundra soils, northern Alaska. Journal of Geophysical Research: Biogeosciences, 114(G3), G03002. https://doi.org/10.1029/2008JG000846

Yang, Y., Dou, Y., Wang, B., Wang, Y., Liang, C., An, S., Soromotin, A., & Kuzyakov, Y. (2022). Increasing contribution of microbial residues to soil organic carbon in grassland restoration chronosequence. *Soil Biology and Biochemistry*, *170*, 108688. https://doi.org/10.1016/j.soilbio.2022.108688

Yu, W., Huang, W., Weintraub-Leff, S. R., & Hall, S. J. (2022). Where and why do particulate organic matter (POM) and mineral-associated organic matter (MAOM) differ among diverse soils? *Soil Biology and Biochemistry*, *172*, 108756. https://doi.org/10.1016/j.soilbio.2022.108756

Zhang, Y., Lavallee, J. M., Robertson, A. D., Even, R., Ogle, S. M., Paustian, K., & Cotrufo, M. F. (2021). Simulating measurable ecosystem carbon and nitrogen dynamics with the mechanistically defined MEMS 2.0 model. *Biogeosciences*, *18*(10), 3147–3171. https://doi.org/10.5194/bg-18-3147-2021

Zhu, Q., Riley, W. J., Tang, J., & Koven, C. D. (2016). Multiple soil nutrient competition between plants, microbes, and mineral surfaces: Model development, parameterization, and example applications in several tropical forests. *Biogeosciences*, *13*(1), 341–363. https://doi.org/10.5194/bg-13-341-2016

APPENDIX

Supplementary Information for Chapter 2

Table A2.1. Complete citations for the 72 studies included in our synthesized dataset. Studies located via the International Soil Radiocarbon Database (ISRaD; Lawrence et al., 2020) are noted in the rightmost column.

	Full citation	In ISRaD?
1	Balabane, M., & Plante, A. F. (2004). Aggregation and carbon storage in silty soil using physical fractionation techniques. European Journal of Soil Science, 55(2), 415–427. https://doi.org/10.1111/j.1351-0754.2004.0608.x	
2	Balesdent, J., Besnard, E., Arrouays, D., & Chenu, C. (1998). The dynamics of carbon in particle-size fractions of soil in a forest-cultivation sequence. Plant and Soil, 201(1), 49–57. https://doi.org/10.1023/A:1004337314970	
3	Barthès, B. G., Kouakoua, E., Larré-Larrouy, M.-C., Razafimbelo, T. M., de Luca, E. F., Azontonde, A., Neves, C. S. V. J., de Freitas, P. L., & Feller, C. L. (2008). Texture and sesquioxide effects on water-stable aggregates and organic matter in some tropical soils. Geoderma, 143(1–2), 14–25. https://doi.org/10.1016/j.geoderma.2007.10.003	
4	Berhe, A. A., Harden, J. W., Torn, M. S., Kleber, M., Burton, S. D., & Harte, J. (2012). Persistence of soil organic matter in eroding versus depositional landform positions. Journal of Geophysical Research: Biogeosciences, 117(G2). https://doi.org/10.1029/2011JG001790	Yes
5	Błońska, E., Lasota, J., Tullus, A., Lutter, R., & Ostonen, I. (2019). Impact of deadwood decomposition on soil organic carbon sequestration in Estonian and Polish forests. Annals of Forest Science, 76(4), 102. https://doi.org/10.1007/s13595-019-0889-9	
6	Caravaca, F., Lax, A., & Albaladejo, J. (1999). Organic matter, nutrient contents and cation exchange capacity in fine fractions from semiarid calcareous soils. Geoderma, 93(3–4), 161–176. https://doi.org/10.1016/S0016-7061(99)00045-2	
7	Conen, F., Zimmermann, M., Leifeld, J., Seth, B., & Alewell, C. (2008). Relative stability of soil carbon revealed by shifts in $\delta^{15}N$ and C:N ratio. Biogeosciences, 5(1), 123–128. https://doi.org/10.5194/bg-5-123-2008	Yes
8	Cui, J., Li, Z., Liu, Z., Ge, B., Fang, C., Zhou, C., & Tang, B. (2014). Physical and chemical stabilization of soil organic carbon along a 500-year cultived soil chronosequence originating from estuarine wetlands: Temporal patterns and land use effects. Agriculture, Ecosystems & Environment, 196, 10–20. https://doi.org/10.1016/j.agee.2014.06.013	
9	Dietterich, L. H., Karpman, J., Neupane, A., Ciochina, M., & Cusack, D. F. (2021). Carbon content of soil fractions varies with season, rainfall, and soil fertility across a lowland tropical moist forest gradient. Biogeochemistry, 155(3), 431–452. https://doi.org/10.1007/s10533-021-00836-1	
10	Doetterl, S., Stevens, A., Six, J., Merckx, R., Van Oost, K., Casanova Pinto, M., Casanova-Katny, A., Muñoz, C., Boudin, M., Zagal Venegas, E., & Boeckx, P.	

	(2015). Soil carbon storage controlled by interactions between geochemistry and climate. Nature Geoscience, 8(10), 780–783. https://doi.org/10.1038/ngeo2516	
11	Dutta, K., Schuur, E. A. G., Neff, J. C., & Zimov, S. A. (2006). Potential carbon release from permafrost soils of Northeastern Siberia. Global Change Biology, 12(12), 2336–2351. https://doi.org/10.1111/j.1365-2486.2006.01259.x	Yes
12	Feller, C., Albrecht, A., & Tessier, D. (1996). Aggregation and Organic Matter Storage in Kaolinitic and Smectitic Tropical Soils. In M. R. Carter & B. A. Stewart (Eds.), Structure and Organic Matter Storage in Agricultural Soils (1st ed., pp. 309–359). CRC Press. https://doi.org/10.1201/9781003075561-12	
13	Gong, W., Yan, X., Wang, J., Hu, T., & Gong, Y. (2009). Long-term manure and fertilizer effects on soil organic matter fractions and microbes under a wheat–maize cropping system in northern China. Geoderma, 149(3–4), 318–324. https://doi.org/10.1016/j.geoderma.2008.12.010	
14	Guggenberger, G., Christensen, B. T., & Zech, W. (1994). Land-use effects on the composition of organic matter in particle-size separates of soil: I. Lignin and carbohydrate signature. European Journal of Soil Science, 45(4), 449–458. https://doi.org/10.1111/j.1365-2389.1994.tb00530.x	
15	Guibert, H., Fallavier, P., & Roméro, J. (1999). Carbon content in soil particle size and consequence on cation exchange capacity of Alfisols. Communications in Soil Science and Plant Analysis, 30(17–18), 2521–2537. https://doi.org/10.1080/00103629909370392	
16	Gutiérrez del Arroyo, O., & Silver, W. L. (2018). Disentangling the long-term effects of disturbance on soil biogeochemistry in a wet tropical forest ecosystem. Global Change Biology, 24(4), 1673–1684. https://doi.org/10.1111/gcb.14027	
17	Hall, S. J., Berhe, A. A., & Thompson, A. (2018). Order from disorder: Do soil organic matter composition and turnover co-vary with iron phase crystallinity? Biogeochemistry, 140(1), 93–110. https://doi.org/10.1007/s10533-018-0476-4	
18	Hall, S. J., McNicol, G., Natake, T., & Silver, W. L. (2015). Large fluxes and rapid turnover of mineral-associated carbon across topographic gradients in a humid tropical forest: Insights from paired $\delta^{13}C$ analysis. Biogeosciences, 12(8), 2471–2487. https://doi.org/10.5194/bg-12-2471-2015	
19	Harden, J. W. (1987). Soils developed in granitic alluvium near Merced, California. https://doi.org/10.3133/b1590A	Yes
20	Harden, J. W., Fries, T. L., & Pavich, M. J. (2002). Cycling of Beryllium and Carbon through hillslope soils in Iowa. Biogeochemistry, 60(3), 317–336. https://doi.org/10.1023/A:1020308729553	Yes
21	Hatton, P.-J., Kleber, M., Zeller, B., Moni, C., Plante, A. F., Townsend, K., Gelhaye, L., Lajtha, K., & Derrien, D. (2012). Transfer of litter-derived N to soil mineral–organic associations: Evidence from decadal ^{15}N tracer experiments. Organic Geochemistry, 42(12), 1489–1501. https://doi.org/10.1016/j.orggeochem.2011.05.002	Yes
22	Heckman, K. A. (2010). Pedogenesis & carbon dynamics across a lithosequence under ponderosa pine. https://doi.org/10.5281/ZENODO.1486081	Yes
23	Heckman, K., Lawrence, C. R., & Harden, J. W. (2018). A sequential selective dissolution method to quantify storage and stability of organic carbon associated with Al and Fe hydroxide phases. Geoderma, 312, 24–35. https://doi.org/10.1016/j.geoderma.2017.09.043	Yes
24	Herndon, E., AlBashaireh, A., Singer, D., Roy Chowdhury, T., Gu, B., & Graham, D. (2017). Influence of iron redox cycling on organo-mineral associations in Arctic	

	tundra soil. Geochimica et Cosmochimica Acta, 207, 210–231. https://doi.org/10.1016/j.gca.2017.02.034	
25	Jindaluang, W., Kheoruenromne, I., Suddhiprakarn, A., Singh, B. P., & Singh, B. (2013). Influence of soil texture and mineralogy on organic matter content and composition in physically separated fractions soils of Thailand. Geoderma, 195–196, 207–219. https://doi.org/10.1016/j.geoderma.2012.12.003	
26	Keller, A. B., Borer, E. T., Collins, S. L., DeLancey, L. C., Fay, P. A., Hofmockel, K. S., Leakey, A. D. B., Mayes, M. A., Seabloom, E. W., Walter, C. A., Wang, Y., Zhao, Q., & Hobbie, S. E. (2022). Soil carbon stocks in temperate grasslands differ strongly across sites but are insensitive to decade-long fertilization. Global Change Biology, 28(4), 1659–1677. https://doi.org/10.1111/gcb.15988	
27	Khomo, L., Trumbore, S., Bern, C. R., & Chadwick, O. A. (2017). Timescales of carbon turnover in soils with mixed crystalline mineralogies. SOIL, 3(1), 17–30. https://doi.org/10.5194/soil-3-17-2017	Yes
28	King, A. E., Amsili, J. P., Córdova, S. C., Culman, S., Fonte, S. J., Kotcon, J., Liebig, M., Masters, M. D., McVay, K., Olk, D. C., Schipanski, M., Schneider, S. K., Stewart, C. E., & Cotrufo, M. F. (2023). A soil matrix capacity index to predict mineral-associated but not particulate organic carbon across a range of climate and soil pH. Biogeochemistry, 165(1), 1–14. https://doi.org/10.1007/s10533-023-01066-3	
29	Kölbl, A., von Lützow, M., & Kögel-Knabner, I. (2006). Decomposition and distribution of ^{15}N labelled mustard litter (Sinapis alba) in physical soil fractions of a cropland with high- and low-yield field areas. Soil Biology and Biochemistry, 38(11), 3292–3302. https://doi.org/10.1016/j.soilbio.2006.04.010	Yes
30	Kong, A. Y. Y., Fonte, S. J., van Kessel, C., & Six, J. (2009). Transitioning from standard to minimum tillage: Trade-offs between soil organic matter stabilization, nitrous oxide emissions, and N availability in irrigated cropping systems. Soil and Tillage Research, 104(2), 256–262. https://doi.org/10.1016/j.still.2009.03.004	
31	Larré-Larrouy, M. C., Albrecht, A., Blanchart, E., Chevallier, T., & Feller, C. (2003). Carbon and monosaccharides of a tropical Vertisol under pasture and market-gardening: Distribution in primary organomineral separates. Geoderma, 117(1–2), 63–79. https://doi.org/10.1016/S0016-7061(03)00135-6	
32	Lawrence, C. R., Beem-Miller, J., Hoyt, A. M., Monroe, G., Sierra, C. A., Stoner, S., Heckman, K., Blankinship, J. C., Crow, S. E., McNicol, G., Trumbore, S., Levine, P. A., Vindušková, O., Todd-Brown, K., Rasmussen, C., Hicks Pries, C. E., Schädel, C., McFarlane, K., Doetterl, S., … Wagai, R. (2020). An open-source database for the synthesis of soil radiocarbon data: International Soil Radiocarbon Database (ISRaD) version 1.0. Earth System Science Data, 12(1), 61–76. https://doi.org/10.5194/essd-12-61-2020	Entries under Lemke_2006
33	Li, Y., Xu, M., Zou, X., Shi, P., & Zhang, Y. (2005). Comparing soil organic carbon dynamics in plantation and secondary forest in wet tropics in Puerto Rico. Global Change Biology, 11(2), 239–248. https://doi.org/10.1111/j.1365-2486.2005.00896.x	
34	Liang, A., Yang, X., Zhang, X., McLaughlin, N., Shen, Y., & Li, W. (2009). Soil organic carbon changes in particle-size fractions following cultivation of Black soils in China. Soil and Tillage Research, 105(1), 21–26. https://doi.org/10.1016/j.still.2009.05.002	
35	Lugato, E., Lavallee, J. M., Haddix, M. L., Panagos, P., & Cotrufo, M. F. (2021). Different climate sensitivity of particulate and mineral-associated soil organic	

	matter. Nature Geoscience, 14(5), 295–300. https://doi.org/10.1038/s41561-021-00744-x	
36	Lybrand, R. A., Heckman, K., & Rasmussen, C. (2017). Soil organic carbon partitioning and $\Delta^{14}C$ variation in desert and conifer ecosystems of southern Arizona. Biogeochemistry, 134(3), 261–277. https://doi.org/10.1007/s10533-017-0360-7	Yes
37	Machmuller, M., et al. Unpublished data.	
38	Marín-Spiotta, E., Swanston, C. W., Torn, M. S., Silver, W. L., & Burton, S. D. (2008). Chemical and mineral control of soil carbon turnover in abandoned tropical pastures. Geoderma, 143(1–2), 49–62. https://doi.org/10.1016/j.geoderma.2007.10.001	Yes
39	Mirabito, A. J., & Chambers, L. G. (2023). Quantifying mineral-associated organic matter in wetlands as an indicator of the degree of soil carbon protection. Geoderma, 430, 116327. https://doi.org/10.1016/j.geoderma.2023.116327	
40	Mosier, S., Apfelbaum, S., Byck, P., Calderon, F., Teague, R., Thompson, R., & Cotrufo, M. F. (2021). Adaptive multi-paddock grazing enhances soil carbon and nitrogen stocks and stabilization through mineral association in southeastern U.S. grazing lands. Journal of Environmental Management, 288, 112409. https://doi.org/10.1016/j.jenvman.2021.112409	
41	Mosier, S., Paustian, K., Davies, C., Kane, M., & Cotrufo, M. F. (2019). Soil organic matter pools under management intensification of loblolly pine plantations. Forest Ecology and Management, 447, 60–66. https://doi.org/10.1016/j.foreco.2019.05.056	
42	Mujuru, L., Mureva, A., Velthorst, E. J., & Hoosbeek, M. R. (2013). Land use and management effects on soil organic matter fractions in Rhodic Ferralsols and Haplic Arenosols in Bindura and Shamva districts of Zimbabwe. Geoderma, 209–210, 262–272. https://doi.org/10.1016/j.geoderma.2013.06.025	
43	Nacro, H. B., Benest, D., & Abbadie, L. (1996). Distribution of microbial activities and organic matter according to particle size in a humid savanna soil (Lamto, Côte d'Ivoire). Soil Biology and Biochemistry, 28(12), 1687–1697. https://doi.org/10.1016/S0038-0717(96)00246-5	
44	Piñeiro, G., Paruelo, J. M., Jobbágy, E. G., Jackson, R. B., & Oesterheld, M. (2009). Grazing effects on belowground C and N stocks along a network of cattle exclosures in temperate and subtropical grasslands of South America. Global Biogeochemical Cycles, 23(2), n/a-n/a. https://doi.org/10.1029/2007GB003168	
45	Pold, G., Grandy, A. S., Melillo, J. M., & DeAngelis, K. M. (2017). Changes in substrate availability drive carbon cycle response to chronic warming. Soil Biology and Biochemistry, 110, 68–78. https://doi.org/10.1016/j.soilbio.2017.03.002	
46	Rasmussen, C., Throckmorton, H., Liles, G., Heckman, K., Meding, S., & Horwath, W. (2018). Controls on Soil Organic Carbon Partitioning and Stabilization in the California Sierra Nevada. Soil Systems, 2(3), 41. https://doi.org/10.3390/soilsystems2030041	Yes
47	Rasmussen, C., & White, D. A. (2010). Vegetation Effects on Soil Organic Carbon Quality in an Arid Hyperthermic Ecosystem. Soil Science, 175(9), 438–446. https://doi.org/10.1097/SS.0b013e3181f38400	Yes
48	Riggs, C. E., Hobbie, S. E., Bach, E. M., Hofmockel, K. S., & Kazanski, C. E. (2015). Nitrogen addition changes grassland soil organic matter decomposition. Biogeochemistry, 125(2), 203–219. https://doi.org/10.1007/s10533-015-0123-2	
49	Santos, R. S., Oliveira, F. C. C., Ferreira, G. W. D., Ferreira, M. A., Araújo, E. F., & Silva, I. R. (2020). Carbon and nitrogen dynamics in soil organic matter fractions	

	following eucalypt afforestation in southern Brazilian grasslands (Pampas). Agriculture, Ecosystems & Environment, 301, 106979. https://doi.org/10.1016/j.agee.2020.106979	
50	Santos, R. S., Wiesmeier, M., Oliveira, D. M. S., Locatelli, J. L., Barreto, M. S. C., Demattê, J. A. M., & Cerri, C. E. P. (2022). Conversion of Brazilian savannah to agricultural land affects quantity and quality of labile soil organic matter. Geoderma, 406, 115509. https://doi.org/10.1016/j.geoderma.2021.115509	
51	Schmidt, M. W. I., & Kögel- Knabner, I. (2002). Organic matter in particle-size fractions from A and B horizons of a Haplic Alisol: Organic matter in particle-size fractions. European Journal of Soil Science, 53(3), 383–391. https://doi.org/10.1046/j.1365-2389.2002.00460.x	
52	Schrumpf, M., Kaiser, K., Guggenberger, G., Persson, T., Kögel-Knabner, I., & Schulze, E.-D. (2013). Storage and stability of organic carbon in soils as related to depth, occlusion within aggregates, and attachment to minerals. Biogeosciences, 10(3), 1675–1691. https://doi.org/10.5194/bg-10-1675-2013	Yes
53	Schulten, H.-R., Leinweber, P., & Sorge, C. (1993). Composition of organic matter in particle-size fractions of an agricultural soil. Journal of Soil Science, 44(4), 677–691. https://doi.org/10.1111/j.1365-2389.1993.tb02332.x	
54	Schuur, E. A. G., Chadwick, O. A., & Matson, P. A. (2001). Carbon cycling and soil carbon storage in mesic to wet Hawaiiian montane forests. Ecology, 82(11), 3182–3196. https://doi.org/10.1890/0012-9658(2001)082[3182:CCASCS]2.0.CO;2	Yes
55	Sleutel, S., De Neve, S., Singier, B., & Hofman, G. (2006). Organic C levels in intensively managed arable soils—Long-term regional trends and characterization of fractions. Soil Use and Management, 22(2), 188–196. https://doi.org/10.1111/j.1475-2743.2006.00019.x	
56	Sollins, P., Kramer, M. G., Swanston, C., Lajtha, K., Filley, T., Aufdenkampe, A. K., Wagai, R., & Bowden, R. D. (2009). Sequential density fractionation across soils of contrasting mineralogy: Evidence for both microbial- and mineral-controlled soil organic matter stabilization. Biogeochemistry, 96(1–3), 209–231. https://doi.org/10.1007/s10533-009-9359-z	Yes
57	Sollins, P., Swanston, C., Kleber, M., Filley, T., Kramer, M., Crow, S., Caldwell, B. A., Lajtha, K., & Bowden, R. (2006). Organic C and N stabilization in a forest soil: Evidence from sequential density fractionation. Soil Biology and Biochemistry, 38(11), 3313–3324. https://doi.org/10.1016/j.soilbio.2006.04.014	Yes
58	Soong, J. L., Janssens, I. A., Grau, O., Margalef, O., Stahl, C., Van Langenhove, L., Urbina, I., Chave, J., Dourdain, A., Ferry, B., Freycon, V., Herault, B., Sardans, J., Peñuelas, J., & Verbruggen, E. (2020). Soil properties explain tree growth and mortality, but not biomass, across phosphorus-depleted tropical forests. Scientific Reports, 10(1), 2302. https://doi.org/10.1038/s41598-020-58913-8	
59	Sousa, R. F. D., Brasil, E. P. F., Figueiredo, C. C. D., & Leandro, W. M. (2015). Soil organic matter fractions in preserved and disturbed wetlands of the cerrado biome. Revista Brasileira de Ciência Do Solo, 39(1), 222–231. https://doi.org/10.1590/01000683rbcs20150048	
60	Steffens, M., Kölbl, A., & Kögel-Knabner, I. (2009). Alteration of soil organic matter pools and aggregation in semi-arid steppe topsoils as driven by organic matter input. European Journal of Soil Science, 60(2), 198–212. doi:10.1111/j.1365-2389.2008.01104.x	
61	Sun, R., Sun, B., Li, X., Wei, S., Zhao, M., Chu, X., Song, W., Yuan, J., & Han, G. (2023). Seven-year experimental warming decreases labile but not recalcitrant soil	

	organic carbon fractions in a coastal wetland. Journal of Soils and Sediments, 23(8), 3071–3081. https://doi.org/10.1007/s11368-023-03536-5	
62	Tian, J., McCormack, L., Wang, J., Guo, D., Wang, Q., Zhang, X., Yu, G., Blagodatskaya, E., & Kuzyakov, Y. (2015). Linkages between the soil organic matter fractions and the microbial metabolic functional diversity within a broad-leaved Korean pine forest. European Journal of Soil Biology, 66, 57–64. https://doi.org/10.1016/j.ejsobi.2014.12.001	
63	Tian, Q., Wang, D., Li, D., Huang, L., Wang, M., Liao, C., & Liu, F. (2020). Variation of soil carbon accumulation across a topographic gradient in a humid subtropical mountain forest. Biogeochemistry, 149(3), 337–354. https://doi.org/10.1007/s10533-020-00679-2	
64	Trumbore, S. E. (1993). Comparison of carbon dynamics in tropical and temperate soils using radiocarbon measurements. Global Biogeochemical Cycles, 7(2), 275–290. https://doi.org/10.1029/93GB00468	Yes
65	van der Pol, L. K., Robertson, A., Schipanski, M., Calderon, F. J., Wallenstein, M. D., & Cotrufo, M. F. (2022). Addressing the soil carbon dilemma: Legumes in intensified rotations regenerate soil carbon while maintaining yields in semi-arid dryland wheat farms. Agriculture, Ecosystems & Environment, 330, 107906. https://doi.org/10.1016/j.agee.2022.107906	
66	Verret, M., Wang, Y., Bjornson, J., & Lacelle, D. (2019). Hummocks in alpine tundra, northern British Columbia, Canada: Distribution, morphology and organic carbon composition. Arctic Science, 5(3), 127–147. https://doi.org/10.1139/as-2018-0021	
67	Wagai, R., Kajiura, M., Asano, M., & Hiradate, S. (2015). Nature of soil organo-mineral assemblage examined by sequential density fractionation with and without sonication: Is allophanic soil different? Geoderma, 241–242, 295–305. https://doi.org/10.1016/j.geoderma.2014.11.028	Yes
68	Wang, Q., Zhang, P.-J., Liu, M., & Deng, Z.-W. (2014). Mineral-associated organic carbon and black carbon in restored wetlands. Soil Biology and Biochemistry, 75, 300–309. https://doi.org/10.1016/j.soilbio.2014.04.025	
69	Wood, S. A., Sokol, N., Bell, C. W., Bradford, M. A., Naeem, S., Wallenstein, M. D., & Palm, C. A. (2016). Opposing effects of different soil organic matter fractions on crop yields. Ecological Applications, 26(7), 2072–2085. https://doi.org/10.1890/16-0024.1	
70	Xu, C., Guo, L., Dou, F., & Ping, C.-L. (2009). Potential DOC production from size-fractionated Arctic tundra soils. Cold Regions Science and Technology, 55(1), 141–150. https://doi.org/10.1016/j.coldregions.2008.08.001	
71	Xu, C., Guo, L., Ping, C.-L., & White, D. M. (2009). Chemical and isotopic characterization of size-fractionated organic matter from cryoturbated tundra soils, northern Alaska. Journal of Geophysical Research: Biogeosciences, 114(G3). https://doi.org/10.1029/2008JG000846	
72	Yang, W., Zhao, H., Leng, X., Cheng, X., & An, S. (2017). Soil organic carbon and nitrogen dynamics following Spartina alterniflora invasion in a coastal wetland of eastern China. CATENA, 156, 281–289. https://doi.org/10.1016/j.catena.2017.03.021	

Table A2.2. Linear regression coefficients for net primary production (NPP; Mg C ha^{-1} yr^{-1}) and particulate (POC; g C kg $soil^{-1}$), mineral-associated (MAOC; g C kg $soil^{-1}$), and soil organic carbon (SOC; g C kg $soil^{-1}$) as predicted by climate and soil properties.

Response variable	Predictor	Intercept	Slope	Multiple r^2	*p*-value	Significance
NPP	MAT	5.1098	0.08348	0.04851	1.43e-8	***
NPP	MAP-PET	6.9995	0.00192	0.2205	<2e-16	***
POC	MAT	2.0924	-0.05649	0.09192	2.9e-15	***
POC	MAP-PET	1.667	6.484e-04	0.1039	<2e-16	***
POC	NPP	1.064	0.05182	0.01111	0.0072	**
POC	pH	3.2368	-0.3018	0.09314	1.862e-15	***
POC	% sand	1.3274	0.00129	0.00084	0.461	
MAOC	MAT	2.6576	-0.00886	0.00565	0.0556	
MAOC	MAP-PET	2.7658	0.000501	0.1549	<2e-16	***
MAOC	NPP	1.9243	0.101	0.1055	<2e-16	***
MAOC	pH	2.6437	-0.01585	0.00064	0.519	
MAOC	% sand	3.0354	-0.01135	0.1619	<2e-16	***
SOC	MAT	3.1889	-0.01655	0.02047	0.000255	***
SOC	MAP-PET	3.191	4.798e-4	0.1477	<2e-16	***
SOC	NPP	2.4653	0.08377	0.0754	1.09e-12	***
SOC	pH	3.7221	-0.1206	0.03864	4.47e-7	***
SOC	% sand	3.2367	-0.00593	0.04595	3.5e-8	***

Table A2.3. Coefficients for path analysis of environmental controls on particulate (POC; g C kg $soil^{-1}$) and mineral-associated organic carbon (MAOC; g C kg $soil^{-1}$) storage.

		Standardized				
Dependent variable	**Predictor**	**Path coeff.**	**Std. error**	**z-value**	***p*-value**	**Significance**
NPP	MAT	0.39	0.033	11.868	0.0	***
NPP	MAP-PET	0.583	0.033	17.75	0.0	***
POC	MAT	-0.24	0.042	-5.647	0.0	***
POC	MAP-PET	0.015	0.053	0.285	0.776	
POC	NPP	0.028	0.046	0.605	0.545	
POC	pH	-0.203	0.046	-4.435	0.0	***
POC	% sand	0.064	0.041	1.556	0.12	
MAOC	MAT	0.024	0.04	0.6	0.548	
MAOC	MAP-PET	0.187	0.05	3.731	0.0	***
MAOC	NPP	0.182	0.044	4.178	0.0	***
MAOC	pH	-0.021	0.043	-0.477	0.633	
MAOC	% sand	-0.286	0.039	-7.282	0.0	***

Table A2.4. Coefficients for path analysis of environmental controls on soil organic carbon (SOC; g C kg $soil^{-1}$) storage.

		Standardized				
Dependent variable	**Predictor**	**Path coeff.**	**Std. error**	**z-value**	***p*-value**	**Significance**

NPP	MAT	0.39	0.033	11.868	0.0	***
NPP	MAP-PET	0.583	0.033	17.75	0.0	***
SOC	MAT	-0.126	0.042	-2.966	0.003	**
SOC	MAP-PET	0.123	0.053	2.343	0.019	*
SOC	NPP	0.116	0.046	2.53	0.011	*
SOC	pH	-0.155	0.046	-3.395	0.001	**
SOC	% sand	-0.131	0.041	-3.182	0.001	**

Table A2.5. Linear regression coefficients for the fraction of soil carbon stored as mineral-associated organic carbon (MAOC) relative to bulk soil organic carbon (SOC; f_{MAOC}, %) as predicted by climate and soil properties.

Response variable	**Predictor**	**Intercept**	**Slope**	**Multiple r^2**	***p*-value**	**Significance**
f_{MAOC}	MAT	63.4012	0.44423	0.02407	6.94e-6	***
f_{MAOC}	MAP-PET	4.1571	1.5788e-5	0.0005	0.525	
f_{MAOC}	NPP	65.421	0.5735	0.00741	0.014	*
f_{MAOC}	pH	3.6372	0.08998	0.06724	2.89e-12	***
f_{MAOC}	% sand	80.9196	-0.2568	0.112	<2e-16	***

Table A2.6. Results from Games-Howell *post-hoc* pairwise comparisons of differences of the fraction of mineral-associated organic carbon (MAOC) relative to total bulk soil organic C (SOC), represented as f_{MAOC} (%; (g MAOC kg $soil^{-1}$/g SOC kg $soil^{-1}$)*100), across land cover types.

Comparison		**Estimate**	**Std. error**	**Games-Howell q-value**	***p*-value**	**Significance**
Cropland	Shrubland	-14.018	1.994	4.9711	1.93e-4	***
Cropland	Grassland	-13.2368	0.9229	10.142	6.33e-11	***
Cropland	Forest	-24.6162	1.2271	14.1853	8.63e-13	***
Cropland	Wetland	-37.3522	4.6856	5.6368	0.003	**
Cropland	Tundra	-44.8386	5.1297	6.1808	0.006	**
Shrubland	Grassland	0.7812	2.0829	0.2652	1.0	
Shrubland	Forest	-10.5982	2.2344	3.3539	0.017	*
Shrubland	Wetland	-23.3342	5.044	3.2712	0.057	
Shrubland	Tundra	-30.8206	5.459	3.9922	0.0330	*
Grassland	Forest	-11.3794	1.3667	5.8867	1.24e-7	***
Grassland	Wetland	-24.1154	4.7242	3.6096	0.043	*
Grassland	Tundra	-31.6018	5.165	4.3264	0.032	*
Forest	Wetland	-12.736	4.7927	1.879	0.464	
Forest	Tundra	-20.2224	5.2279	2.7352	0.187	
Wetland	Tundra	-7.4864	6.9123	0.7658	0.969	

Table A2.7. Results from Games-Howell *post-hoc* pairwise comparisons of differences in mean annual temperature (MAT, °C), mean annual precipitation minus potential evapotranspiration (MAP-PET, mm), annual net primary production (NPP, Mg C ha^{-1} yr^{-1}), soil pH, and % sand across land cover types.

MAT (°C)						
Comparison		**Estimate**	**Std. error**	**Games-Howell q-value**	***p*-value**	**Significance**
Cropland	Forest	0.4384	0.4699	0.6597	0.986	
Cropland	Grassland	-0.2469	0.3823	0.4563	0.998	
Cropland	Shrubland	1.3805	1.6046	1.6046	0.599	
Cropland	Tundra	-19.1035	1.0724	12.5966	1.38e-5	***
Cropland	Wetland	5.0769	0.7933	4.5253	0.005	**
Forest	Grassland	-0.6853	0.461	1.0511	0.9	
Forest	Shrubland	0.9421	0.6604	1.0087	0.914	
Forest	Tundra	-19.5419	1.1028	12.5306	5.55e-6	***
Forest	Wetland	4.6386	0.8339	3.9332	0.011	*
Grassland	Shrubland	1.6274	0.6015	1.9131	0.406	
Grassland	Tundra	-18.8566	1.0685	12.4787	1.66e-5	***
Grassland	Wetland	5.3239	0.7881	4.7769	0.003	**
Shrubland	Tundra	-20.484	1.1685	12.3959	8.19e-7	***
Shrubland	Wetland	3.6964	0.9191	2.8439	0.085	
Tundra	Wetland	24.1804	1.2746	13.7423	3.5e-8	***
MAP-PET (mm)						
Comparison		**Estimate**	**Std. error**	**Games-Howell q-value**	***p*-value**	**Significance**
Cropland	Forest	503.0567	41.5825	8.5544	9.85e-11	***
Cropland	Grassland	136.2303	30.614	3.1466	0.021	*
Cropland	Shrubland	-659.6325	88.4755	5.2719	9.86e-5	***
Cropland	Tundra	520.2945	38.004	9.6807	3.26e-4	**
Cropland	Wetland	138.0678	54.7709	1.7825	0.515	
Forest	Grassland	-366.8264	44.987	5.7659	2.41e-7	***
Forest	Shrubland	-1162.6892	94.4168	8.7076	4.98e-10	***
Forest	Tundra	17.2379	50.3082	0.2423	1.0	
Forest	Wetland	-364.9889	63.9255	4.0373	0.008	**
Grassland	Shrubland	-795.8628	90.1257	6.2442	4.0e-6	***
Grassland	Tundra	384.0642	41.7017	6.5123	8.41e-4	***
Grassland	Wetland	1.8375	57.3984	0.02264	1.0	
Shrubland	Tundra	1179.927	92.8964	8.9813	1.53e-9	***
Shrubland	Wetland	797.7003	100.9222	5.5891	2.71e-5	***
Tundra	Wetland	-382.2268	61.6576	4.3835	0.009	**
NPP (Mg C ha^{-1} yr^{-1})						
Comparison		**Estimate**	**Std. error**	**Games-Howell q-value**	***p*-value**	**Significance**
Cropland	Forest	2.1951	0.234	6.6341	2.16e-9	***
Cropland	Grassland	0.5544	0.1364	2.8745	0.048	*
Cropland	Shrubland	0.3639	0.4684	0.5945	0.994	
Cropland	Tundra	-4.0831	0.2808	10.2833	9.85e-4	***
Cropland	Wetland	0.4276	0.5233	0.5778	0.99	
Forest	Grassland	-1.6507	0.2361	4.9141	2.1e-5	***
Forest	Shrubland	-1.8312	0.5065	2.5567	0.128	

Forest	Tundra	-6.2783	0.3405	13.0367	6.26e-7	***
Forest	Wetland	-1.7675	0.5578	2.241	0.293	
Grassland	Shrubland	-0.1905	0.4694	0.287	1.0	
Grassland	Tundra	-4.6376	0.2825	11.6069	4.76e-4	***
Grassland	Wetland	-0.1268	0.5243	0.1711	1.0	
Shrubland	Tundra	-4.4471	0.5297	5.9364	2.02e-5	***
Shrubland	Wetland	0.06368	0.6897	0.06529	1.0	
Tundra	Wetland	4.5107	0.5789	5.5098	0.002	**
Soil pH						
Comparison		**Estimate**	**Std. error**	**Games-Howell q-value**	***p*-value**	**Significance**
Cropland	Forest	-1.5275	0.07095	15.2228	0.0	***
Cropland	Grassland	-0.7086	0.06285	7.9729	1.76e-10	***
Cropland	Shrubland	-0.333	0.1344	1.7527	0.507	
Cropland	Tundra	-2.0493	0.2848	5.0877	0.061	
Cropland	Wetland	0.06536	0.4798	0.09634	1.0	
Forest	Grassland	0.8189	0.06942	8.3412	1.0	
Forest	Shrubland	1.1945	0.1376	6.1404	3.22e-6	***
Forest	Tundra	-0.5218	0.2863	1.2885	0.781	
Forest	Wetland	1.593	0.4807	2.3432	0.301	
Grassland	Shrubland	0.3756	0.1336	1.9886	0.367	
Grassland	Tundra	-1.3407	0.2844	3.3329	0.182	
Grassland	Wetland	0.774	0.4795	1.1413	0.849	
Shrubland	Tundra	-1.7163	0.3082	3.9372	0.082	
Shrubland	Wetland	0.3984	0.494	0.5702	0.99	
Tundra	Wetland	2.1146	0.5542	2.6981	0.17	
% sand						
Comparison		**Estimate**	**Std. error**	**Games-Howell q-value**	***p*-value**	**Significance**
Cropland	Forest	12.442	1.665	5.2834	3.12e-6	***
Cropland	Grassland	4.9149	1.4528	2.4056	0.156	
Cropland	Shrubland	14.9689	3.2384	3.2685	0.026	*
Cropland	Tundra	21.123	7.9412	1.8815	0.564	
Cropland	Wetland	-4.9517	10.2143	0.3428	0.999	
Forest	Grassland	-7.5001	1.6939	3.1314	0.023	*
Forest	Shrubland	2.5269	3.3533	0.5328	0.994	
Forest	Tundra	8.6879	7.9888	0.769	0.952	
Forest	Wetland	-17.3937	10.2513	1.1998	0.822	
Grassland	Shrubland	10.027	3.2531	2.1795	0.271	
Grassland	Tundra	16.188	7.9473	1.4403	0.724	
Grassland	Wetland	-9.8936	10.219	0.6846	0.976	
Shrubland	Tundra	6.1611	8.4579	0.5151	0.991	
Shrubland	Wetland	-19.9206	10.621	1.3262	0.765	
Tundra	Wetland	-26.0817	12.8601	1.4341	0.71	

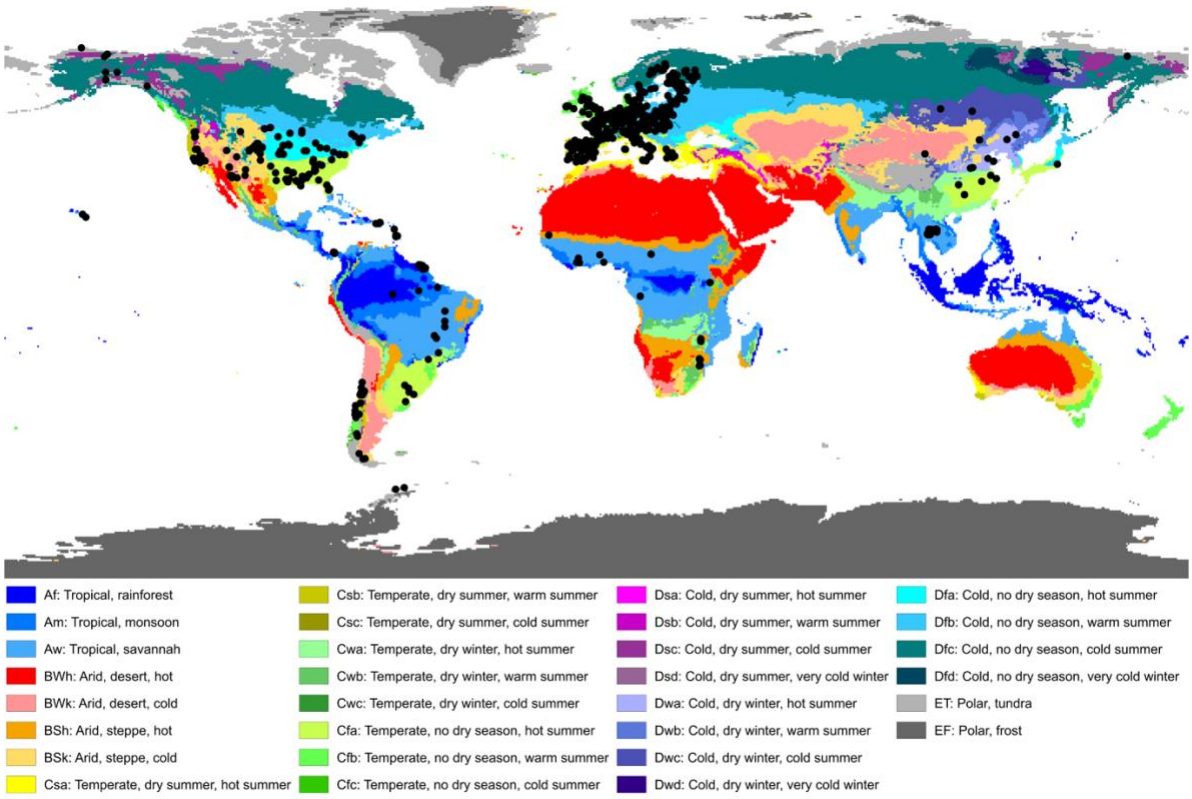

Figure A2.1. Distribution of all data points included in our synthesized dataset across Köppen-Geiger Climate Classification Zones (Beck et al., 2018). Map created using QGIS.

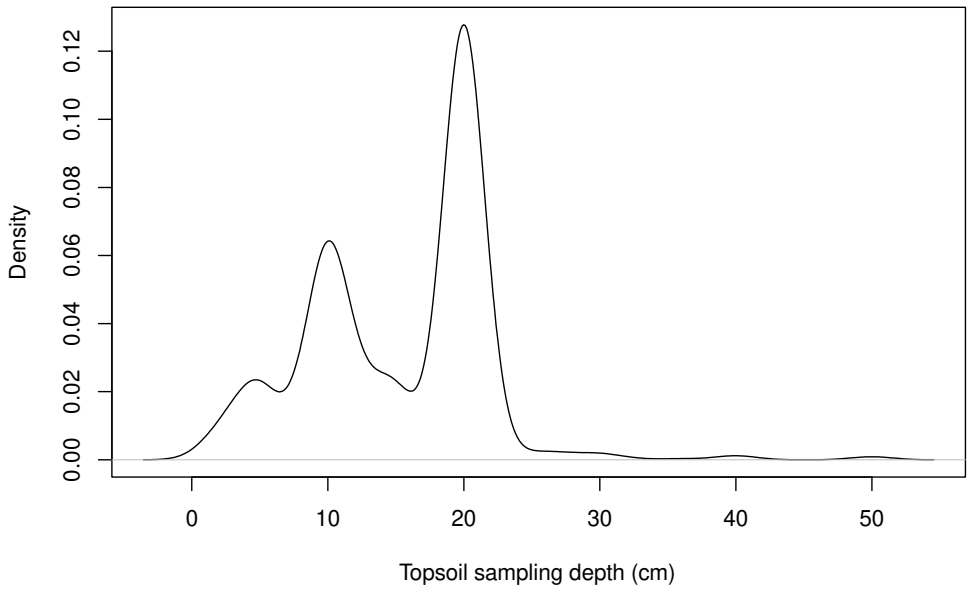

Figure A2.2. Density distribution of sampling depth of all topsoil data points included in our final, synthesized dataset after completion of all data processing.

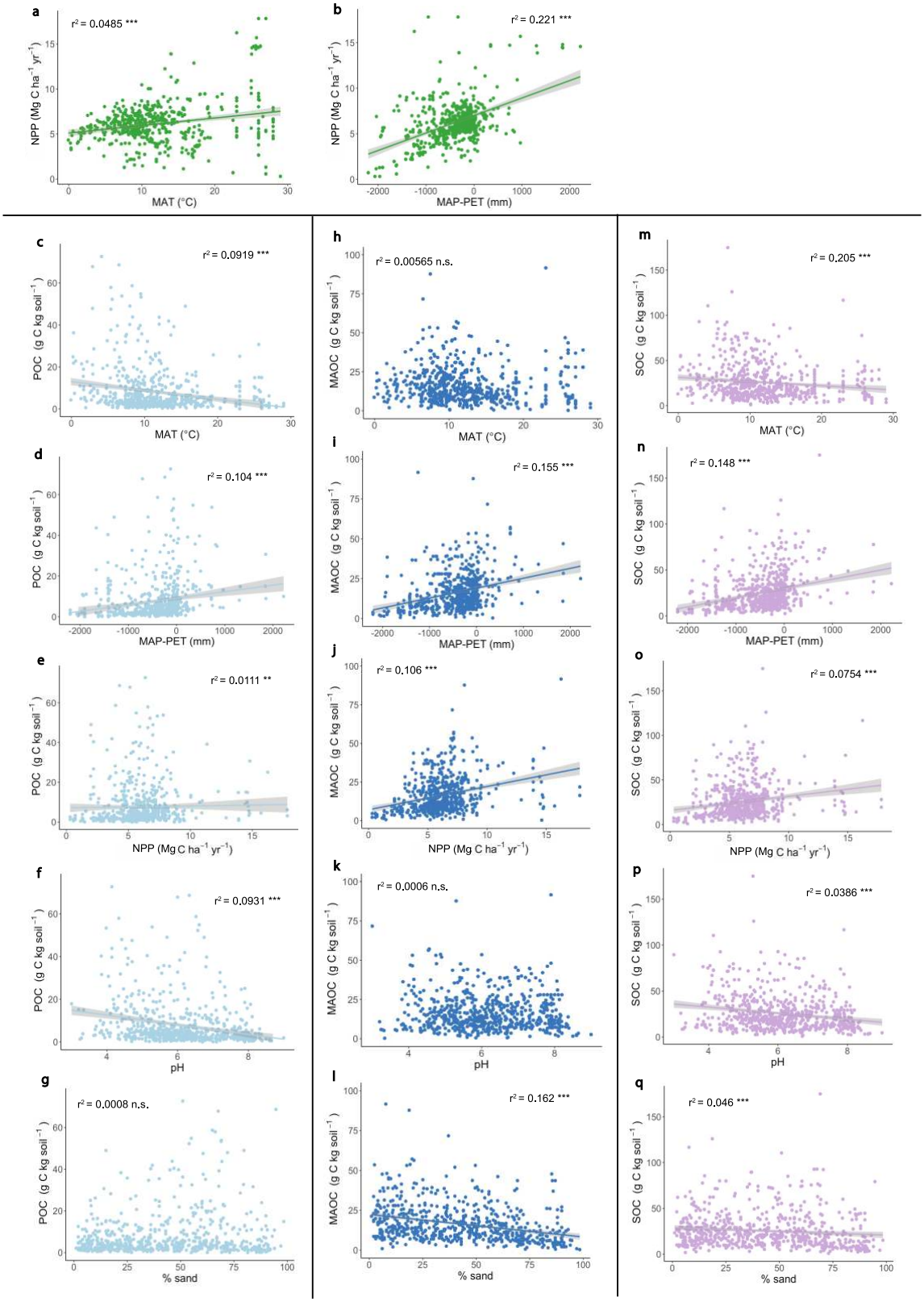

Figure A2.3. Simple linear regressions testing relationships between mean annual temperature (MAT; °C), mean annual precipitation minus potential evapotranspiration (MAP-PET; mm), and net primary

production (NPP; Mg C ha^{-1} yr^{-1}; **a-b**), as well as relationships between MAT, MAP-PET, NPP, soil pH, and % sand, and particulate (POC; g C kg soil^{-1}; **c-g**), mineral-associated (MAOC; g C kg soil^{-1}; **h-l**), and bulk soil organic carbon (SOC; g C kg soil^{-1}; **m-q**) across our global dataset (Table A3.1). The grey shaded area around lines of best fit represents 95% confidence intervals. In all cases, n.s. non-significant, * p < 0.05, ** p <0.01, and *** p < 0.001. Full outputs of all regressions are provided in Table A3.2.

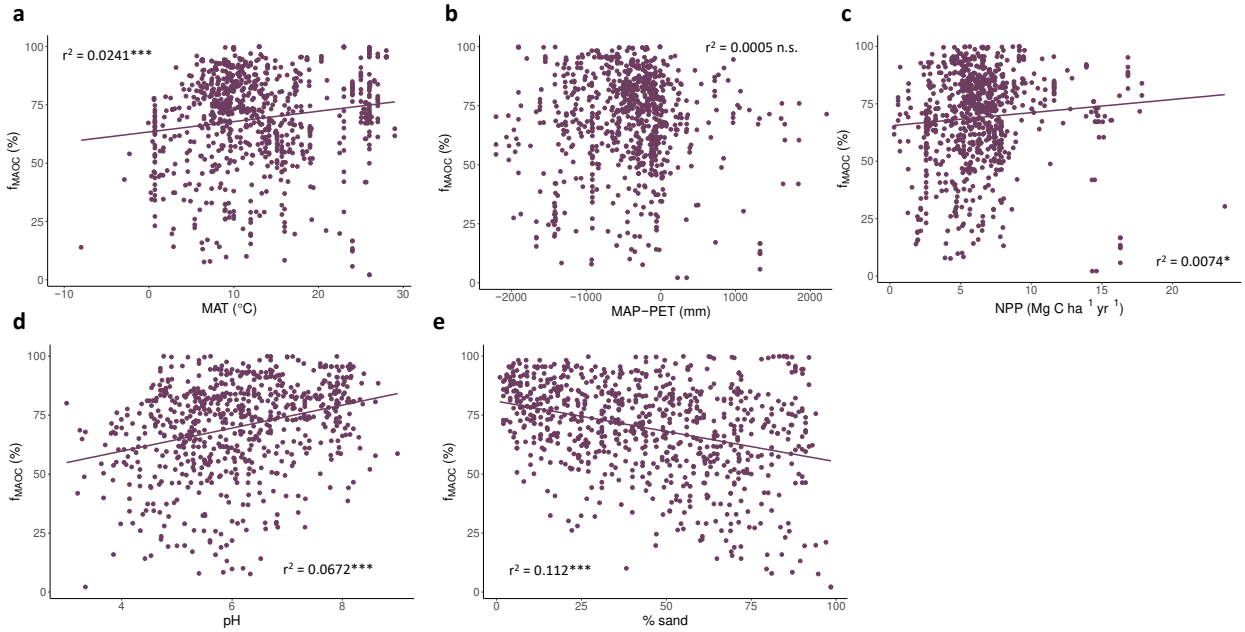

Figure A2.4. Simple linear regressions testing relationships between **a**) mean annual temperature (MAT; °C), **b**) mean annual precipitation minus potential evapotranspiration (MAP-PET; mm), **c**) net primary production (NPP; Mg C ha^{-1} yr^{-1}), **d**) soil pH, and e) % sand with the fraction of carbon stored in mineral-associated organic carbon (MAOC) relative to bulk soil organic carbon (SOC; $f_{MAOC,\%}$) across our global dataset (Table A3.1). The grey shaded area around lines of best fit represents 95% confidence intervals. In all cases, n.s. non-significant, * p < 0.05, ** p <0.01, and *** p < 0.001. Full outputs of all regressions are provided in Table A3.5.

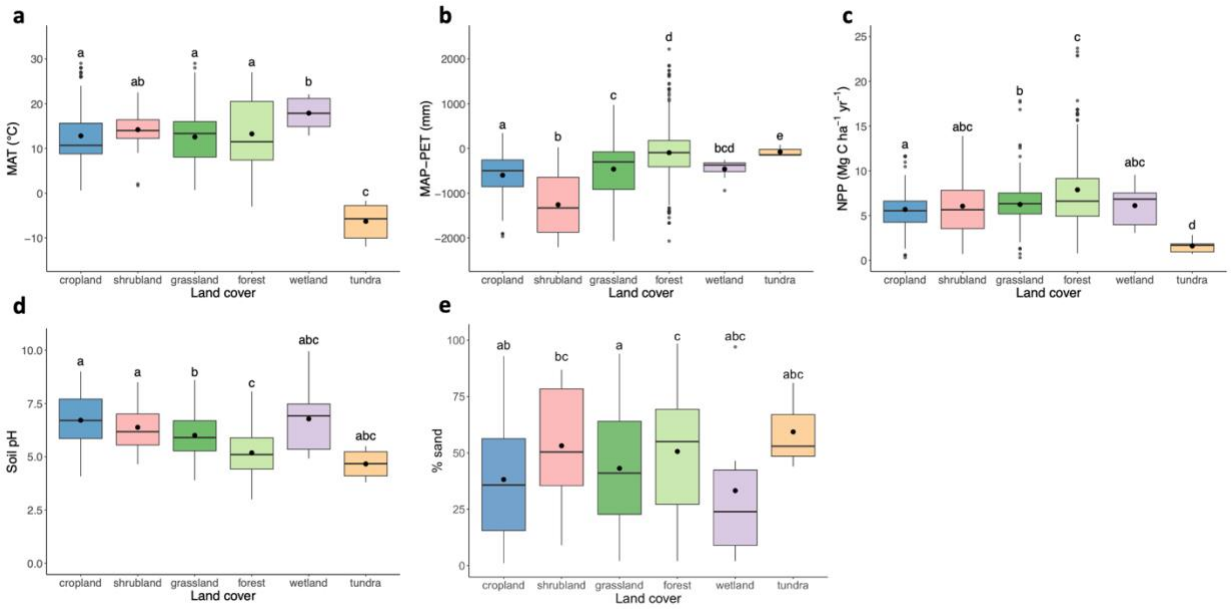

Figure A2.5. Comparisons of **a**) mean annual temperature (MAT; °C), **b**) mean annual precipitation minus potential evapotranspiration (MAP-PET; mm), **c**) net primary production (NPP; Mg C ha^{-1} yr^{-1}), **d**) soil pH, and **e**) % sand with across land cover types. Solid black dots inside each box indicate group means, and letters above bars indicate significant differences between groups. Statistical results are provided in Table A1.7.

Supplementary Information for Chapter 3

Table A3.1. General model parameters, reproduced following Kaiser et al., 2015 with modifications to match the current model.

Parameter	Description	Value
Enzyme kinetics		
k_{cat}: number of enzymatic reactions catalyzed per enzyme (mol substrate C decomposed mol enzyme C^{-1})		
$k_{cat}POM$	k_{cat} of enzymes degrading POM	0.22 $timestep^{-1*}$
$k_{cat}CRN$	k_{cat} of enzymes degrading C-rich microbial necromass	0.63 $timestep^{-1}$
$k_{cat}NRN$	k_{cat} of enzymes degrading N-rich microbial necromass	0.3 $timestep^{-1}$
k_m: half saturation constant for substrates in one microsite		
k_mPOM	k_m of POM	0.29 fmol C
k_mCRN	k_m of C-rich microbial necromass	0.28 fmol C
k_mNRN	k_m of N-rich microbial necormass	0.25 fmol C
K_{enz}	First order rate constant for inactivation of all enzymes	0.036 $timestep^{-1}$
Microbial physiology		
R_{maint}	Maintenance respiration (as fraction of cell biomass)	0.002667 $timestep^{-1}$
R_{eg}	Respiration associated with enzyme production and growth (as fraction of C uptake allocated to enzyme production and growth)	0.26 $timestep^{-1}$
U_{max}	Maximum C uptake rate (as fraction of cell biomass, to be multiplied by cell surface area:volume ratio)	0.0019 $timestep^{-1}$
Pr_{inv}	Probability that an already-occupied microsite will be invaded and colonized by a neighboring, reproducing cell	0.01
F_M	In the case of random catastrophic death, factor that links maximum cell size to mortality rate	0.1133
Initial pools in each microsite		
C_{enz}	Active extracellular enzymes	0.5 fmol C
C_{CRN}	C-rich microbial necromass	100 fmol C
C_{NRN}	N-rich microbial necromass	30 fmol C
C_{DOM}	DOM available for immediate uptake (initial C:N=8)**	7 fmol C
C_{POM}	POM	8333 fmol C
Pool C:N ratios		
CN_{CRN}	C:N of C-rich, complex substrates (e.g., cell wall compounds, lipids, starch) released upon microbial cell death	150
CN_{NRN}	C:N of N-rich, complex substrates (e.g., proteins, DNA, RNA) released upon microbial cell death	5
$CN_{N\text{-}DOM}$	C:N of soluble substrates released upon microbial cell death	15
CN_{POM}	Initial C:N of POM	10-100, depending on scenario
Initial number of microsites occupied by microbes		
M_O	Microsites occupied by microbes, randomly distributed over 10,000 microsites	1666

*One model timestep=1 h.
**the C:N of immediately assimilable DOM has an initial value of 8, but is not a parameter and can change over the course of the simulation.

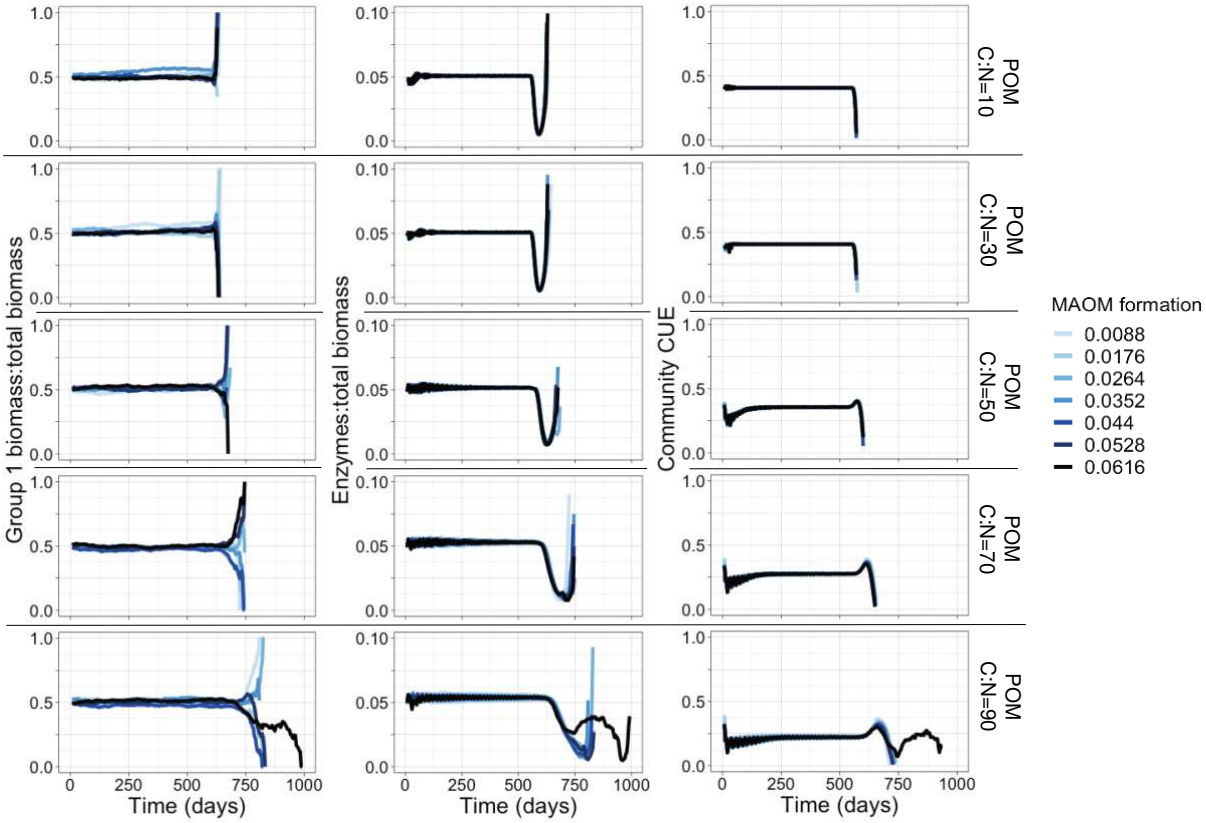

Figure A3.1. All results from simulations of communities containing microbes that produce enzymes at the full rate only. The x-axis of each plot indicates simulation time in days, and the y-axis represents cheater biomass:total biomass, total enzyme production:total biomass, and community carbon use efficiency (CUE), depending on column Each row represents particulate organic matter (POM) carbon:nitrogen (C:N) ratio at the start of the simulations. Line colors represent rates of mineral-associated organic matter (MAOM) formation. Note that values of MAOM formation values are technically values of the parameter f_{diff} (see *Materials and Methods*; Table 1) but are labeled "MAOM formation" for ease of interpretability, as f_{diff} controls MAOM formation rates. Additionally, for the first column depicting group 1:total biomass, both groups of microbes possess the exact same suite of enzyme investment traits, and the group 1:total biomass ratio serves as a proof of concept that each group comprises ~50% of the total biomass when all microbial composition, enzyme production, and growth traits are equal.

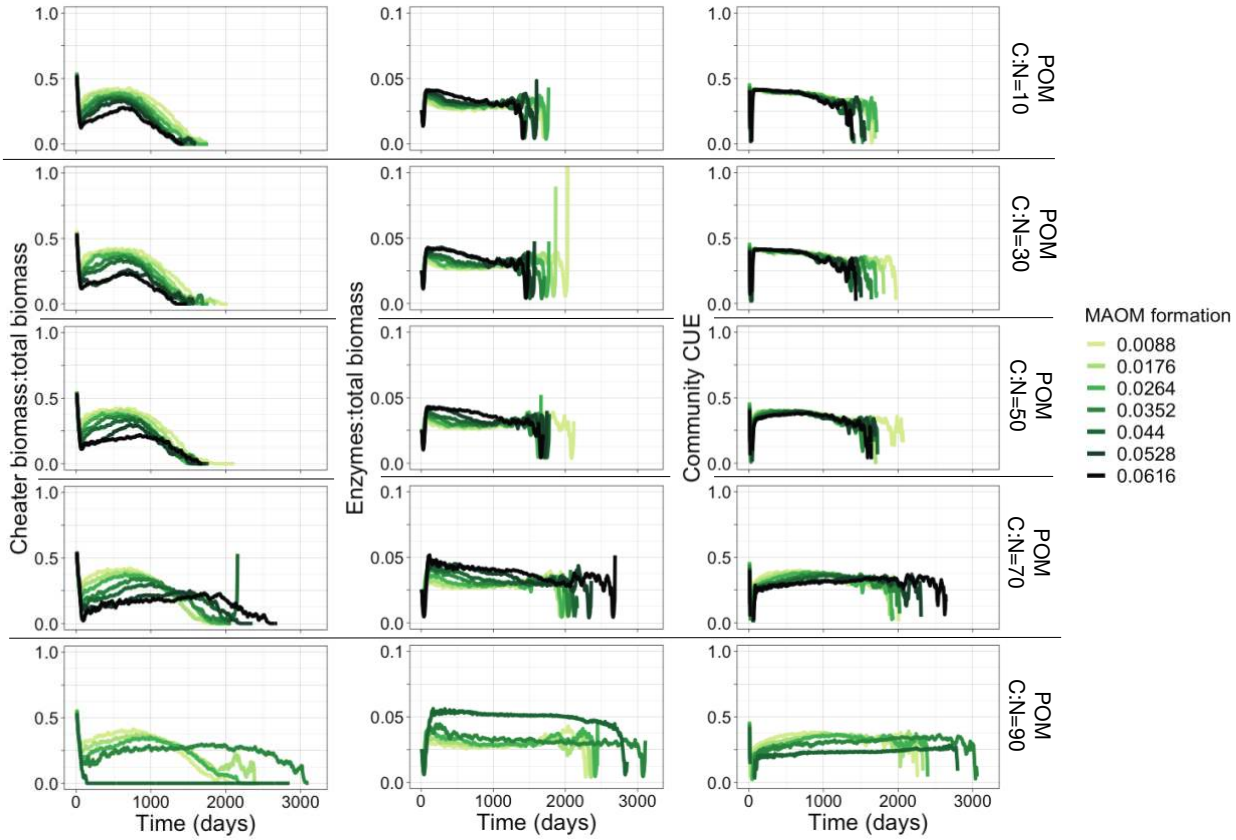

Figure A3.1. All results from simulations of communities containing microbes that produce enzymes at the full rate (i.e., 0.12 of C uptake is invested in enzyme production; producers), and those that do not produce any enzymes at all (i.e., full cheaters). The x-axis of each plot indicates simulation time in days, and the y-axis represents cheater biomass:total biomass, total enzyme production:total biomass, and community carbon use efficiency (CUE), depending on column. Each row represents particulate organic matter (POM) carbon:nitrogen (C:N) ratio at the start of the simulations. Line colors represent rates of mineral-associated organic matter (MAOM) formation. Note that values of MAOM formation values are technically values of the parameter f_{diff} (see *Materials and Methods*; Table 1) but are labeled "MAOM formation" for ease of interpretability, as f_{diff} controls MAOM formation rates.

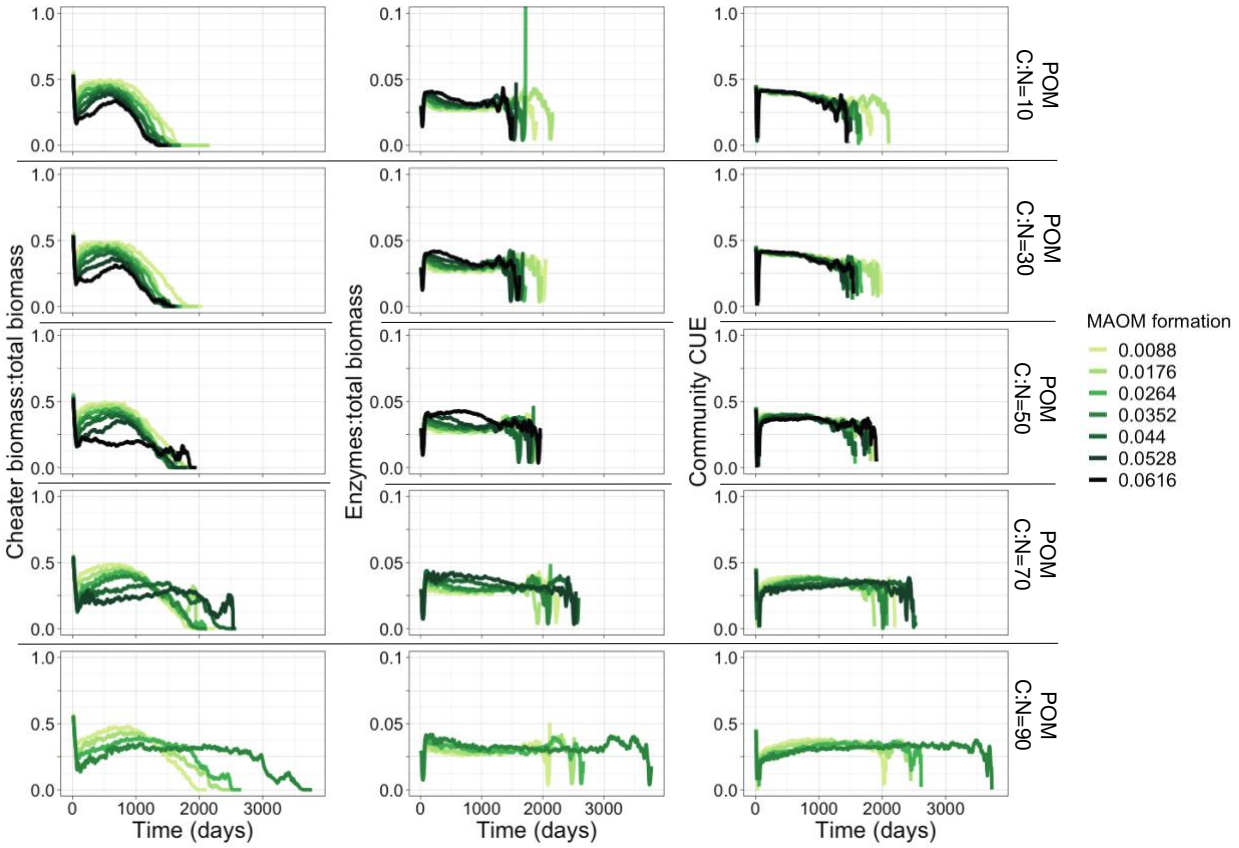

Figure A3.2. All results from simulations of communities containing microbial 'producers' that synthesize enzymes at the full rate (i.e., 0.12 of C uptake is invested in enzyme production), and microbial 'cheaters' that synthesize enzymes at 1/6 that rate (i.e., 0.02 of C uptake). The x-axis of each plot indicates simulation time in days, and the y-axis represents cheater biomass:total biomass, total enzyme production:total biomass, and community carbon use efficiency (CUE), depending on column. Each row represents particulate organic matter (POM) carbon:nitrogen (C:N) ratio at the start of the simulations. Line colors represent rates of mineral-associated organic matter (MAOM) formation. Note that values of MAOM formation values are technically values of the parameter f_{diff} (see *Materials and Methods*; Table 1) but are labeled "MAOM formation" for ease of interpretability, as f_{diff} controls MAOM formation rates.

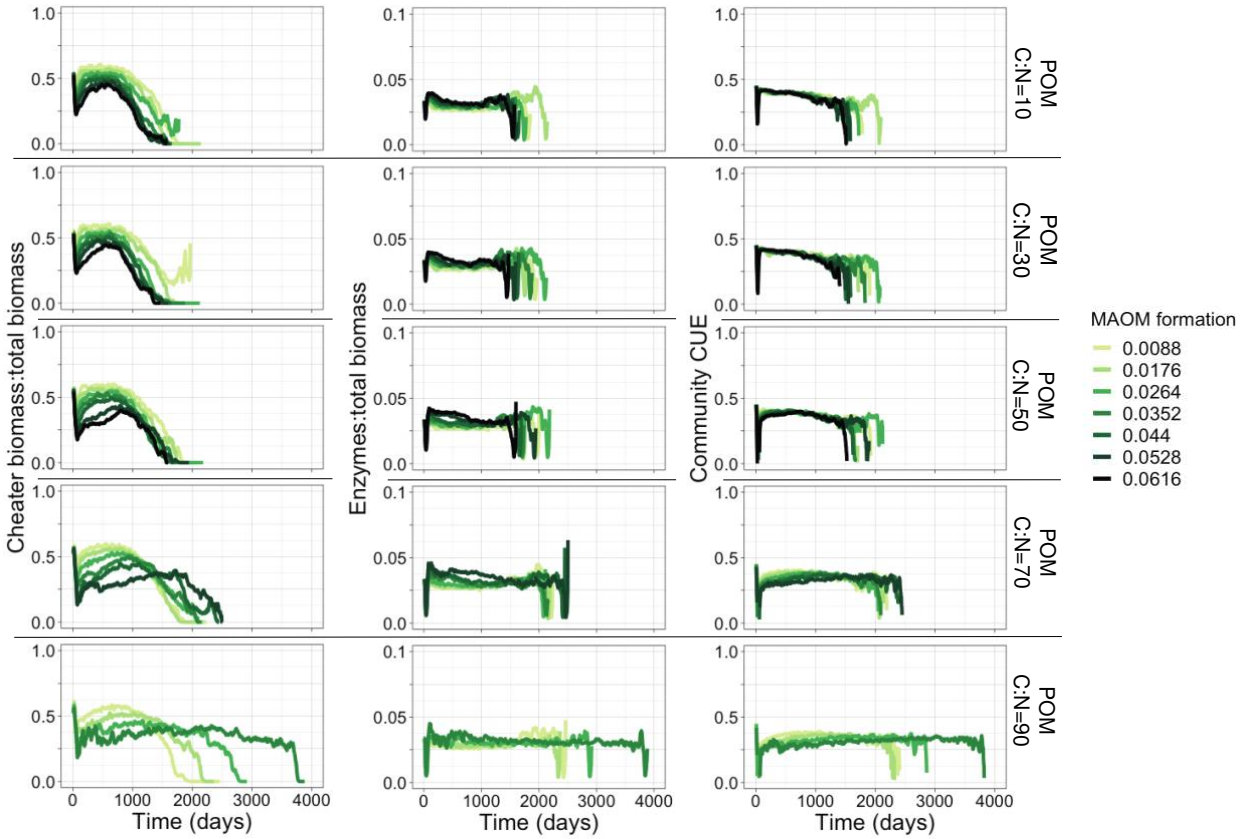

Figure A3.3. All results from simulations of communities containing microbial 'producers' that synthesize enzymes at the full rate (i.e., 0.12 of C uptake is invested in enzyme production), and microbial 'cheaters' that synthesize enzymes at 1/3 that rate (i.e., 0.04 of C uptake). The x-axis of each plot indicates simulation time in days, and the y-axis represents cheater biomass:total biomass, total enzyme production:total biomass, and community carbon use efficiency (CUE), depending on column. Each row represents particulate organic matter (POM) carbon:nitrogen (C:N) ratio at the start of the simulations. Line colors represent rates of mineral-associated organic matter (MAOM) formation. Note that values of MAOM formation values are technically values of the parameter f_{diff} (see *Materials and Methods*; Table 1) but are labeled "MAOM formation" for ease of interpretability, as f_{diff} controls MAOM formation rates.

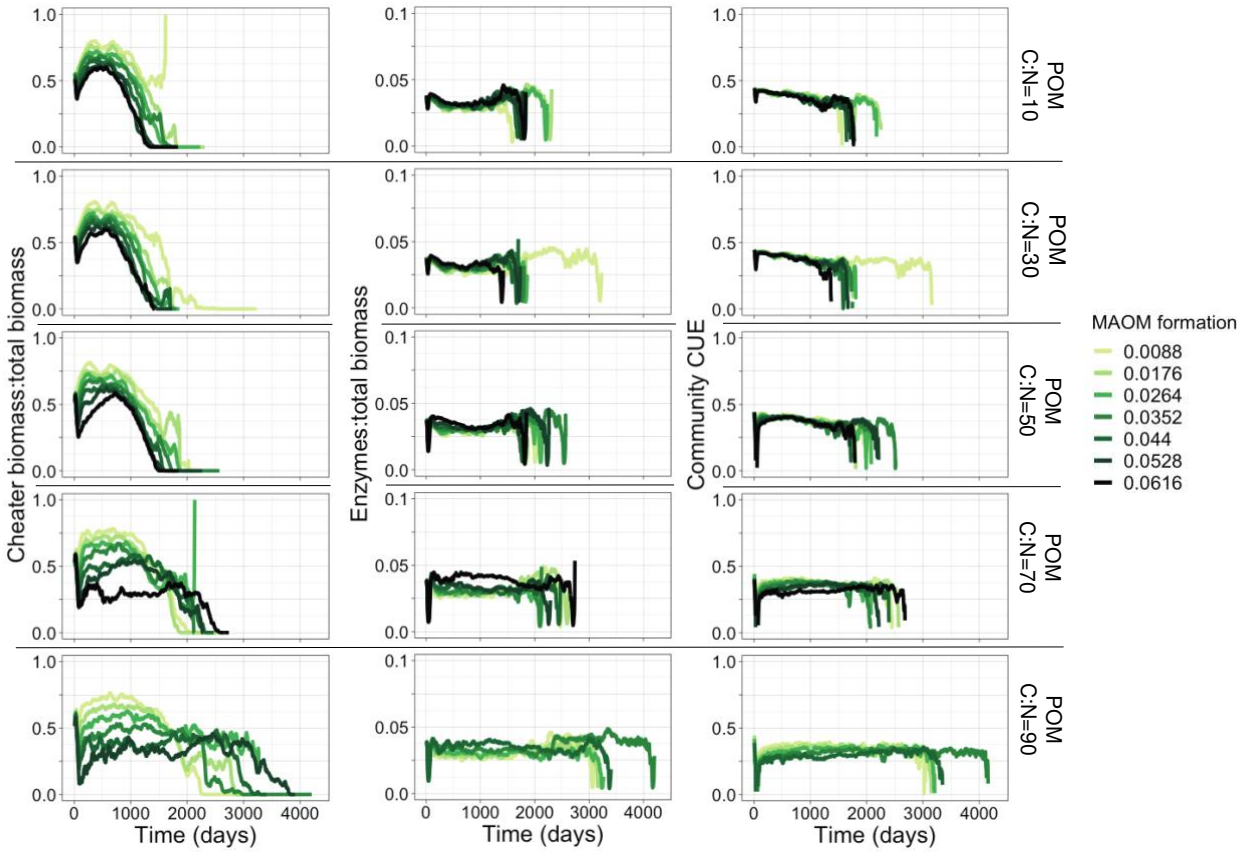

Figure A3.4. All results from simulations of communities containing microbial 'producers' that synthesize enzymes at the full rate (i.e., 0.12 of C uptake is invested in enzyme production), and microbial 'cheaters' that synthesize enzymes at 1/2 that rate (i.e., 0.06 of C uptake). The x-axis of each plot indicates simulation time in days, and the y-axis represents cheater biomass:total biomass, total enzyme production:total biomass, and community carbon use efficiency (CUE), depending on column. Each row indicates particulate organic matter (POM) carbon:nitrogen (C:N) ratio at the start of the simulations. Line colors represent rates of mineral-associated organic matter (MAOM) formation. Note that values of MAOM formation values are technically values of the parameter f_{diff} (see *Materials and Methods*; Table 1) but are labeled "MAOM formation" for ease of interpretability, as f_{diff} controls MAOM formation rates.

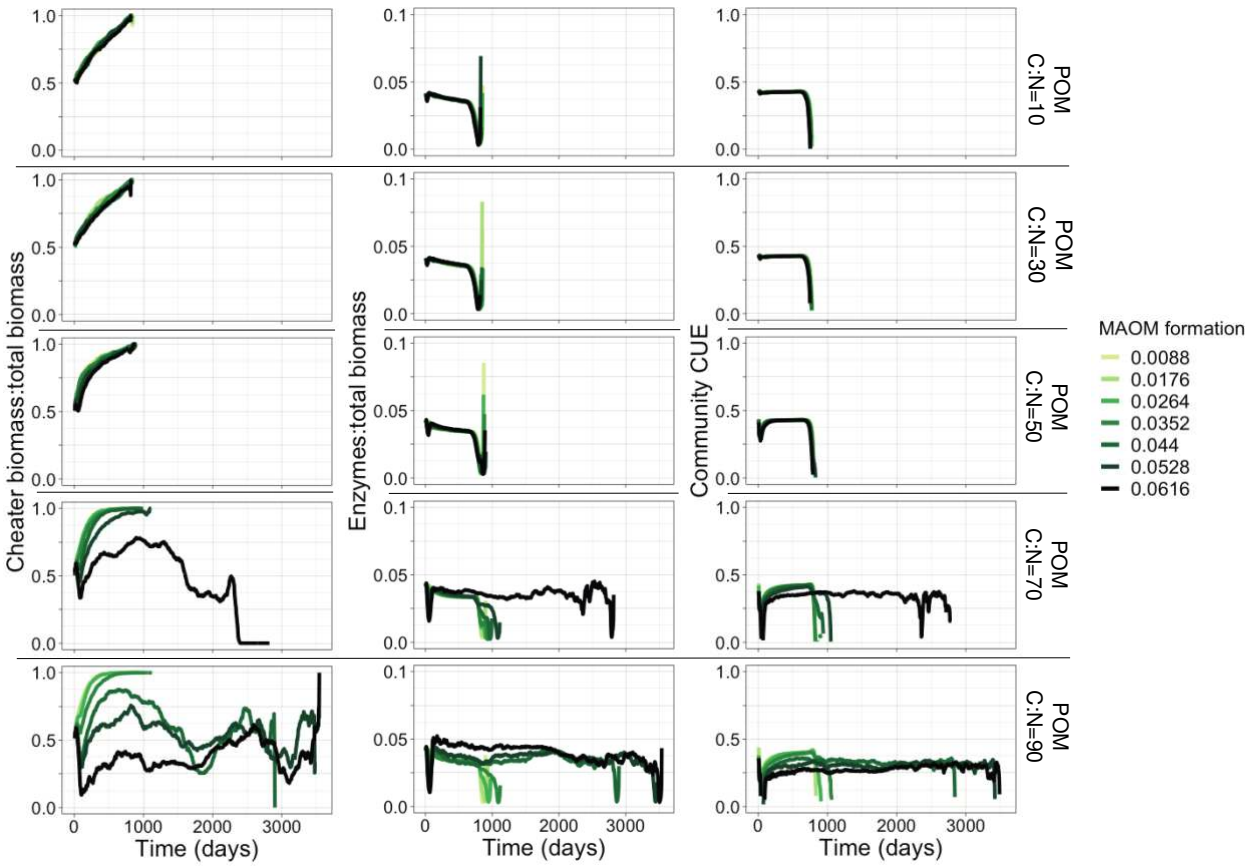

Figure A3.5. All results from simulations of communities containing microbial 'producers' that synthesize enzymes at the full rate (i.e., 0.12 of C uptake is invested in enzyme production), and microbial 'cheaters' that synthesize enzymes at 3/4 that rate (i.e., 0.08 of C uptake). The x-axis of each plot indicates simulation time in days, and the y-axis represents cheater biomass:total biomass, total enzyme production:total biomass, and community carbon use efficiency (CUE), depending on column. Each row represents particulate organic matter (POM) carbon:nitrogen (C:N) ratio at the start of the simulations. Line colors represent rates of mineral-associated organic matter (MAOM) formation. Note that values of MAOM formation values are technically values of the parameter f_{diff} (see *Materials and Methods*; Table 1) but are labeled "MAOM formation" for ease of interpretability, as f_{diff} controls MAOM formation rates.

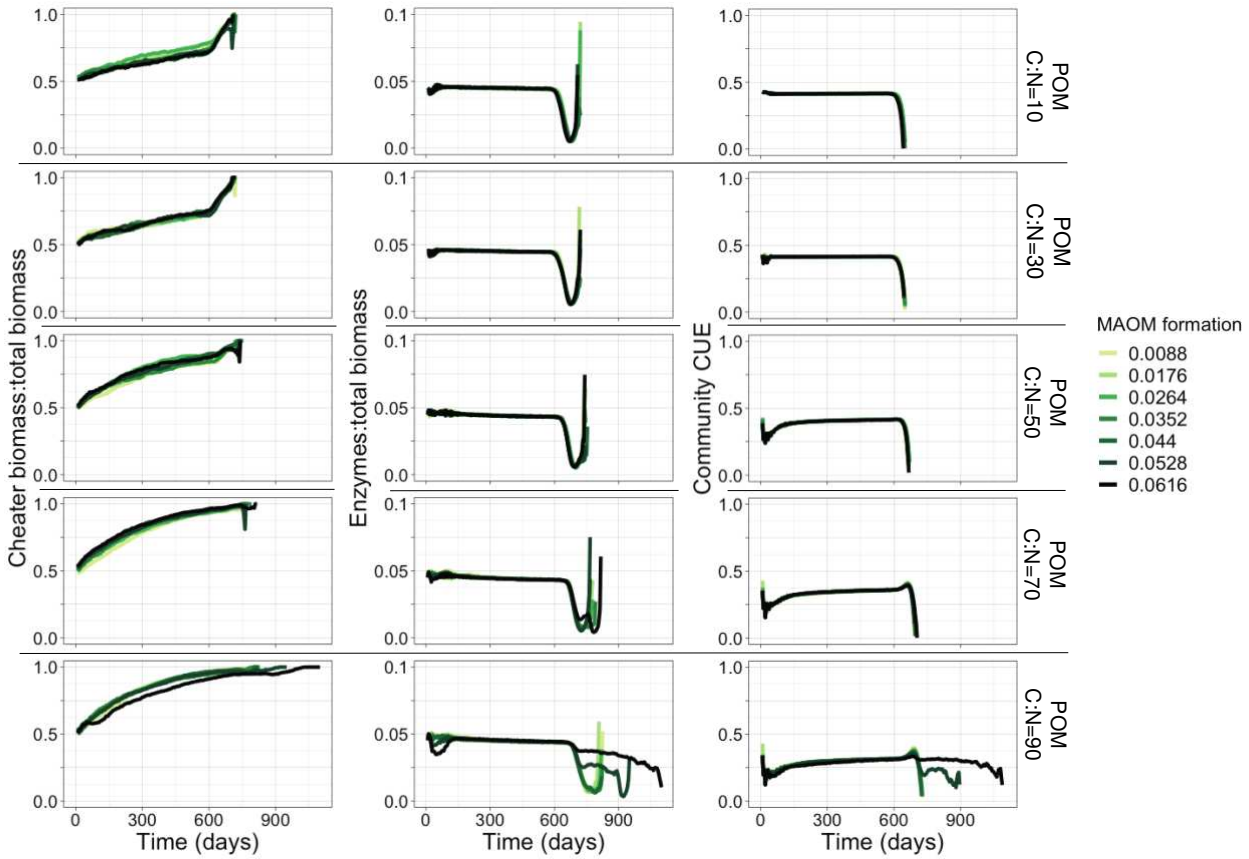

Figure A3.6. All results from simulations of communities containing microbial 'producers' that synthesize enzymes at the full rate (i.e., 0.12 of C uptake is invested in enzyme production), and microbial 'cheaters' that synthesize enzymes at 5/6 that rate (i.e., 0.10 of C uptake). The x-axis of each plot indicates simulation time in days, and the y-axis represents cheater biomass:total biomass, total enzyme production:total biomass, and community carbon use efficiency (CUE), depending on column. Each row represents particulate organic matter (POM) carbon:nitrogen (C:N) ratio at the start of the simulations. Line colors represent rates of mineral-associated organic matter (MAOM) formation. Note that values of MAOM formation values are technically values of the parameter f_{diff} (see *Materials and Methods*; Table 1) but are labeled "MAOM formation" for ease of interpretability, as f_{diff} controls MAOM formation rates.

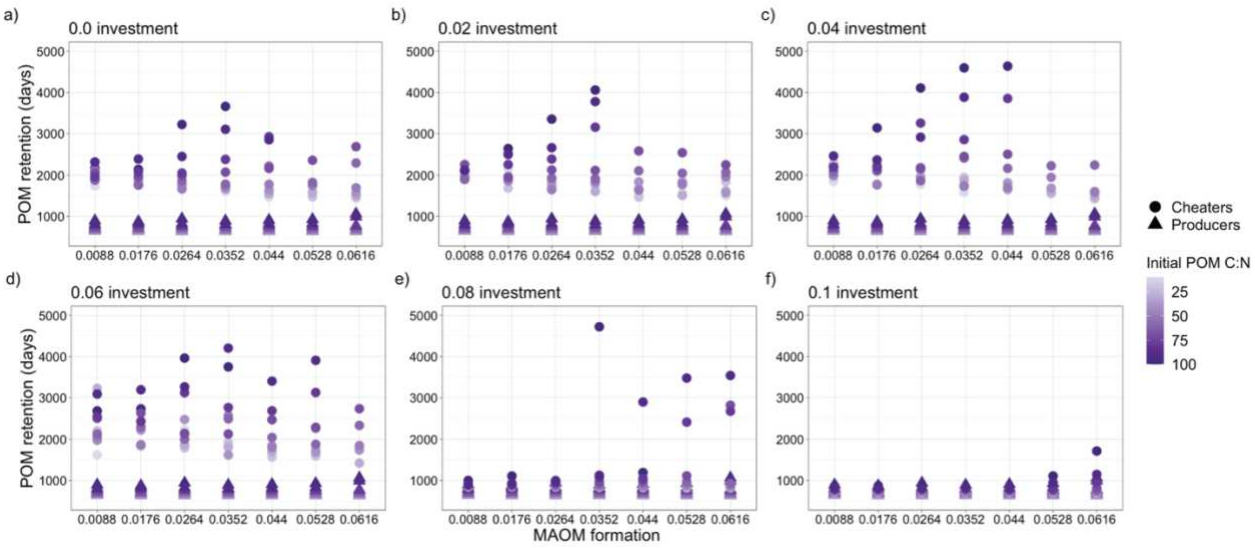

Figure A3.7. Effects of initial particulate organic matter (POM) carbon:nitrogen (C:N) ratio and mineral-associated organic matter (MAOM) formation on POM retention in simulations that contain microbial cheaters compared to those that contain only enzyme producers. Panels **a-f** represent different cheater enzyme investments. In each, the x-axis indicates MAOM formation, and the y-axis indicates the length of time POM is retained in the system. Note that values of MAOM formation values are technically values of the parameter f_{diff} (see *Materials and Methods*; Table 1) but are labeled "MAOM formation" for ease of interpretability, as f_{diff} controls MAOM formation rates. Different colors represent initial POM C:N, with darker shades of purple indicating higher C:N. Different shapes indicate whether simulations contain cheaters (circles) or producers only (triangles).

Supplementary Information for Chapter 4

Table A4.1. Results from one-way Analysis of Variance (ANOVA) tests assessing effects of fresh dissolved organic matter (DOM) additions on the mass-specific growth rate of individual microbial groups.

Microbial group	**Df**	**F value**	***P* value**	**Significance**
Gram+ bacteria	3,76	0.982	0.406	n.s.
Gram- bacteria	3,76	0.718	0.544	n.s.
Actinomycetes	3,76	1.036	0.382	n.s.
Saprotrophic fungi	3,76	1.883	0.14	n.s.
AMF	3,76	0.207	0.891	n.s.
General PLFAs	3,76	1.102	0.354	n.s.

Table A4.2. Results from one-way Analysis of Variance (ANOVA) tests and associated Tukey *post-hoc* pairwise comparisons assessing effects of fresh dissolved organic matter (DOM) additions on incorporation efficiencies of the applied DOM of individual microbial groups. Only statistically significant pairwise comparisons are included.

One-way ANOVA results				
Microbial group	**Df**	**F value**	***P* value**	**Significance**
Gram+ bacteria	2,57	3.872	0.0265	*
Gram- bacteria	2,57	4.545	0.0147	*
Actinomycetes	2,57	0.802	0.454	n.s.
Saprotrophic fungi	2,57	2.136	0.127	n.s.
AMF	2,57	5.66	0.00572	**
General PLFAs	2,57	9.995	0.00019	***
Tukey *post hoc* pairwise comparisons				
Microbial group	**Comparison**	**Difference**	***P* value**	**Significance**
Gram+ bacteria	High-low	-0.1795	0.0199	*
Gram- bacteria	High-low	-0.1593	0.0107	*
AMF	High-low	-0.2059	0.0049	**
General PLFAs	Medium-low	-0.0974	0.0438	*
	High-low	-0.1765	0.00011	***

Table A4.3. Results from one-way Analysis of Variance (ANOVA) and associated Tukey *post-hoc* pairwise comparisons assessing effects of fresh dissolved organic matter (DOM) additions on the total biomass of individual microbial groups. Only statistically significant pairwise comparisons are included

One-way ANOVA results				
Microbial group	**Df**	**F value**	***P* value**	**Significance**
Gram+ bacteria	3,76	0.257	0.856	n.s.
Gram- bacteria	3,76	0.626	0.6	n.s.

Actinomycetes	3,76	0.284	0.837	n.s.
Saprotrophic fungi	3,76	1.561	0.206	n.s.
AMF	3,76	1.546	0.21	n.s.
General PLFAs	3,76	2.973	0.037	*
Tukey *post hoc* pairwise comparisons				
Microbial group	**Comparison**	**Difference**	***P* value**	**Significance**
General PLFAs	DI-medium	0.1694	0.0503	*

Table A4.4. Results from one-way Analysis of Variance (ANOVA) tests and associated Tukey *post-hoc* pairwise comparisons assessing effects of fresh dissolved organic matter (DOM) additions on DOM-derived respiration and carbon (C) in each soil organic matter (SOM) fraction.

One-way ANOVA results				
Carbon pool	**Df**	**F value**	***P* value**	**Significance**
Cumulative respiration	2,57	1148	<2e-16	***
Light POM	2,57	9.246	0.000333	***
CHAOM	2,57	16.96	1.74e-6	***
MAOM	2,57	162.7	<2e-16	***
DOM	2,57	21.98	9.02e-8	***
Tukey *post hoc* pairwise comparisons				
Carbon pool	**Comparison**	**Difference**	***P* value**	**Significance**
Cumulative respiration	Medium-low	7.35	<2e-16	***
	High-low	15.064	<2e-16	***
	High-medium	7.7138	<2e-16	***
Light POM	High-low	0.7149	0.000198	***
CHAOM	Medium-low	0.3044	0.0075	**
	High-low	0.5569	9e-7	***
	High-medium	0.2525	0.0312	*
MAOM	Medium-low	2.45	<2e-16	***
	High-low	5.088	<2e-16	***
	High-medium	2.638	<2e-16	***
DOM	Medium-low	0.385	0.00972	**
	High-low	0.8264	<2e-16	***
	High-medium	0.4414	0.00267	**

Table A4.5. Results from one-way Analysis of Variance (ANOVA) tests and associated Tukey *post-hoc* pairwise comparisons assessing effects of fresh dissolved organic matter (DOM) additions on cumulative total respiration and carbon (C) in each soil organic matter (SOM) fraction.

One-way ANOVA results				
Carbon pool	**Df**	**F value**	***P* value**	**Significance**
Cumulative respiration	3,76	5.354	0.00213	**
Light POM	3,76	6.601	0.000504	***

CHAOM	3,76	13.83	2.75e-7	***
MAOM	3,76	3.335	0.0237	*
DOM	3,74	20.12	1.23e-9	***
Tukey *post hoc* pairwise comparisons				
Carbon pool	**Comparison**	**Difference**	***P* value**	**Significance**
Cumulative respiration	DI-medium	-121.816	0.01	**
	DI-high	-138.19	0.00264	**
Light POM	DI-low	1.1645	0.00055	***
	DI-medium	0.8764	0.0142	*
	DI-high	0.9543	0.00629	**
CHAOM	DI-low	-0.6179	6.8e-6	***
	DI-medium	-0.6248	5.4e-6	***
	DI-high	-0.6	1.24e-5	***
MAOM	DI-low	-0.6435	0.0285	*
DOM	DI-low	-0.0238	1e-8	***
	DI-medium	-0.0259	<2e-16	***
	DI-high	-0.0212	2.2e-7	***

Table A4.5. Results from linear regressions assessing the effects of microbial traits including growth rate, carbon use efficiency (CUE), dissolved organic matter (DOM) incorporation efficiency, and total biomass on DOM-derived fraction formation efficiency, as well as change in fraction carbon (C) relative to DI water controls.

Response var.	Predictor	Intercept	Slope	r^2	*p*-value	Significance
DOM-derived light POM formation efficiency	Growth	0.767	-0.0262	0.0053	0.5823	n.s.
	CUE	0.9544	-1.3814	0.0308	0.1837	n.s.
	DOM incorp. efficiency	0.9498	-7.4427	0.0379	0.1361	n.s.
	Total biomass	0.9137	-0.0607	0.0099	0.4505	n.s.
DOM-derived CHAOM formation efficiency	Growth	0.569	-0.0068	0.0026	0.702	n.s.
	CUE	0.6177	-0.3847	0.0179	0.3171	n.s.
	DOM incorp. efficiency	0.5271	0.3663	0.0007	0.8446	n.s.
	Total biomass	0.3965	0.0343	0.0233	0.2485	n.s.
DOM-derived MAOM formation efficiency	Growth	4.3639	-0.0092	0.00045	0.8735	n.s.
	CUE	4.0275	1.3853	0.0213	0.2701	n.s.
	DOM incorp. efficiency	4.0901	6.0692	0.0173	0.3168	n.s.
	Total biomass	4.521	-0.0456	0.0038	0.6398	n.s.
DOM-derived DOM formation efficiency	Growth	0.8616	0.0099	0.0027	0.7011	n.s.
	CUE	0.8791	0.1057	0.0006	0.8537	n.s.
	DOM incorp. efficiency	0.9347	-0.8154	0.0017	0.7619	n.s.
	Total biomass	1.2514	-0.082	0.0628	0.0579	.
Change in light POM	Growth	-1.045	0.012	0.00056	0.858	n.s.
	CUE	-0.7918	-1.0285	0.0085	0.4866	n.s.

	DOM incorp. efficiency	-0.5537	-11.3235	0.0439	0.108	n.s.
	Total biomass	-0.6545	-0.0815	0.0089	0.4736	n.s.
Change in CHAOM	Growth	0.653	-0.0092	0.0021	0.7334	n.s.
	CUE	0.5437	0.3529	0.0063	0.5511	n.s.
	DOM incorp. efficiency	0.6259	-0.2956	0.00019	0.9174	n.s.
	Total biomass	0.4445	0.0402	0.0135	0.3761	n.s.
Change in MAOM	Growth	0.6587	-0.0285	0.0072	0.522	n.s.
	CUE	0.4672	0.4763	0.004	0.634	n.s.
	DOM incorp. efficiency	0.7462	-4.7937	0.0171	0.3192	n.s.
	Total biomass	0.7801	-0.0527	0.0081	0.495	n.s.
Change in DOM	Growth	0.0255	-0.00041	0.0048	0.6077	n.s.
	CUE	0.029	-0.0245	0.0374	0.1494	n.s.
	DOM incorp. efficiency	0.0276	-0.0996	0.0255	0.2308	n.s.
	Total biomass	0.033	-0.0022	0.0445	0.112	n.s.

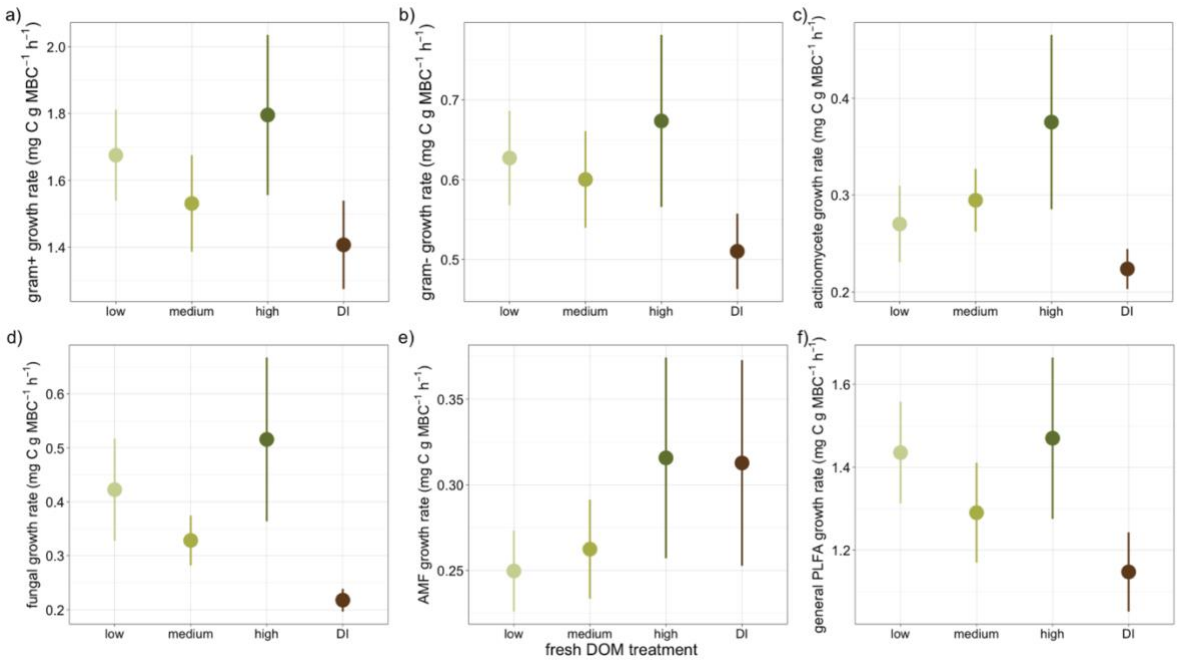

Figure A4.1. Effects of fresh dissolved organic matter (DOM) addition on the mass-specific growth rate of individual microbial groups, including **a**) gram positive bacteria, **b**) gram negative bacteria, **c**) actinomycetes, **d**) saprotrophic fungi, **e**) arbuscular mycorrhizal fungi (AMF), and **f)** general microbial phospholipid fatty acid (PLFA) biomarkers. Data points and error bars indicate group means and standard error. There were no statistical differences between groups. Statistical results are described in more detail in Table A2.1.

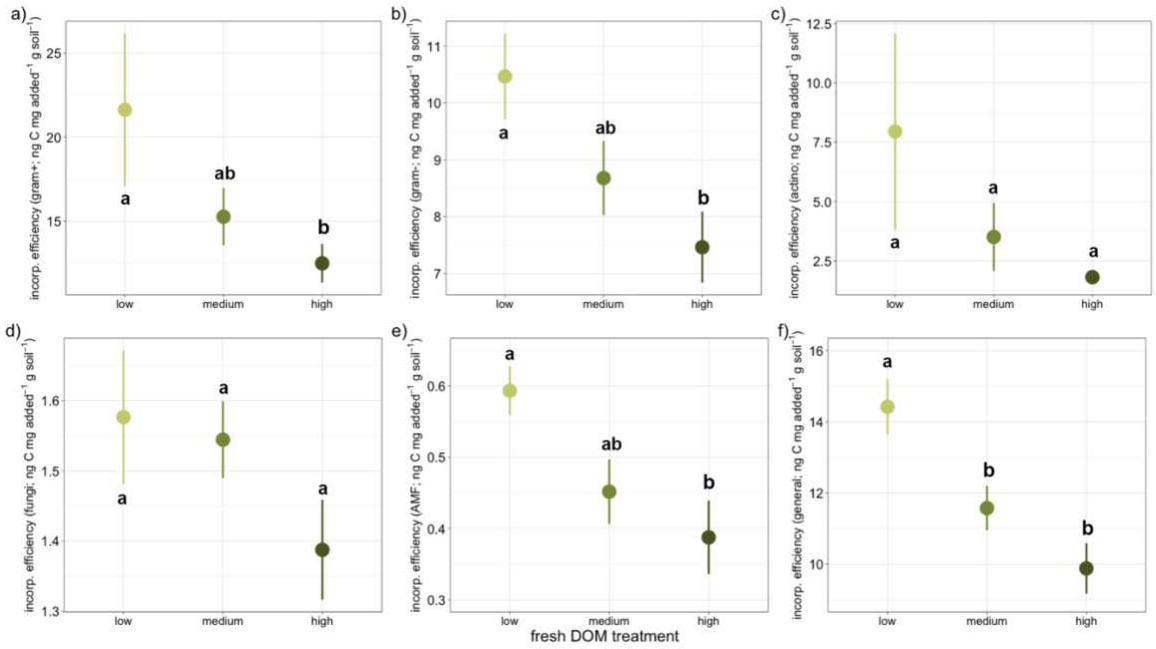

Figure A4.2. Effects of fresh dissolved organic matter (DOM) addition on efficiency of fresh dissolved organic matter (DOM) incorporation into individual microbial groups, including **a)** gram positive bacteria, **b)** gram negative bacteria, **c**) actinomycetes, **d**) saprotrophic fungi, **e**) arbuscular mycorrhizal fungi (AMF), and **f**) general microbial phospholipid fatty acid (PLFA) biomarkers. Data points and error bars indicate group means and standard error. Statistical differences between groups are described in Table A2.2, and indicated with letters above data points.

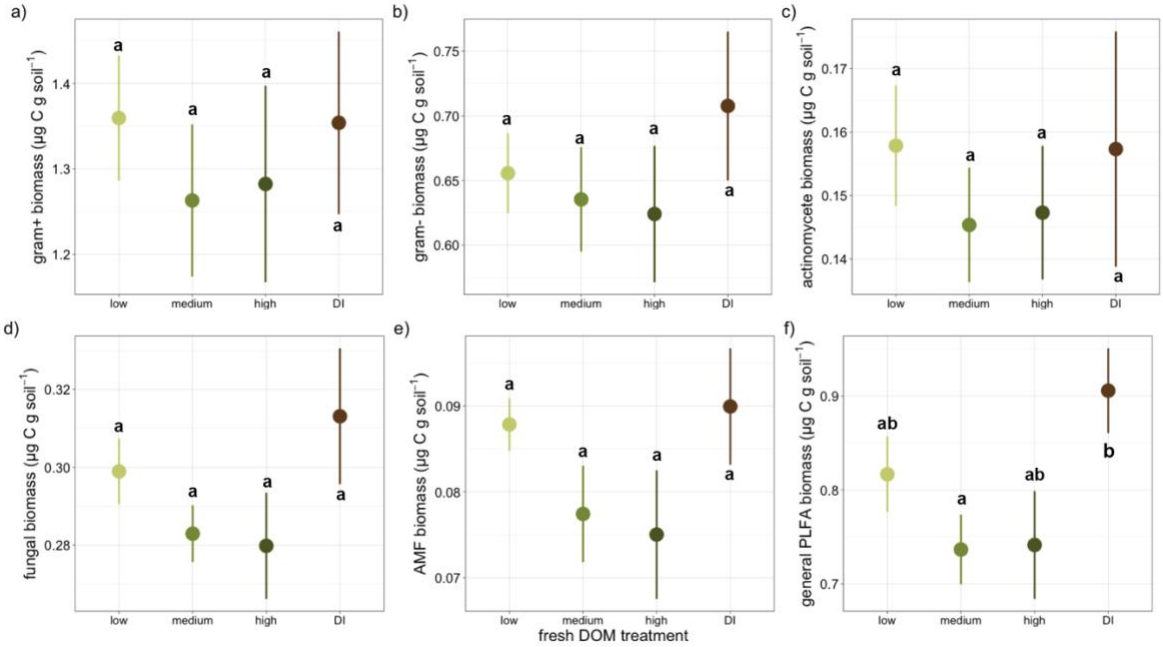

Figure A4.3. Effects of fresh dissolved organic matter (DOM) addition on the total biomass of individual microbial groups including **a**) gram positive bacteria, **b**) gram negative bacteria, **c**) actinomycetes, **d**) saprotrophic fungi, **e)** arbuscular mycorrhizal fungi (AMF), and **f**) general microbial phospholipid fatty

acid (PLFA) biomarkers. Data points and error bars indicate group means and standard error. Statistical differences between groups are described in Table A2.3, and indicated with letters above data points.

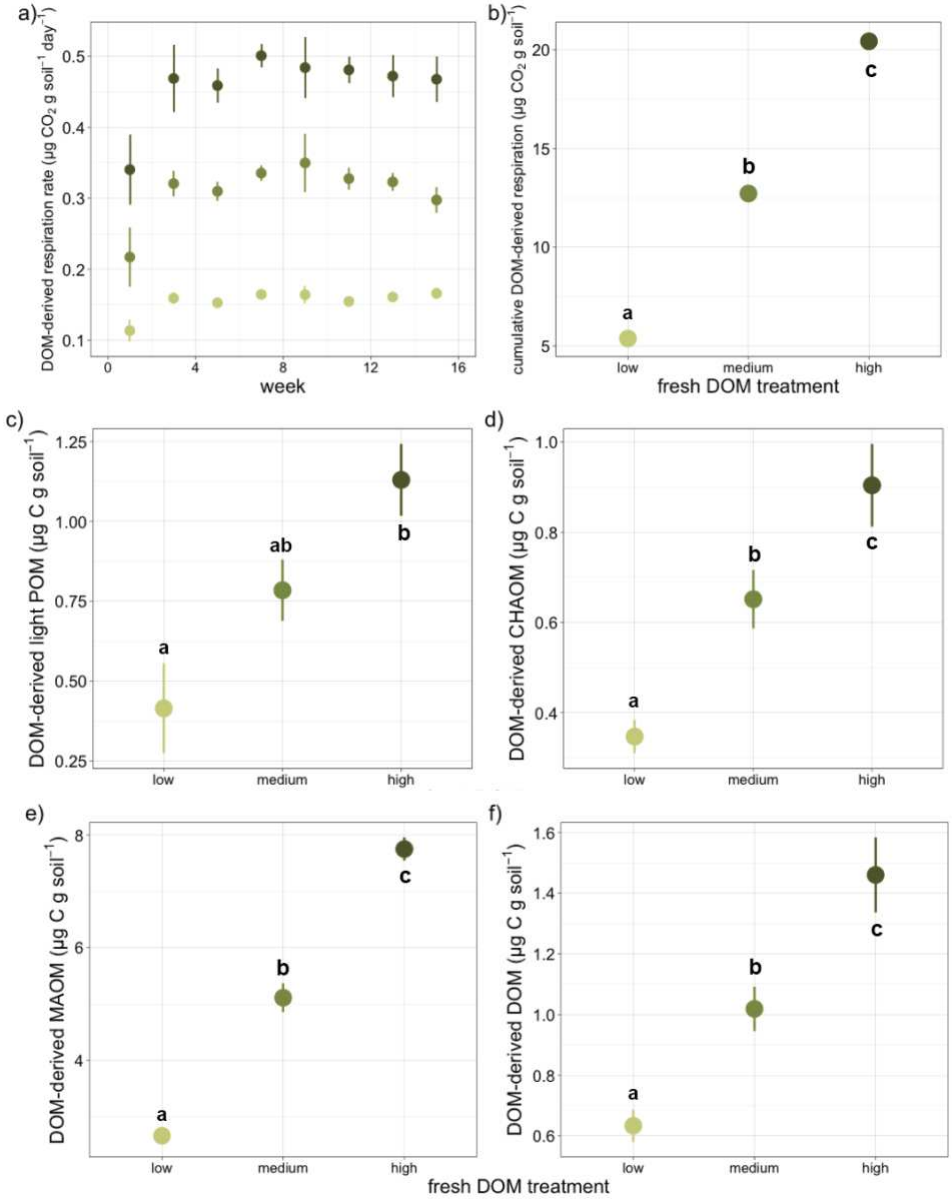

Figure A4.4. Effects of fresh dissolved organic matter (DOM) addition on DOM-derived **a**) respiration rate, **b**) cumulative respiration, **c**) light particulate organic matter (POM), **d**) organic matter associated with coarse, heavy minerals (CHAOM); **e**) mineral-associated organic matter (MAOM), and **f**) dissolved organic matter (DOM). In **a**), different colors indicate fresh DOM addition treatment. Data points and error bars indicate group means and standard error. Statistical differences between groups are described in Table A2.4, and indicated with letters above data points.

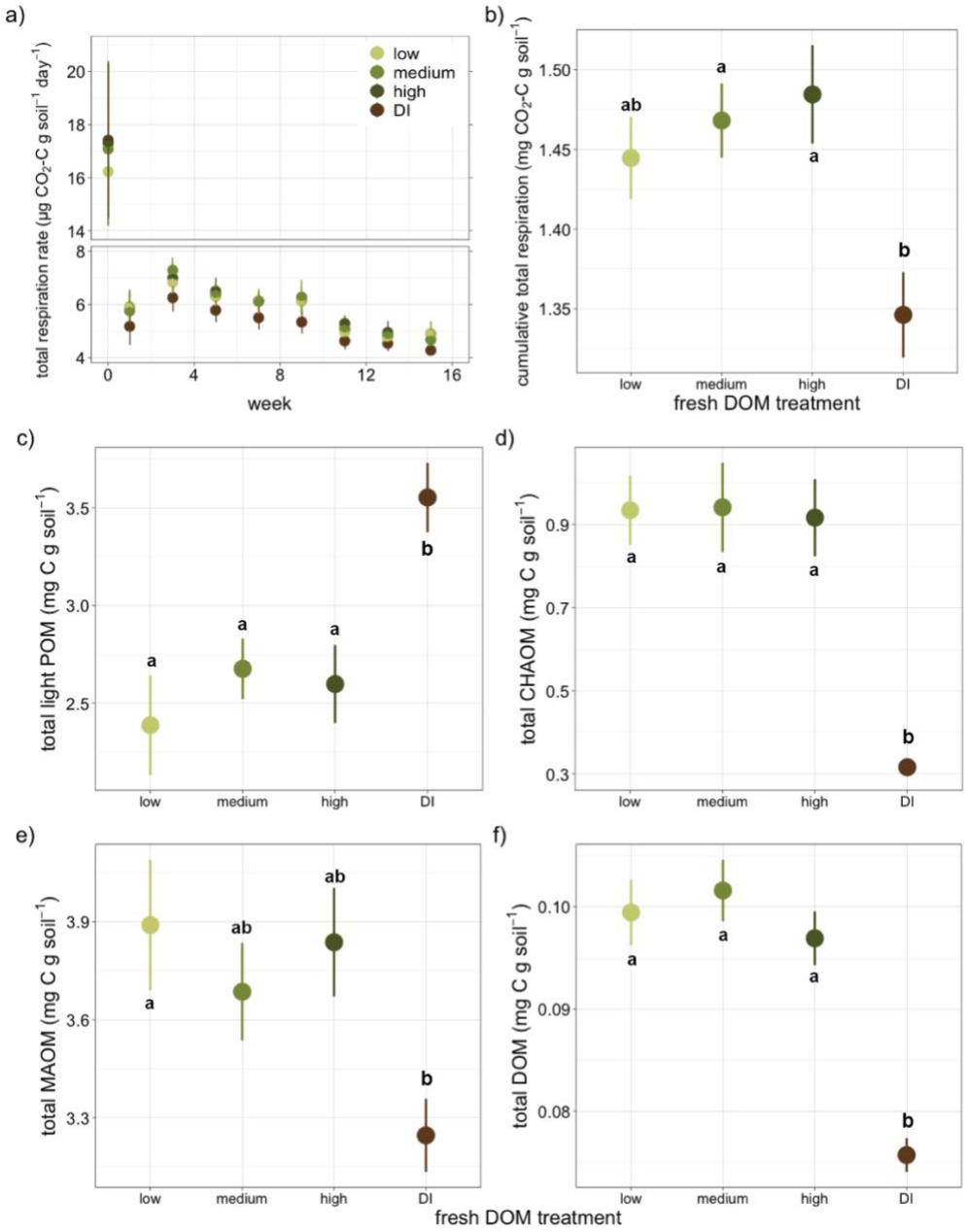

Figure A4.5. Effects of fresh dissolved organic matter (DOM) addition on total carbon (C) storage in **a**) total respiration, **b**) cumulative total respiration, **c**) light particulate organic matter (POM), **d**) organic matter associated with coarse, heavy minerals (CHAOM), **e**) mineral-associated organic matter (MAOM), and **f)** DOM. Data points and error bars indicate group means and standard error. Statistical differences between groups are described in Table A2.5, and indicated with letters above data points.